LASER DIAGNOSITIC SYSTEM VALIDATION AND ULTRA-COMPACT

COMBUSTOR CHARACTERIZATION

THESIS

Terry B. Hankins, Captain, USAF

AFIT/GAE/ENY/08-M14

DEPARTMENT OF THE AIR FORCE
AIR UNIVERSITY
AIR FORCE INSTITUTE OF TECHNOLOGY

Wright-Patterson Air Force Base, Ohio

The views expressed in this thesis are those of the author and do not reflect the official policy or position of the United States Air Force, Department of Defense, or the United States Government.

AFIT/GAE/ENY/08-M14

LASER DIAGNOSITIC SYSTEM VALIDATION AND ULTRA-COMPACT COMBUSTOR CHARACTERIZATION

THESIS

Presented to the Faculty

Department of Aeronautics and Astronautics

Graduate School of Engineering and Management

Air Force Institute of Technology

Air University

Air Education and Training Command

In Partial Fulfillment of the Requirements for the

Degree of Master of Science in Aeronautical Engineering

Terry B. Hankins, BS

Captain, USAF

March 2008

APPROVED FOR PUBLIC RELEASE; DISTRIBUTION UNLIMITED.

AFIT/GAE/ENY/08-M14

LASER DIAGNOSITIC SYSTEM VALIDATION AND ULTRA-COMPACT

COMBUSTOR CHARACTERIZATION

Terry B. Hankins, BS
Captain, USAF

Approved:

_____   _____
Maj Richard Branam, USAF (Chairman)   date

_____   _____
Dr. Paul King (Member)   date

_____   _____
Dr. Mark Reeder (Member)   date

AFIT/GAE/ENY/08-M14

Abstract

The AFIT combustion optimization and analysis laser (COAL) lab is now completely operational and is state-of-the-art in combustion diagnostics. The objective of this research is to perform a validation of a laser diagnostic system and to begin the characterization of a small-scale model of an ultra-compact combustor (UCC). Validation of the laser system was accomplished by using planar laser induced fluorescence (PLIF) on a laminar premixed hydrogen-air flame produced by a Hencken burner. OH species concentrations are measured. Flame temperatures are determined with a two line fluorescence technique using different transitions in the (1,0) band of the OH (A-X) electronic transition system. Comparisons are made to existing research to prove accuracy. Characterization of the UCC began by developing an operational procedure. A proper starting condition and operating regime has been established. Pressures, temperature, and emissions data have been recorded for a range of equivalence ratios. Comparisons are made to previous computational fluid dynamic (CFD) research. Combustion efficiencies of over 99% have been recorded when operating the small-scale UCC. Future work will involve using PLIF to take non-intrusive measurements inside the combustor through optically clear quartz windows to study cavity-vane interactions.

To my mother, the late Billie Jean Hankins. Since her passing I have gone from high school graduate to Master's graduate. She always told me I could do anything I set my mind to. Thanks for looking out for me from Heaven Mom!

Acknowledgements

First, I would like to thank my wife Kerry for having the utmost confidence in me. She has truly been an inspiration by taking care of things around the house, being a full-time nursing student, still having the time to listen to my problems, and help me in anyway she could. She is not only my lover, she is my best friend and together we make a great team.

I would like to thank my advisor Major Rich Branam. He gave me free reign in the COAL lab and the opportunity to "play with fire" as he would call it. Most importantly I would like to thank him for all the patience he has shown me during all the visits to his office. No matter how busy he was he would always take the time to answer all my questions, even when I asked the same one two or three different times.

Thank you so much to Dr. Terry Meyer for your constant availability and answering all my questions about laser spectroscopy. A special thanks goes to Keith Grinstead for the numerous times he helped me in the lab and always getting the laser to operate correctly when I couldn't. Last but certainly not least, thank you to the lab technicians John Hixenbaugh and Chris Zickafoose. All their hard work in the lab is truly appreciated.

Finally, I give all the thanks to God. For I know, I am truly blessed.

Terry B. Hankins

Table of Contents

List of Figures

List of Tables

List of Symbols

Symbol

$\overset{\circ}{A}$ Angstrom (1×10^{-10} meters)

atm   Atmospheric pressure

ºC   Degrees Celsius

C_pT Stagnation Enthalpy (J/mol)

CO   Carbon monoxide

CO_2 Carbon dioxide

CH   Methylidyne radical

C_xH_y Chemical equation for hydrocarbon fuel

$C_{12}H_{23}$ Kerosene

$C_{12}H_{26}$ n-dodecane

C_2H_4 Ethylene

CH_4 Methane

ºF   Degrees Fahrenheit

g   Gravitational constant (m/s^2)

H_2 Hydrogen

H_2O Water

k   Boltzmann's Constant $\left(\dfrac{m^2 kg}{s^2 K} \right)$

K   Kelvin

KDP   Potassium dideuterium phosphate

MW_{air} Molecular weight of air (kg/kmol)

MW_{fuel}	Molecular weight of fuel (kg/kmol)
$\dot{m}_f$	Mass flow rate (kg/s)
NO_X	Nitrous-oxide
N_2	Nitrogen
OH	Hydroxyl radical
O_2	Oxygen
S_B	Buoyant flame speed (m/s)
$\mathscr{T}$	Thrust (N)
T_4	Temperature of the combustor outlet – turbine inlet (K)
UHC	Unburned Hydrocarbon
ϕ	Equivalence ratio
χ	Mole fraction
η_b	Combustion efficiency (%)
σ	Molecule cross section
2-D	Two dimensional
3-D	Three dimensional

List of Abbreviations

Abbreviation or Symbol

AFIT	Air Force Institute of Technology
AFRL	Air Force Research Laboratory
CARS	Coherent Anti-Stokes Raman Spectroscopy
CFD	Computational Fluid Dynamics
COAL	Combustion Optimization and Analysis Laser lab
cm	centimeter
CT	Constant Temperature
DOD	Department of Defense
DOE	Department of Energy
EI	Emissions Index
FWHM	Full-Width Half-Maximum
GE	General Electric
HPT	High Pressure Turbine
ICCD	Intensifying Charged-Coupled Device
IGV	Inlet Guide Vanes
IHPTET	Integrated High Performance Turbine Engine Technology
ISSI	Innovative Scientific Solutions Inc.
ITB	Inter-Stage Turbine Burner
J	Joule
kg	kilogram
LHV	Lower Heating Value (J/kg)
LMLP	Low Mass, Low Pressure
LII	Laser-Induced Incandescence
LPT	Low Pressure Turbine
min	minute
mJ	milliJoule
ml	milliliter
mm	millimeter

ms	milliseconds
NASA	National Aeronautics and Space Administration
Nd:YAG	Neodymium-doped Yttrium Aluminium Garnet
nm	nanometer
ns	nanoseconds
Pa	Pascal (N/m^2)
PLIF	Planar Laser Induced Fluorescence
psi	pounds per square inch
PIV	Particle Imaging Velocimetry
ppm	parts per million
Q	Quality of the Resonator
RVC	Radial Vane Cavity
s	Second
slpm	standard liters per minute
ST	Specific Thrust
TSFC	Thrust Specific Fuel Consumption
TVC	Trapped Vortex Combustion
UCC	Ultra-Compact Combustor
UV	Ultra Violet
VAATE	Versatile Affordable Advanced Turbine Engines
VI	Virtual Instrument
WPAFB	Wright-Patterson Air Force Base

LASER DIAGNOSITIC SYSTEM VALIDATION AND ULTRA-COMPACT

COMBUSTOR CHARACTERIZATION

I.   Introduction

1.1   *Research and Design Perspective*

Military and commercial aircraft consumption of hydrocarbon fuels continues to increase at an exponential pace. The profound dependence on these fuels whose cost continues to rise at an alarming rate shows no sign of dissipating in the near future. As a result, it is imperative future gas turbine engine development focus on technological advancements quantified by increased thrust-to-weight ratio as well as combustion efficiency and decreased thrust specific fuel consumption (TSFC). Also, environmental concerns demand decreased exhaust noise and pollutant emissions. Current design efforts focus on requirements to fly aircraft at supersonic speeds, greater distances, and higher altitudes while achieving decreased life cycle cost in categories such as research and development, investment, and operating and support. If the U.S. Military is to maintain global air superiority and the commercial aircraft industry is to remain economically stable, a main focus must be on the advancement of gas turbine engine technology.

One engine advancement currently in development is the Ultra-Compact Combustor (UCC). It is a shortened combustor placed after the compressor section of the

engine circumferentially over the turbine thus increasing the thrust-to-weight ratio. More specifically, it makes use of the inter-stage turbine burner (ITB) concept employed so a reheat cycle is located between the high and low-pressure turbine stages. Also, the circumferential design of the UCC will feature a trapped vortex combustor (TVC) enhanced airflow capability and greater fuel mixing to increase combustion efficiency. Theoretically, various designs of the UCC have shown potential in accomplishing these improvements through extensive research using computational fluid dynamics (CFD). Until now however, no experimental research has been done to prove accurately what interactions actually occur inside the cavity-vane section of the UCC to facilitate these improvements. The author believes the UCC is a major step in the right direction for the advancement of gas turbine engine technology.

One way to quantify this advancement is through the study of a laminar premixed flame using state-of-the art non-intrusive laser diagnostic techniques. More specifically, advanced analytical tools grounded with proven diagnostic capabilities such as planar laser-induced fluorescence (PLIF) will be used to analyze species concentrations and flame temperatures. A Hencken burner will be used specifically for this purpose. Once the laser diagnostic system is validated, it will be used to take measurements of interactions inside a small-scale UCC through optically clear quartz windows. This will occur after the characterization process of this UCC is completed. During this process emissions data will be captured using a portable emissions analyzer. This data will be used to calculate combustion efficiency. Research will be performed in the Combustion Optimization and Analysis Laser (COAL) lab located at the Air Force Institute of Technology (AFIT).

1.2   *Versatile Affordable Advanced Turbine Engines (VAATE) Initiative*

Air superiority of the United States military is a direct result of gas turbine engine technology. War fighter requirements continue to raise the bar resulting in the need for even more capable, durable, and cost-effective aircraft systems. As a result, greater advancements must be made in propulsion technology. However, investment in gas turbine engine research has considerably declined over the past years (Ref. 1). A continued decline in research could jeopardize the military's capability to remain air dominant in the future.

The Versatile Affordable Advanced Turbine Engines (VAATE) initiative, modeled after the highly successful Integrated High Performance Turbine Engine Technology (IHPTET) program, seeks specific improvements in turbine engine technology such as a 200% increase in engine thrust-to-weight ratio, a 25% reduction in engine fuel consumption, and a 60% reduction in engine development, procurement, and life cycle maintenance cost (Ref. 1)**. To promote continued advancement in gas turbine engine technology research, VAATE will be modeled after a prominent characteristic that made IHPTET so successful – an integrated technology plan between the Department of Defense (DOD), National Aeronautics and Space Administration (NASA), Department of Energy (DOE), academia and industry. A follow on to this plan, the UCC is a proponent of a combined effort between academia – AFIT, industry – General Electric (GE) Engines, and DOD – Air Force Research Lab (AFRL) Propulsion Directorate and will help accomplish the improvement goals set into place by the VAATE initiative.

1.3   *The AFIT Laser Diagnostic System*

The laser diagnostic system makes the COAL lab a state-of-the-art combustion diagnostics facility. The overall arrangement consists of lasers, various optics to include visible light and ultra-violet (UV) filters, lenses, rails and electronically controlled traverse systems for accurate location of optics and cameras for image collection. The system is mounted on several mobile optics tables located around the UCC in the AFIT COAL laboratory (Ref. 2). The laser system is a Quanta-Ray PIV-Series dual pulsed Nd:YAG made by Spectra-Physics, see Fig. 1.

Fig. 1. Quanta-Ray PIV-Series dual pulsed Nd:YAG laser

Some features of this advanced laser include dual oscillators, beam combination, harmonic generation, and wavelength separation. It produces 200 mJ to 400 mJ of pulsed energy at 1064 nm. Pulse separation times range from 100 ns to 100 ms. There is also a Continuum ND6000 narrowband dye laser with a frequency doubler, see Fig. 2, and a broadband dye laser all assembled by Innovative Scientific Solutions, Inc. (ISSI).
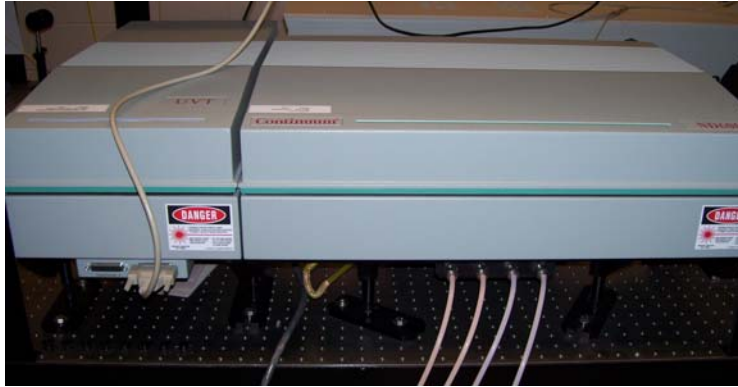
Fig. 2. ND6000 narrowband dye laser with frequency doubler

The camera is an intensifying charged-coupled device (ICCD) camera made by Princeton Instruments (PI-Max, 512 x 512 pixels) with a Nikon PK-11A and PK-12 lens and one CVI camera filter, see Fig. 3.
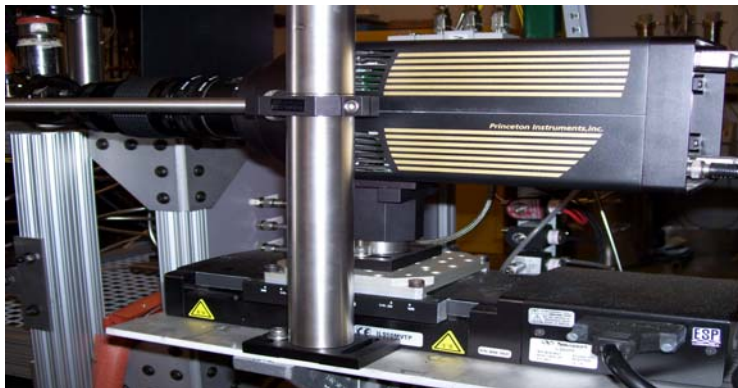
Fig. 3. Princeton Instruments ICCD camera

Operational procedures for the laser and camera can be found in Koether's thesis (Ref. 3).   In addition to PLIF, the Quanta-Ray PIV-Series dual pulsed Nd:YAG laser and surrounding components will also be used for Coherent Anti-Stokes Raman Scattering (CARS), Instantaneous Raman Scattering, Raman Spectroscopy, Laser Induced

Incandescence (LII), and Particle Image Velocimetry (PIV). This laser diagnostic capability distinguishes the AFIT COAL laboratory as a highly advanced combustion diagnostics facility.

1.4 *The AFIT Small-Scale Ultra-compact Combustor*

A small-scale model of a UCC made of stainless steel has been designed and built for combustion research in the COAL lab at AFIT (Ref. 2). Numerous details about supporting equipment for the small-scale model can be found in Koether's thesis (Ref. 3). As for basic support, the UCC has a main and secondary airflow. They both can be heated to temperatures of up to 500 Kelvin (K). The main airflow has delivery rates up to 7 kg/min and secondary airflow has delivery rates up to 2 kg/min. JP-8 fuel can be delivered at constant pressure or constant flow to the combustor through the use of a dual syringe pump. Up to 5.67 ml/s of JP-8 can be delivered with nanoliter precision. Ethylene (C_2H_4) or hydrogen (H_2) can be metered with high precision mass flow controllers through a spark ignition system to light a fire inside the combustor.

In future work, combustion diagnostics will include measurements taken of interactions inside the UCC through optically clear quartz windows to quantify flame speeds, mixing, and vorticity thus validating combustion efficiency measurements. Fig. 4 shows the small-scale model of the UCC with arrows pointing to areas to be fitted with optically clear quartz windows for non-intrusive laser diagnostics. The upper arrow points to the cavity section and the lower arrow points to the axial section.
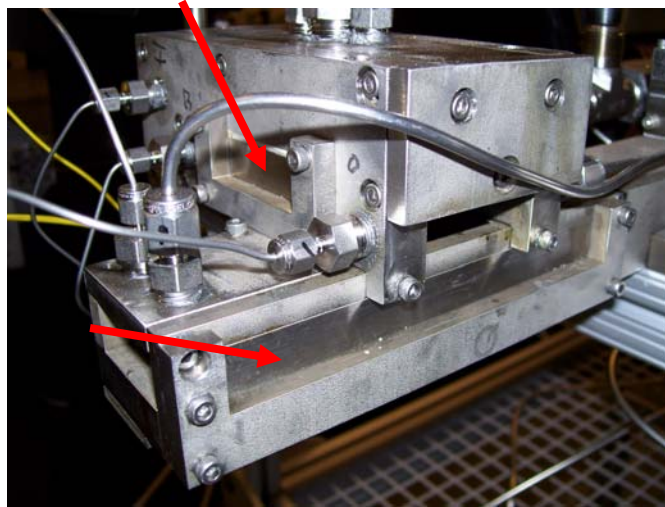
Fig. 4. Side view of the AFIT small-scale model of the UCC

This current model utilizes a flat cavity representing an infinite radius of curvature. After

analysis is complete, measurements will be made on a curved section. Fig. 5 shows a

complete assembly drawing of this section designed using Solid Works.
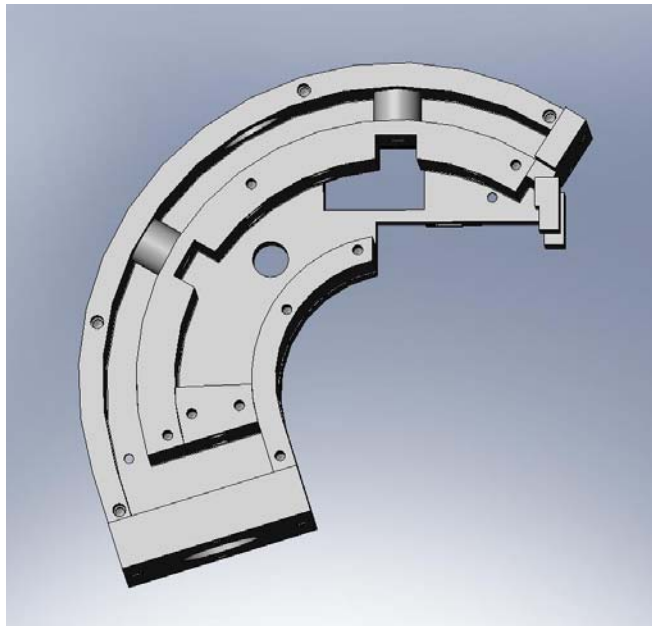
Fig. 5. Curved small-scale model designed with Solid Works

Windows were designed to also allow optical access. It is purposely displayed without one side to show the internal design. This section is currently being built by the AFIT model shop.

1.5   *Objectives*

The AFIT COAL lab is up and running. Several areas of research are in progress. After Koether (Ref. 3) finished in August of 2007 the laser diagnostics system still needed some final calibration. This is being done by the characterization of a laminar flame produced by a Hencken burner, Fig. 6.

Fig. 6. Laminar Flame Produce by a Hencken Burner (photo by Chris Zickafoose)

Once the calibration is done satisfactorily, the lines and optics used on the burner will be reconfigured to be used on the small-scale flat sectional model of the UCC. Final installations and equipment checks will be accomplished prior to lighting a flame in the UCC. Once a flame is successfully lit, data collection will begin. Emissions data will be gathered first. Immediately after, optics will be put in place to take PLIF images for the

characterization of the turbulent flame burning inside the UCC. Emissions data as well as species and temperature measurements from PLIF images will be compared to find the most efficient areas of burning. This data will be used to accomplish the objectives of UCC research and to validate previous CFD results. When enough data is gathered from the flat section, a curved section will be installed and the previously described data gathering process will be repeated providing additional information to support UCC objectives.

There are three main objectives of UCC research and they provide a background for the current research. The first objective is to study the effect of body forces on the performance of the UCC independent of velocity effects. It is necessary to determine if the effect of decreasing turbulent Reynolds number within the main cavity, as cavity mass is increased, is due to body forces or flow shear. Depending on which of these is responsible, main airflow velocity, equivalence ratio, and air jet geometry will be investigated to determine if they have an effect on decreasing the turbulent Reynolds number. The second objective is to determine whether the vortex flow in the main cavity of the UCC can be trapped simulating the Trapped Vortex Combustor (TVC) concept. Initial design of the UCC is based on this concept and will be supported by CFD modeling. Combustor performance such as combustion efficiency, low noise, and operating range will be evaluated through a parametric study of various air injection rates and geometries. The third objective is to investigate the interaction between the main cavity, the vane cavity, and the main flow. It will be determined if the vane cavity can retrieve optimal mass extraction from the main cavity maintaining increased combustion efficiency, low pressure drop and low noise. The effect of vane geometry on flame strain

and combustion reaction will be evaluated based on cavity-vane interactions. These objectives represent the overall goal of research on the UCC so it can be further developed for use in advanced gas turbine engines.

The objective of the current research is to perform a validation of a state-of-the-art laser diagnostic system and to begin the characterization of a small-scale model of a UCC. Validation of the laser system will be accomplished by using laser diagnostics to capture PLIF images of a laminar premixed hydrogen-air flame to determine species concentrations and flame temperatures. Comparisons will be made to existing research to estimate accuracy. Characterization of the UCC will begin with making sure the AFIT COAL lab is fully functional. Once the lab is up and running, a proper starting condition and operating regime will be determined for the small-scale model using JP-8. Pressures and temperatures inside the combustor will be determined for a range of equivalence ratios. This data will be compared to emissions measurements captured using a portable emission analyzer to determine combustor operating parameters such as emissions index and combustion efficiency. Comparisons will be made to selected previous CFD research. Future work will involve emissions data collection using a gas chromatograph, an industry standard gas analyzer made by California Analysis. Also, characterization of cavity-vane interactions inside the model will be made non-intrusively using PLIF.

II.   Theory and Background

2.1   *Standard Gas Turbine Engine Combustor*

A typical gas turbine engine consists of an inlet, compressor, combustor, turbine, and nozzle. These components make up what is known as the gas generator of the engine and is common to the turbojet, turboprop, turbofan, and turboshaft engines. The combustion section makes up a significant portion of the engine as shown in Fig. 7. Its optimal performance is very important to efficient engine operation. The primary goal is to supply high-temperature and high-pressure gas to the engine. The following properties of a gas turbine engine combustor are preferred (Ref. 4): total combustion, pressure losses held to a minimum, combustion stability, even temperature distribution, short length, small cross section, reduced chance of flameout, relight ability, and operation over a broad range of mass flow rates, pressures, and temperatures.
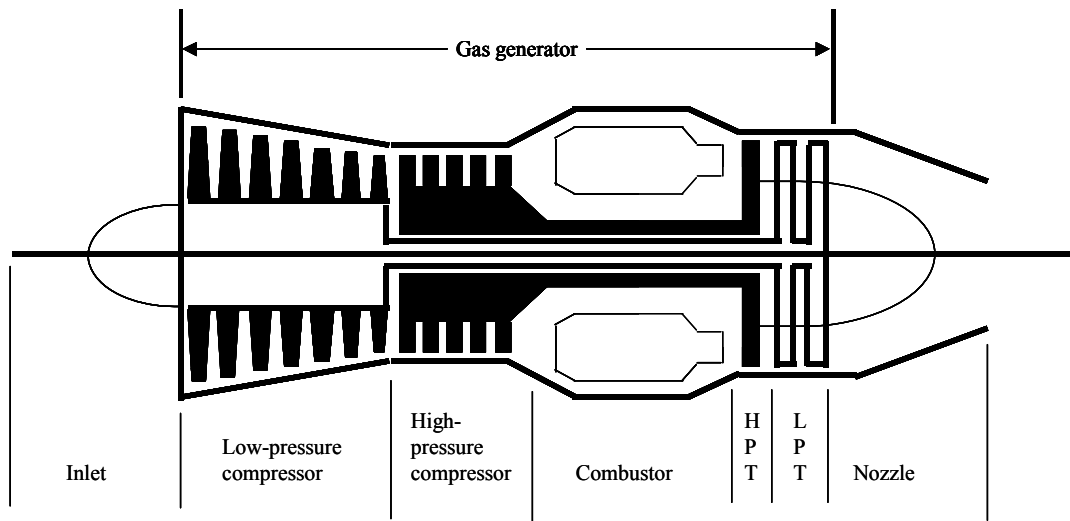
Fig. 7. Schematic of a turbojet with dual axial compressor and turbine (Ref. 4)

A standard combustor contains primary and secondary air mixed with vaporized fuel injected in the axial direction as depicted in Fig. 8.
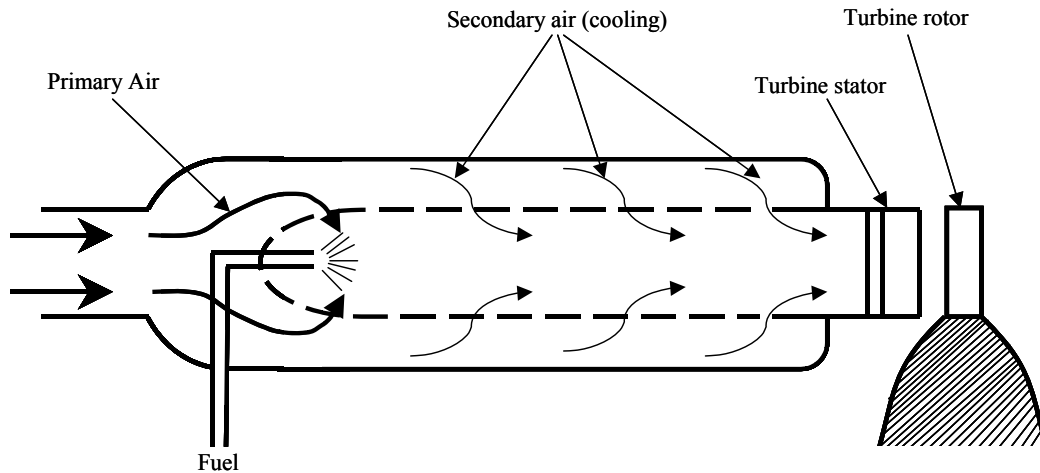
Fig. 8. Flow through standard combustor (Ref. 4)

It is desired for the mixture to burn at a uniform temperature. Combustors designed to operate in this configuration are of the can, annular, or can-annular type and often are referred to as a flame tube. Inside these type chambers, combustion occurs in two zones. In the primary zone high-temperature, high-pressure air enters from the compressor and flows around fuel injectors spraying atomized liquid-droplet fuel and the combustion process begins (Ref. 4). As air recirculates around fuel injectors, flame stability is accomplished. The fuel-air mixture in this primary zone is slightly fuel-rich resulting in higher temperatures and increased emissions such as unburned hydrocarbons, carbon monoxide and nitrous oxides. The addition of air creates a fuel-lean mixture in the secondary or dilution zone and provides cooling so the allowable structural temperature limit of the turbine is not exceeded (Ref. 4). As this process occurs in the axial direction,

all of the fuel does not have time to totally combust. Therefore, losses occur in standard combustors resulting in decreased efficiencies and increased emissions.

The UCC operates like a standard combustor only on a smaller scale. The primary zone is the circumferential cavity, and the secondary zone is made up of each of the radial vane cavities (Ref. 5). This particular configuration provides for increased residence time for fuel to more completely combust resulting in a decreased amount of unburned hydrocarbons lowering the amount of harmful emissions produced.

2.2   Ultra-Compact Combustor Concept

Advancements in gas turbine engine technology are rigorously sought after with the cost of hydrocarbon fuels continuing to rise. One parameter used to measure these advancements is thrust specific fuel consumption (TSFC) calculated using the following formula:

$$TSFC = \frac{\dot{m}_f}{\mathcal{T}} \tag{1}$$

where $\dot{m}_f$ equals mass flow rate of fuel (kg/s) and $\mathcal{T}$ equals thrust (N).

Another parameter is specific thrust (ST). The goal is for ST to increase while TSFC decreases or stays the same. Researchers at the University of California at Irvine (Ref. 6) have proposed the idea of a constant temperature (CT) cycle gas turbine engine to accomplish this goal. They have shown a large increase in ST with equal or reduced TSFC. However, there is a problem with a true CT cycle. It requires burning take place inside the turbine rotor, a technically complex and expensive process. The next best option is an inter-stage turbine burner (ITB) burning fuel between stages in the turbine.

This idea has been shown to increase ST by over 50% with no increase in TSFC in a turbofan engine (Ref. 7). Since a traditional combustor is too big to fit between turbine stages, the idea of an ultra-compact combustor emerged. This advanced engine concept (Ref. 8), shown in Fig. 9, can significantly decrease the size of a standard gas turbine engine and increase thrust without sacrificing combustion efficiency.
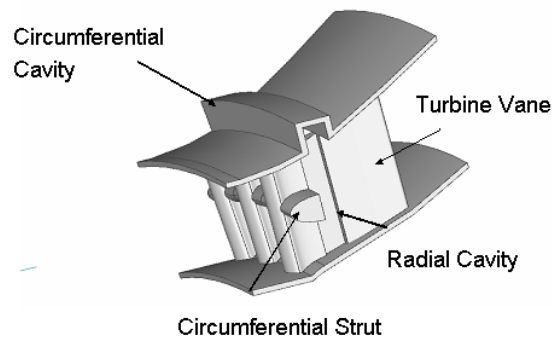
Fig. 9. UCC concept; direction of flow from left to right (Ref. 8).

Originated by the AFRL Propulsion Directorate at Wright-Patterson Air Force Base (WPAFB) in Dayton, OH, the main goal of the UCC is to reduce engine size and weight while increasing combustion efficiency and decreasing fuel consumption. To accomplish this goal, combustion is designed to take place inside a circumferential cavity seen in Fig. 9. Fuel is injected into the cavity through nozzles in recessed ports as air is injected through angled inlets creating a swirling motion. As a result, a centripetal acceleration creates a high g-load resulting in a pressure gradient. Airfoils placed on the center body act as inlet guide vanes (IGV) and create a radial vane cavity (RVC)(Ref. 9). These help draw flow from the cavity into the axial direction and enhance the pressure

gradient see Fig. 10. There are numerous benefits to this process. First, the swirling

motion gives the fuel more time to burn rather than in the axial direction such as in a

standard combustor. The centripetal acceleration promotes rapid mixing and the high g-

loading reduces chemical residence time or time needed for combustion. Also, the

pressure gradient resulting from this high g-loading traps unreacted products in the cavity

to help extract more energy from the fuel. In conclusion, more fuel is burned faster and

flame stability is achieved through trapped vortex combustion all promoting increased

combustion efficiency.
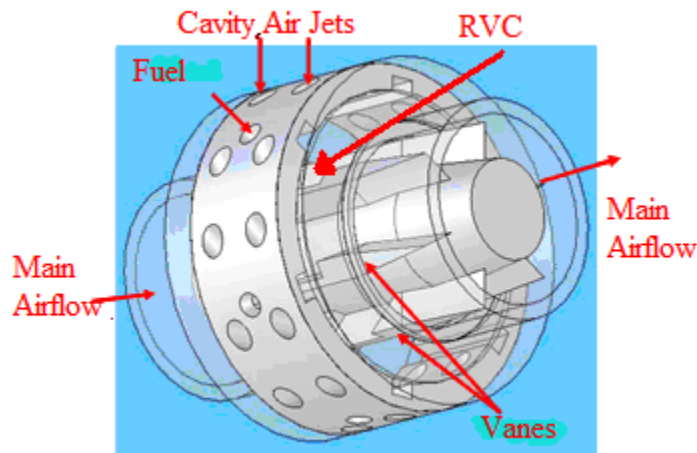
Fig. 10. Components of UCC (Ref. 9)

2.3   Past and Present Research on the UCC

Inter-Stage Turbine Burning

Ideally, gas turbine engines would operate on a constant temperature (CT) cycle

(Ref. 6). However, as mentioned previously, a true CT cycle would require burning in

the turbine rotor, a method too technically complex and expensive. An option is an inter-

stage turbine burner (ITB) acting as a reheat cycle located between high pressure turbine

(HPT) and low pressure turbine (LPT) stages. Sirignano and Liu (Ref. 6) have verified

promising results of increased ST with little gain in TSFC in the use of a reheat cycle

over the conventional non-reheat Brayton cycle.

An ITB consist of a fueled-cavity type flame holder combined with an injection of

air in an angled manner from the outer casing in a turbine vane and it is located between

the HPT and LPT (Ref. 5). The goal is to promote additional thrust without significantly

increasing engine size and weight. As seen in Fig. 11, a circumferential cavity is aligned

with radial vane cavities (RVC) for each turbine vane (Ref. 10).
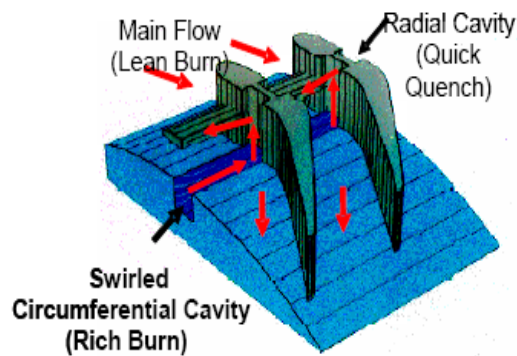
Fig. 11. UCC/ITB Concept for Advance Combustion System (Ref. 10)

Fuel burns rich in the circumferential cavity and has more residence time to burn as it

recirculates, thus more power is extracted from increased burning of the fuel. This

method is superior to conventional combustors burning fuel in the axial direction. Flame

stability is also created, hence the name flame holder, allowing combustion products to

burn more completely thus increasing combustion efficiency and producing less harmful

emissions.

Numerous CFD studies have been done to optimize the design of the ITB.

Analysis with FLUENT® predicts the radial transport of hot combustion products from

the cavity to the main flow is better using an angled as opposed to a straight RVC (Ref.

11). Radial transport describes the migration of hot combustion products from the

circumferential cavity into the main air flow to promote lean burning as seen in Fig. 11.

Also predicted is an optimal temperature profile peaking at the central portion at the exit

of the ITB. A continuous temperature increase, obtained when employing a straight

RVC, could potentially exceed the structural temperature limit of the turbine.

A particular CFD study has been done to evaluate the ITB concept with three

different RVC shapes such as angled, backward, and forward, seen respectively in Fig.

12.
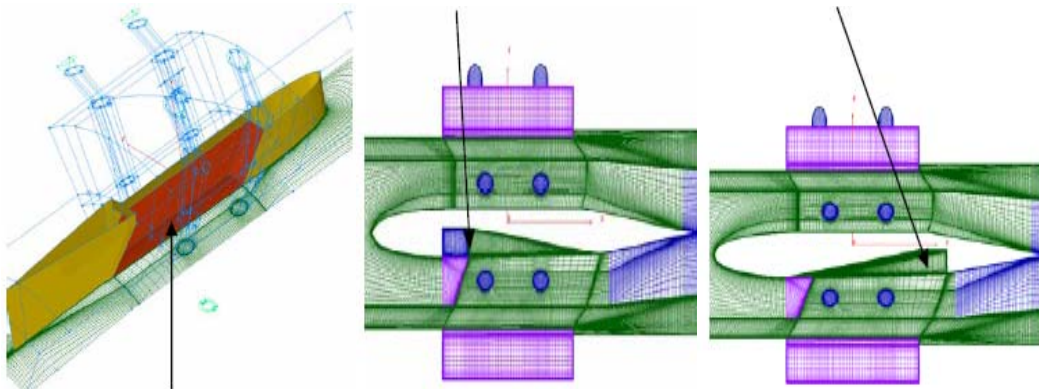
Fig. 12. Various radial vane cavity shapes (Ref. 10)

The angled RVC is predicted to be the best design for optimal radial transport and the

results are comparable to those produced with the forward facing cavity. Radial transport

was predicted to be substantially lower for the backward facing cavity. Overall this study

shows the performance of the ITB is inherently dependent on the shape of the RVC.

Since a conventional combustor is too large to fit between turbine stages, a UCC is needed to implement the ITB concept. The UCC combines trapped vortex and centrifugally loaded combustion with the performance capabilities of the ITB. This could result in more efficient burning of fuel in a shorter axial length therefore reducing engine size and improving cycle efficiency. The small-scale UCC in the AFIT COAL lab has an angled RVC.

Trapped Vortex Combustion

The purpose of trapped vortex combustion (TVC) is to provide flame stability inside the cavity of the UCC. Essentially a vortex is created by injecting fuel and air in a way to promote a swirling motion like a vortex as seen in Fig. 13.
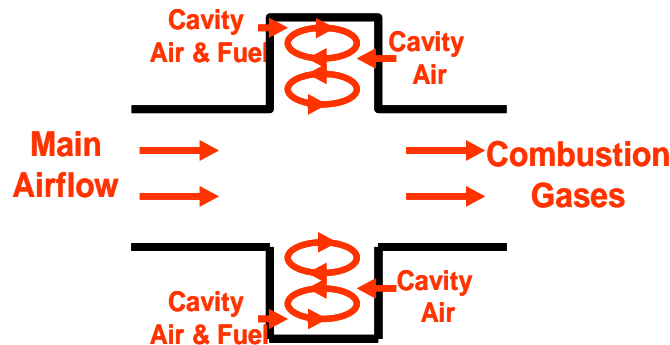
Fig. 13. The Trapped Vortex Combustor (TVC) concept (Ref. 9)

Air also travels along the axial direction. When these two flows meet, the vortex is enhanced creating increased mixing. This produces a stable flame region in the combustion zone for increased burning. As a result, very low overall lean-blow-out equivalence ratios are obtained along with an enhanced combustion efficiency of about

18

99% (Ref. 12).   Compared to traditional swirl stabilized combustors, TVC has been shown to give a wider operating range, improved altitude relight, and decreased nitrous-oxide (NO_X) emissions (Ref. 13). The UCC will utilized the TVC concept to improve mixing of the fuel and prolong flame stabilization. Future work will involve the use of laser diagnostic techniques to determine the location and strength of trapped vortices inside a small-scale UCC using different geometries.

Centrifugally Enhanced Combustion

Greater residence time is achieved as fuel and air travel circumferentially around the engine. Positive effects on combustion occur such as increased mixing and burning. This effect is further enhanced by centrifugal acceleration. Also known as centrifugally loaded combustion, flame speed is increased as it accelerates. As a result, buoyancy forces are created and the flame is transported into less dense flame regions maximizing the burning process. Lewis (Ref. 14) found flame speeds from buoyant forces are greater than laminar or turbulent flame speeds. As the flow is centrifugally loaded, centripetal acceleration is increased causing buoyant flame speeds to become very large. Lewis (Ref. 14) also determined for a g-loading of up to 800, buoyant flame speed increases with increasing acceleration. Buoyant flame speed (S_B) can be found using the following relation:

$$S_B \propto 1.25\sqrt{g} \tag{2}$$

Above a g-loading of 800, speed immediately decreases causing flame extinction.

Yonezawa et al. (Ref. 15) incorporated this idea of high g-loading into a jet-swirled combustor where a ring of inclined combustor air inlets brings air in creating swirling vortexes. They determined increased combustion efficiency could be achieved with this combination.

The UCC will operate with both trapped vortex and centrifugally enhanced combustion to promote flame stability and increased flame speeds. These concepts enable the UCC to remain small without negatively impacting performance.

Computational Fluid Dynamics Research on the UCC

CFD has been proven to be a valuable tool for theoretically determining the physical interactions inside the UCC. Much research has been done by researchers at AFRL and previous students at AFIT. Anderson's thesis (Ref. 2) provides a comprehensive list and description of this previous CFD research. In several studies, combustion and mixing qualities have been predicted and compared with experimental results.

CFD research by Moenter (Ref. 16) was done to design a planar and curved sectional small-scale model of the UCC in 2006. The planar, or infinite, radius of curvature small-scale model (see Fig. 4) is now being operated in the AFIT COAL lab. Predictions from Moenter's code will be compared to experimental data from initial operation of this model. Results will be discussed in Chapter 4.2. The curved sectional model is currently being built by the AFIT Model Shop and will be used in future research.

Moenter's CFD code, a follow on from the codes of Anisko (Ref. 17) and

Greenwood (Ref. 9), predicted certain operational conditions for a planar and curved 60-

degree sector rig. The main goal was to better understand cavity-vane interactions of the

UCC. An emphasis was placed on the axial aerodynamic vane and effect of the RVC in

pulling flow from the cavity. Experimental operating conditions from a full-scale UCC

operated in the AFRL propulsion lab were used to define the boundary conditions for the

CFD code. Several variable operating conditions were used for the comparison of

different configurations. Three conditions varying pressure and mass flow were used

based on a one-sixth, 60-degree model of a full-scale UCC. Two atmospheric conditions,

ATM 1 and ATM 2, were used to analyze a planar and curved sector rig, see Table 1.

Table 1. Operating Conditions for CFD 3-D, 60-degree Models (Ref. 16)

Condition	Main Flow (kg/min)	Cavity Flow (kg/min)	Fuel Flow (kg/min)	P_{amb} (psia)	P_4 (psia)
LMLP	2.197	0.486	0.0534	40.5	39.7
LMMP	2.246	0.468	0.0538	48.6	47.8
HMHP	4.914	0.962	0.0591	57.4	55.4
ATM 1	1.099	0.243	0.0267	14.7	13.9
ATM 2	0.876	0.195	0.0241	14.7	13.9

It should be noted these two conditions were not derived from any experimental data but

were randomly chosen as 50 and 40 percent mass flow rates from the low mass, low

pressure (LMLP) operating condition in Table 1 (Ref. 16). Several predictions of cavity-

vane interactions were obtained for different configurations, but of particular interest for

this research is the predicted operating conditions of the planar sector rig and the

resulting emissions and temperature data from Tables 2 and 3 respectively. In Table 2,

T4 is the temperature of the combustor outlet - turbine inlet comparative to the main vane

exhaust of the UCC. The tables also list 3-D baseline model data for other comparisons.

Data gathered from the initial operation of the small-scale UCC in the AFIT COAL lab is

compared to the planar sector rig data at conditions ATM 1 and ATM 2 and can be found

in Chapter 4.2. The fuel used for this CFD model is JP-8, a kerosene ($C_{12}H_{23}$) based

fuel, and is the same fuel used experimentally in this research.

Table 2. CFD efficiency and emissions data for 2-D planar sector rig (Ref. 16)

Condition	Model	CO (ppm)	NO_x (ppm)	UHC (ppm)	% O_2	% CO_2	η_b (%)	$\Delta P/P$ (%)
ATM 1	3-D Baseline	1498.03	6.85	19.06	15.66	3.28	97.71	7.86
	Planar Sct Rig	2586.95	43.13	1.35	16.23	2.85	99.12	1.8
ATM 2	3-D Baseline	2793.39	9.45	13.12	15.50	3.29	94.49	4.35
	Planar Sct Rig	1665.53	42.43	0.72	16.01	3.05	99.45	1.15

Table 3. Temperature data for 2-D planar sector rig (Ref. 16)

Condition	Model	T4avg	T4max	Pattern Factor
ATM 1	3-D Baseline	1064.43	2330.46	2.38
	Planar Sct Rig	1027.78	2339.22	2.64
ATM 2	3-D Baseline	1073.25	2342.39	2.34
	Planar Sct Rig	1069.11	2347.27	2.38

2.4   Combustor Operating Parameters

Numerous operational parameters are used to measure the performance of

combustors. Those pertinent to this research will be presented in the following section

and will be used to characterize the operation of a small-scale UCC. The author believes

the text, *An Introduction to Combustion*, by Stephen R. Turns is a an excellent reference

on combustion (Ref. 18) and it will be used as a source for the following parameters

unless stated otherwise.

Stoichiometric Air-Fuel Ratio

A stoichiometric amount of oxidizer means there is just enough oxidizer or air mixed with fuel to completely burn all of the fuel. If there is more than a stoichiometric amount the mixture is fuel-rich and if there is less the mixture is fuel-lean. The stoichiometric air-fuel ratio can be determined from balancing a simple chemical equation under the assumption of complete combustion. The chemical equation for a hydrocarbon fuel such as C_xH_y is represented by the following stoichiometric relation:

$$C_xH_y + a(O_2 + 3.76N_2) \rightarrow xCO_2 + (y/2)H_2O + 3.76N_2 \tag{3}$$
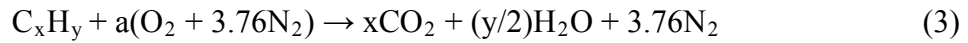
where $a = x + y/4$. Using this formula, the stoichiometric air-fuel ratio can be found by using the following equation:

$$(A/F)_{STOIC} = \frac{4.76a}{1} \frac{MW_{air}}{MW_{fuel}} \tag{4}$$

where MW_{air} and MW_{fuel} are the molecular weights of the air and fuel respectively in units of kg/kmol.

Equivalence Ratio

The equivalence ratio (ϕ) is used to describe the fuel-air mixture and is given by the following equation:

$$\phi = \frac{\left(\dfrac{A}{F}\right)_{STOIC}}{\left(\dfrac{A}{F}\right)_{ACTUAL}} \tag{5}$$

where $\phi > 1$ denotes a fuel-rich mixture and $\phi < 1$ denotes a fuel-lean mixture. When $\phi = 1$ the mixture is stoichiometric.

Emissions Index

The emissions index (EI) is a dimensionless number used to represent the amount of pollutants emitted per quantity of fuel used for a particular engine. The method used to calculate EI listed here is an aerospace recommended practice from the Society of Automotive Engineers (Ref. 19) and is widely accepted. For a hydrocarbon fuel the emission index is determined using the following equation:

$$EI_Z = \left(\frac{\text{moles of Z}}{\text{moles of fuel}} \right) \left(\frac{\text{molecular wt. of Z}}{\text{molecular wt. of fuel}} \right)(1000) \tag{6}$$

where Z is the species of interest.

Combustion Efficiency

Combustion efficiency (η_b) is a measure of how close a combustor comes to operating at an ideal condition, i.e., extracting the most amount of power available from an amount of fuel consumed. It is given in terms of a percentage. Emissions representing incomplete combustion such as unburned hydrocarbons and carbon monoxide are taken into account. The method used to calculate combustion efficiency listed here is also an aerospace recommended practice from the Society of Automotive Engineers (Ref. 19). The equation listed below, taken from Ref. 19, is used for

combustion efficiency calculations based on emissions data from the main vane exhaust of the UCC in this thesis.

$$\eta_b = 100\left[1.00 - 10109\frac{EI_{CO}}{H_C} - \frac{EI_{CxHy}}{1000}\right]$$

(7)

H_C is lower heating value (LHV) of the fuel in units of J/kg. For calculations in Chapter 4.2, a value of 4.4467×10^7 J/kg is used for H_C, a JP-8 equivalent, n-dodecane ($C_{12}H_{26}$) (Ref. 18). This is an approximation for JP-8 fuel and will be further described in Chapter 3.2.

Combustion efficiency is also calculated in terms of mass balance to determine the overall efficiency of the combustor for both cavity and main vane exhaust. The following general equation is used for this calculation:

$$\eta_b = \frac{1}{\dot{m}_f H_c}\left[\left(\dot{m} + \dot{m}_f\right)C_P T_4 - \dot{m}C_P T_3\right]$$

(8)

where H_C is in units of kJ/kg, $\dot{m}$ and $\dot{m}_f$ are mass flow of the air and fuel respectively in units of kg/min, and $C_P T$ is stagnation enthalpy measured in J/mol with 4 and 3 denoting combustor outlet and inlet.

2.5   Laser Structure

Dual Pulsed Nd:YAG Lasers

There are numerous types of lasers in use today in both research and academia. As stated previously, the laser used for testing in the AFIT COAL laboratory is a dual pulsed Nd:YAG laser. It is more technically known as a flash lamp-pumped Q-switched

Nd:YAG laser. Nd:YAG stands for neodymium-doped yttrium aluminum garnet, which

is a well-known solid-state laser media. Q-switching dramatically increases output peak

power and will be discussed in a later section. According to the Quanta-Ray Lab-Series

Pulsed Nd:YAG Laser User's Manual (Ref. 20), the active medium of triply ionized

neodymium is optically pumped by two flash lamps, hence the name dual pulsed. The

output from the flash lamp equals principle absorption bands in the visible part of the

electromagnetic spectrum. Excited electrons drop quickly to the $F_{3/2}$ level (see Fig. 14),

the upper level of the lasing transition, where they remain for about 230 microseconds.

The most probable lasing transition is to the I $_{11/2}$ state, where a photon is emitted at 1064

nm. Because electrons in this state want to naturally relax to the ground state, the

population remains low. Therefore, a population inversion occurs. In other words, an

atom is excited to a higher energy state and will emit a photon at a certain frequency.

This is related to frequency doubling and will be discussed further in a later section. The

Q-switched Nd:YAG laser in the AFIT COAL laboratory produces the power necessary

for the numerous laser diagnostic techniques mentioned previously.
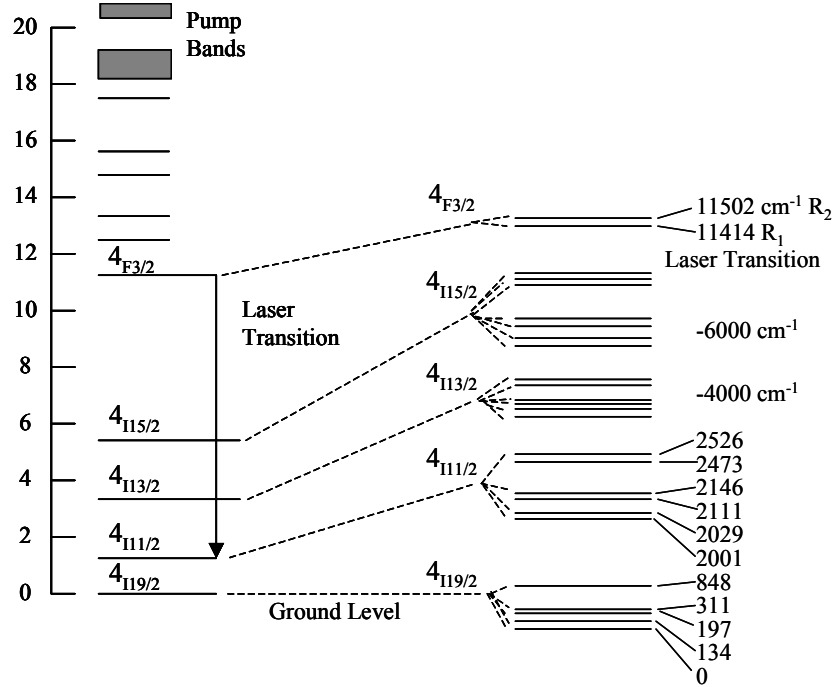
Fig. 14. Energy Level Scheme for the Nd:YAG Laser Source (Ref. 20)

Q-Switching

A Q-switch is an electro-optic device used to make a high cavity loss and prevent oscillation. The letter Q is an acronym for quality of the resonator (Ref. 21). The resonator is switched back and forth from a high quality state to a low quality state. A high quality resonator has low loss. When switched to high quality and one of the laser mirrors is blocked, otherwise known as blocking feedback, a population inversion builds with numerous high-energy photons building up inside of the laser cavity. When switched back to the low quality resonator and feedback is restored, the laser will release a short pulse of high energy light. Output peak power in a laser can be increased dramatically by adding a Q-switch to the resonator as is done to the laser in the AFIT COAL laboratory (Ref. 20).

Frequency Doubling

A clear understanding of the processes by which lasers can provide energy is important when working with them to do research. One such process is called frequency doubling. In a Nd:YAG laser the active medium is triply ionized neodymium, which is optically pumped by a flash lamp. As a result, large populations of excited neodymium ions build up in the YAG rod, much in the same way a capacitor stores electrical energy. Oscillation is prohibited by a Q-switch as described previously while a population inversion builds, and stored energy or a peak power is released and a short pulse of high intensity light is released. Due to relaxation, a photon is emitted at a 1064 nm wavelength. This high peak power permits a wavelength conversion through several non-linear processes. From a photon standpoint, two photons at a fundamental frequency are created in a non-linear crystal known as potassium dideuterium phosphate (KDP). There are many different types and shapes of crystals, but this happens to be the type of crystal inside of the laser in the AFIT COAL lab. The crystal reaches an excited state and naturally relaxes to a ground state and one photon comes out at doubled the frequency. The 1064 nm wavelength decreases to 532 nm, energy increases and frequency doubles, hence the name frequency doubling. This process is also known as second harmonic generation.

2.6   Laser Diagnostic Techniques

Laser diagnostic techniques have become an extremely powerful tool for the non-intrusive analysis and characterization of flames and flame structure in combustion chambers. They are invaluable for temperature measurements where metal probes cannot measure temperature because they will melt. Furthermore, these probes will most

certainly interrupt the very sensitive flow structure of a flame and as a result unavoidable changes in the local temperature distribution will be produced (Ref. 22). These non-intrusive techniques continue to evolve and increased research is being done in this area. The ability to refine and perfect these methods currently exists at the AFIT COAL laboratory. There is the capability to light fire in a small-scale combustion chamber and use laser technology to characterize the flame without disturbing the flow. The purpose of this section will be to summarize current research to provide a background on how laser techniques such as PLIF and PIV can be applied separately and simultaneously to the characterization of laminar and turbulent flames. This section will also describe methods of data reduction from these techniques and how it can be used to support the research objectives of the UCC.

Planar Laser-Induced Fluorescence (PLIF)

PLIF is a two-dimensional (2-D) laser diagnostic technique meaning it makes use of a plane of light from a laser passed through an area of interest. PLIF is based on the emission and absorption of atomic spectra at high energy levels. Photons are "induced" by exciting radicals to higher energy levels through different photo-chemical processes. As the higher energy level is reached by the radical, it wants to naturally revert to a lower energy state. When doing this it emits radiation from this upper energy level giving off light, hence the name fluorescence. Photon emission is important to the combustion process. Numerous radicals such as hydroxyl (OH) are produced during combustion. It has a high fluorescence time. As a laser sheet is directed into a flame, the OH radical will

fluoresce long enough to display the location of combustion. This method can be used to determine species concentrations within a flame.

The usefulness of PLIF makes it one of the most widely used combustion diagnostic techniques (Ref. 23). A major advantage is it can be used to determine temperature measurements. This is a method known either as two-color PLIF, or PLIF thermometry, and will be described in greater detail in the following section. Another key advantage of PLIF is it is a non-intrusive technique. This means flame qualities can go undisturbed while taking measurements since probing the flame can be avoided as described above. This prevents possibly melting thermocouples and other equipment while trying to measure extremely high temperatures. There are disadvantages to PLIF however, and one of them is known as quenching.

Quenching

Quenching is described as dissociation, energy transfer to another molecule or internal energy state, or a general chemical reaction (Ref. 24). When this happens, a fluorescent signal is not released. This can decrease the quantity of fluorescence and skew the interpretation of the data. If all quenching processes and species densities are known, some very good analytical corrections can be made to adjust the PLIF signal. A very good quenching correction method is described in Chapter 3.4. It is an analytical model published by Tamura et. al (Ref. 25) and will be used for analysis of the PLIF results in Chapter 4.1.

OH PLIF Thermometry

The ability to measure temperature in flames is extremely important in the design and characterization of combustion processes. Non-intrusive measurements of 2-D temperature fields (planar thermometry) provides valuable information in determining regions of burned and unburned gases (Ref. 26). The OH radical is used because of its natural abundance in high temperature combustion. Using two different transitions in bands of the OH (A-X) electronic transition system, a fluorescence emission is detected as it originates from laser-pumped upper energy levels. Several OH transition pairs of the (A-X) electronic system exist. They are chosen according to their sensitivity to temperature and their particular wavelength. Generally, a spectral line at a certain wavelength is chosen if it produces a strong OH fluorescence signal and it must be insensitive to changes in temperature. An additional temperature sensitive line is chosen. The signal ratio of these lines obtained from a spectral simulation database known as LIFBASE (Ref. 27) is used to make temperature measurements. LIFBASE is further described in Chapter 3.2.

Temperature can also be determined using spectra analysis by taking a signal from LIFBASE at a particular wavelength and performing a scan around that wavelength. A full-width half-maximum (FWHM) value from a certain measured OH intensity scan is compared to various FWHM values to obtain a temperature. A summary of these two methods and the use of LIFBASE are provided in Chapters 3.4 and 3.2. Additional information on the ratio of intensity method can be found in Koether's thesis (Ref. 3).

Spectral lines from the rotational transitions of the OH (A-X) (1-0) band were chosen for temperature measurements in this research. In addition, lines from this

particular band were chosen because they were used by different researchers doing OH

PLIF thermometry. Seitzman and Hanson et al. (Ref. 26) examined three rotational line

pairs, $Q_2(11)$ - $R_2(5)$, $Q_2(11)$ - $P_1(7)$, and $Q_2(11)$ - $R_2(8)$. They measured a temperature

range from 1000 K to 3000 K with as low as 7% error when using the $Q_2(11)$ - $P_1(7)$

transition pair. The wavelengths for the lines were as follows: $Q_2(11)$ – 285.16 nm, $P_1(7)$

– 285.09 nm, and $R_2(8)$ – 281.72 nm. Giezendanner-Thoben et al. (Ref. 28) used one

vibrational line pair, $P_1(2)$ - $R_2(13)$, to measure a temperature range of 1500 K to 2200 K

with an error of 4 to 7% depending on the location within the flame and the temperature

level. The wavelengths for these lines were as follows: $P_1(2)$ – 282.66 nm and $R_2(13)$ –

282.64 nm. Welle et al. (Ref. 29) used one line pair, $Q_1(5)$ - $Q_1(14)$, with wavelengths of

282.75 nm and 286.46 nm respectively. Their experimental set-up used a laser system

calibrated with a CH_4-air flame from a Hencken burner. Also, lines $Q_1(9)$, $Q_2(8)$, and

$P_1(5)$ with respective wavelengths of 284.005 nm, 284.008 nm, and 284.028 nm, were

used for additional comparisons.

Research by Hancock et al. (Ref. 30) consisted of taking temperature

measurements of a hydrogen-air flame also produced with a Hencken burner.

Temperature measurements were made using both nitrogen Coherent anti-Stokes Raman

scattering (CARS) spectroscopy and hydrogen CARS. CARS is another technique used

to take non-intrusive temperature measurements with the OH radical. An explanation of

CARS along with additional references can be found in Anderson's thesis (Ref. 2).

Argon was used as a co-flow around the outside of the flame to keep it as laminar as

possible. Measurements of the flame were taken approximately 3.8 cm above the burner

to reduce heat loss to the burner surface. To take accurate measurements at this height,

fuel flow rates of 13 - 60 standard liters per minute (slpm) were used, and the air flow rate was held constant at 60.6 slpm. This produced flame equivalence ratios of 0.51 - 2.36. Accuracies within 2 to 3% were obtained for temperatures using nitrogen and hydrogen CARS respectively.

A hydrogen-air flame produced with a Hencken burner was used to take PLIF measurements in the AFIT COAL lab. The results from this research include temperature as a function of height above the surface of the burner and equivalence ratio. Comparisons are made to the Hancock data in Chapter 4.1. The goal is to create a calibration method using the Hencken burner for flame thermometry techniques.

Particle Imaging Velocimetry (PIV)

PIV is a 2-D non-intrusive laser diagnostic technique producing an instantaneous velocity vector map of a flow field of interest. This technique may be applied to the UCC after PLIF is completed. Fluids are seeded with tracer particles either reflecting light or resonating as they pass through a laser sheet in a specified area. The size of the particle is important since it must be small enough to follow the flow but large enough to reflect light. A pulsed laser makes a sheet or plane of light big enough to capture enough particles but small enough to reduce the number of particles with out-of-plane velocity components. A CCD camera synchronized with pulses of light from this laser captures images of the particles. There is some very good statistically based data reduction software that will take these images frame by frame and produce a velocity vector field, see Fig. 15.
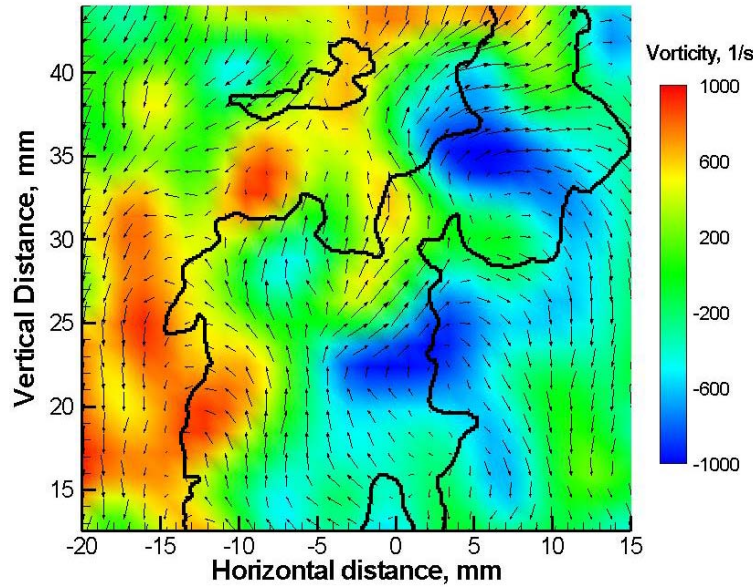
Fig. 15. Instantaneous velocity vector field (Ref. 33, used with permission)

Essentially, velocity vectors of the particles are determined by measuring the distances traveled by the particles in a known time between successive exposures of the camera. Fig. 15 is an example of the kind of imaging data produced using PIV. Similar images of a particular flow were produced from research done by Kahler & Kompenhans (Ref. 31). Using multiple plane stereo particle image velocimetry, all three-velocity components can be determined simultaneously or separately to produce detailed flow patterns in a specified region of interest.

Research has been done with multiple-camera PIV characterizing turbulent premixed combustion in a small-scale geometry by measuring flame position and flow field velocity to assist in the comprehension of flame-vortex interaction (Ref. 32). The effect of flame and obstacle generated vortex interactions within a semi-confined

combustion chamber were studied. This excellent research method could be used to

determine the quality and quantity of trapped vortex flow inside the UCC.

The experimental configuration used by Jarvis and Hargrave consisted of a small-

scale combustion chamber with a 150 mm x 150 mm internal square cross section 500

mm in height. A key point of interest from this research is the combustion chamber made

from transparent polycarbonate to allow for optimal viewing. If the optically clear quartz

windows installed in the AFIT small-scale UCC continually crack due to increased

heating and pressure, the use of transparent polycarbonate could be an alternative

material for use. Solid obstacles were placed inside the chamber for vortex generation.

A 99.5% pure methane-air mixture with a stoichiometric equivalence ratio of one was

used as the burning gas. For complete characterization of the combustion process, a pair

of 2-D laser diagnostic techniques were employed. First, a multiple-camera PIV

technique was used to determine how much interaction occurred between the flames and

vortices occurring in the area of concentration. Two vertical laser sheets 70 mm high and

1 mm wide produced by New Wave Solo III Nd:YAG lasers were positioned through this

area. A two frame CCD TSI PIV Cam 10-30 camera with a resolution of 1000 x 1016

pixels was used for capturing images of flame-vortex interaction similar to Fig. 15. For

their second technique, a high-speed laser sheet 1 mm thick was produced by an Oxford

Lasers copper vapor laser model LS 20-50. It illuminated regions of burnt and unburnt

gas mixture to provide a representation of the interaction process. These images were

captured by a Kodak Ektapro 4540 high-speed digital CCD camera. It was operated with

a resolution of 256 x 128 pixels and used a 55 mm Micro Nikkor lens. This camera and

the Oxford laser were synchronized to produce images at 9000 frames per second. For

both laser techniques, the flow was seeded with 1 - 2 micron sized droplets of olive oil using a TSI 6 jet atomizer. This type of seeding material burns up in the flame revealing areas of burnt and unburnt mixture showing the boundary of the flame front. Images were analyzed using TSI Insight 3 software with a two-frame FFT cross-correlation routine and a Gaussian peak search algorithm. A window of 32 x 32 pixels and a 50% overlap was utilized. This particular configuration used by Jarvis and Hargrave is only one of many. There are numerous ways to conduct a PIV experiment depending on available equipment and budget. A similar PIV experiment may be used to characterize interactions in regions of interest inside the UCC.

One particular region of interest inside the UCC is the cavity-vane area. The location of this area can be seen in Fig. 4. Using PIV, results of cavity-vane interactions such as flame propagation speed and direction as well as trapped vortex flow can be determined. Details from reduced PIV images, such as enlarged vortices depict greater residence times near the flame possibly ensuring a similar wrinkling effect (Ref. 33). Wrinkling in flames increases the frontal area and maximizes the burning rate. This information can be used to ensure burning is occurring in proper locations. PIV can also be performed simultaneously with PLIF, a method that will be used to characterize the numerous unknown interactions inside the UCC and will be described next.

Simultaneous use of PLIF and PIV

Using PLIF and PIV simultaneously to study flame structure and flame-vortex interaction in turbulent premixed flames is an excellent technique. The data produced from these techniques can be analyzed separately and compared with emissions data to

locate optimal areas of burning inside of the UCC for increased combustion efficiency.

Excellent research is being done with simultaneous PLIF and PIV. As stated previously, laser diagnostic techniques are evolving with maturing technology. In one particular research, three-dimensional (3-D) flame propagation speeds are found small enough to allow simultaneous PLIF and PIV techniques to be used to obtain flame orientation information (Ref. 33). In their research, a simultaneous PLIF and PIV technique was used to characterize flames by detecting flame merging and the creation of pockets of both products and reactants. A strong interaction between vortex structures and the flame front was also revealed. This particular research creates an excellent foundation to support two UCC objectives to determine areas of trapped vortex flow and cavity-vane interactions with the main flow.

In order to understand flame behavior inside the UCC, it is important to be able to measure flame temperatures, species concentrations, and flame speed. This information can be compared with emissions data to determine the best locations for efficient burning inside the UCC. PLIF is used to measure flame temperatures and species concentrations allowing the characterization and location of flame structure, as described previously. Besides OH radicals, acetone can also be used for PLIF imaging as was done by Filatyev et al (Ref. 33). It is consumed or in other words reacts upon reaching the flame front, therefore, making it a good marker for flame zone visualization due to its high concentration after combustion takes place. Methylidyne (CH) radicals can also be used for PLIF imaging because the emitted wavelength ranges are very narrow and make a good flame marker. Simultaneous use of CH and OH for PLIF imaging can also be useful as was done by Tanahashi et al in 2005 (Ref. 34), and Driscoll et al in 2003 (Ref.

35). Images with CH and OH reveal isolated burned gas pockets in unburned areas and isolated unburned mixtures in the burned area. Using CH PLIF along with PIV, Driscoll et al (Ref. 35) reports properties such as degree of flamelet extinction, local stretch rates, reaction layer thickness, and wrinkling parameter can all be quantified. Tanahasi et al (Ref. 34) reports at high Reynolds numbers burned gases do not consistently have high-speed velocities and PLIF imaging shows increased wrinkles of the flame at its front. This Reynolds number dependence on flame front geometry is a very valuable piece of information that can be applied to the study of the UCC. Increased wrinkles in the flame signify increased mixing which could mean better burning and fewer emissions.

Numerous properties of combustion can be discovered using combinations of laser diagnostic techniques. Fig. 16 shows a schematic for and experiment of a simultaneous PIV and PLIF technique used by Filatyev et al (Ref. 33).
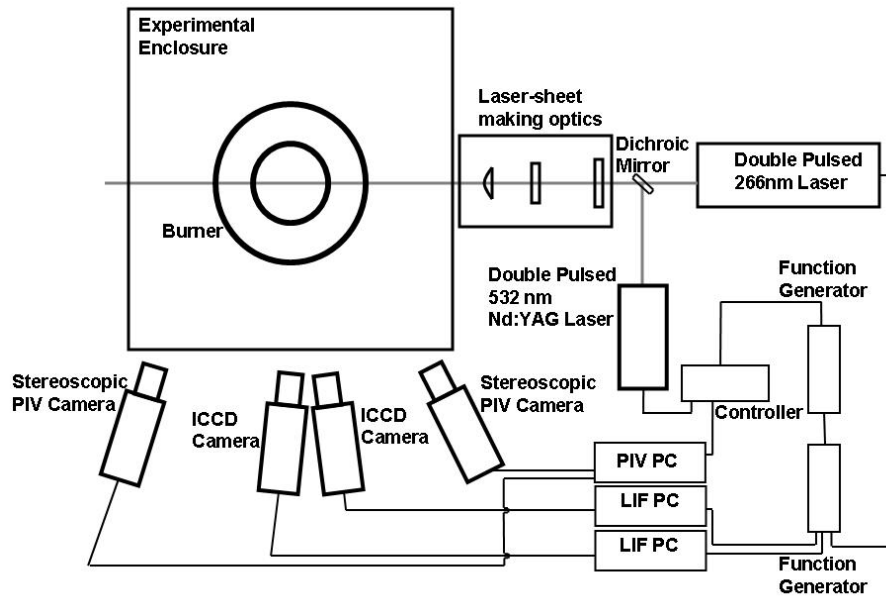
Fig. 16. Schematic of simultaneous double-pulsed acetone and stereoscopic PIV (Ref. 33, used with permission)

A Spectra-Physics Quanta-Ray PIV 400-10 Nd:YAG double-pulsed 266 nm laser was used for PLIF. This laser is similar to the one used in the AFIT COAL laboratory. A unique aspect of this laser allows its use in the double-pulsed PIV mode and the fourth harmonic output of the laser (266 nm, 50 mJ/pulse) for double-pulsed acetone PLIF measurements. The fluorescence was captured using two Roper ICCD cameras and Tamron AF 28-300mmF3.5/6.3 lenses. Filters were not needed because the glass on the combustion chamber totally blocked the scattered light at 266 nm. The other laser used exclusively for PIV was a Blue Sky PIV laser (532 nm, 150 mJ/pulse). The image was captured using two CCD cameras, a synchronizer, and frame grabber software. Nikon AF 105 mm F/2.8 lenses were used to collect laser light for the PIV signal. This is, of course, only a general summary of what can be used for simultaneous PIV and PLIF laser diagnostics and serves as an example of what can used in the combustion lab.

For data analysis, to match PIV images with PLIF results, a calibration technique was applied (Ref. 33). The same target was imaged on all cameras for both PIV and PLIF. To account for the offset of the PLIF cameras to the laser sheet, a fourth-order polynomial fit through the points was applied to minimize image distortion. To measure the absolute value of flame propagation speed, the relative distances of flame positions on two PLIF images were used, see Fig. 17. The flame position of the first frame (left image) propagated according to the local velocity field, measured using PIV and time delay between PLIF images. Then, the distance between flame position in the second frame (right image) and the flame position in the propagated PLIF frame (image to the right of image B) was calculated and divided by the time delay between pulses. This equals the absolute value of propagation speed. This data reduction method clearly

shows how PIV and PLIF combined can detect flame merging and the creation of pockets

of both products and reactants. This is a key analysis method and may be applied to

calculating flame propagation speeds inside the UCC.
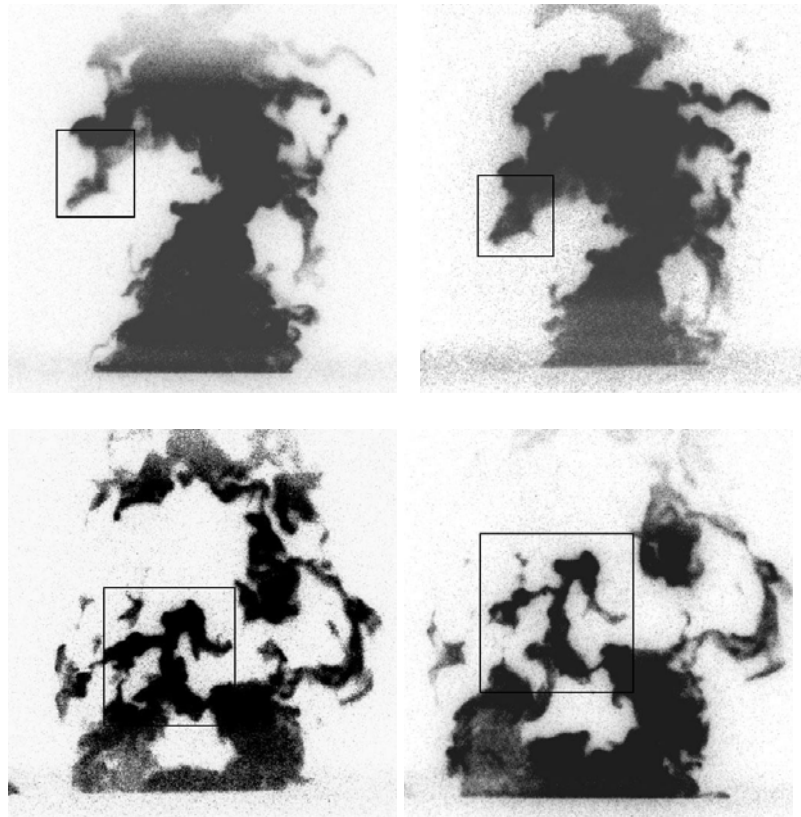
Fig. 17. Acetone PLIF images passing through the burner axis (top) and 7.5 mm away from the
burner axis (bottom). Time delay between left and right image was 400 micro-sec (Ref. 33, used
with permission).

III. Methodology

3.1   Methods

To meet the objective the following steps were taken:

1. *Final calibration of the laser system.* In order to obtain accurate data from PLIF images, the laser was calibrated using a laminar flame produced by a Hencken burner. Species concentrations and temperature measurements are compared to theoretical data to determine the accuracy of measurement.

2. *Configure the lab for UCC operations.* Equipment supporting the Hencken burner will be transferred to the UCC. Lines for air, nitrogen, and ethylene will be connected. Optics for the laser system will be moved to ensure they are not damaged during the initial lighting of the combustor. Also, the ICCD camera will be repositioned to protect it from hot exhaust. Once controlled operation for the UCC is achieved, the goal is to reposition the optics to send a planar laser beam through the cavity and vane to take PLIF images of the interactions.

3. *Perform equipment checks and calibrations.* Support equipment such as fuel pumps, heat exchangers, and gas analyzers will be turned on and controlled to ensure their safe, accurate, and reliable operation. All computers and equipment will be set-up to be controlled from one central computer using a network switch and Lab-View software.

4. *Update operational procedures.* The lab is continuously evolving, and it is imperative to have current step-by-step procedures for continuity. Procedures for operating the Hencken burner are updated. A method for analyzing images with image software will be written. A procedure for a motion controller used for

placement of optics will be written. Finally, procedures for operating the UCC are mainly rewritten to include all the nuances of operation since this was the first time it was actually operated.

5. *Characterize small-scale model of the UCC.* A good starting condition and operating regime will be established for the UCC. Temperature and pressure data will be captured using Lab-View equipment software along with several pressure transducers and thermocouples. Emissions data will be collected from a portable emissions analyzer made by Testo.

3.2   Data Collection

Gathering data in the COAL lab is an easy process due in part to the fact this is a state-of-the-art facility. Numerous equipment upgrades, and arrangements have been made so the data collection process is as efficient as possible. The lab is currently set up in three main stations, each with a computer, keyboard, and monitor. The computer control station can be seen in Fig. 18 and its design is described by Anderson (Ref 2).

Fig. 18. Computer Control Station

There is also a laser control station and a camera control station seen in Fig. 19 and Fig.

20 respectively. Both the design and capability of these systems are described in detail

by Koether (Ref 3). An upgrade to the lab in the near future will be the installment of a

KVM switch so the camera and laser computers can all be operated from one central

location at the computer control station. This will streamline the data gathering process

and also promote increased safety in the lab since everything will be controlled from one

central location away from laser beams and exhaust gases.

Fig. 19. Camera control station

Fig. 20. Laser Control Station

Several software packages are used in the lab to collect data. Software by Lab-View is used for operational control of most of the lab. Win-View 32 software is used to collect and analyze PLIF images. ESP Utility Version 4.2 software by Newport is used to control translational movement of the camera and optics.

Lab-View

A virtual instrument (VI), a component of Lab-View, is installed on the computer at the control station. The front panel can be seen in Fig. 21.
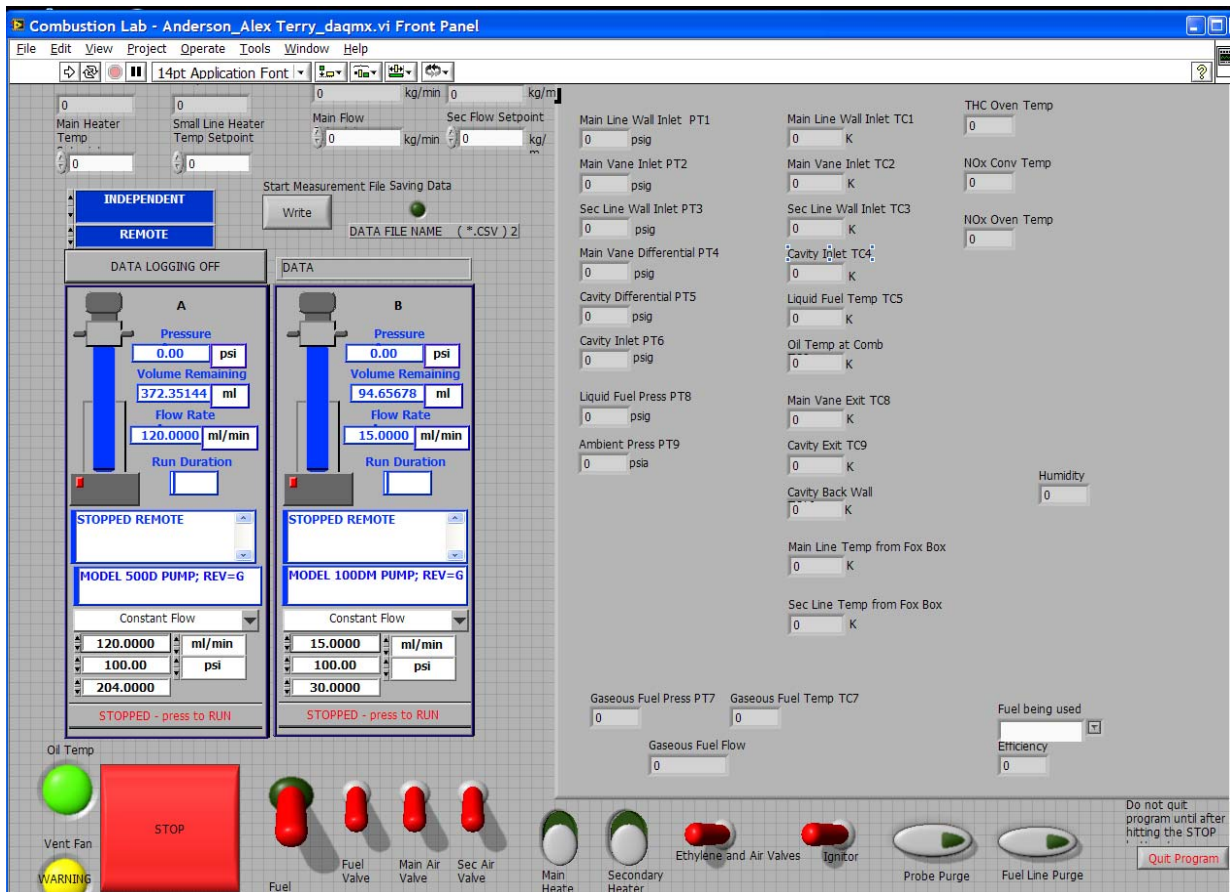
Fig. 21. VI front panel for lab component control

It remotely controls many functions in the lab such as solenoids, fuel pump, igniter, valves and was designed by Anderson (Ref. 2). It can also be used to record pressures, temperatures, and flow rates of different components throughout the lab. The set up for this is also described in Anderson's thesis. The VI is currently configured to output a data file for 36 parameters. Appendix E shows a list of the output parameters and their corresponding numbered location in the file. These output files were used to collect operational data on the UCC and the results are located in Chapter 4.2.

PLIF Image Collection

Image collection is accomplished using an ICCD camera made by Princeton Instruments, see Fig. 3. The description of the camera and how to operate it is located in Koether's thesis (Ref. 3). Image analysis is done using Win-View 32 software, see Fig. 22. This software was used to determine intensities of various PLIF images taken of a laminar premixed flame.
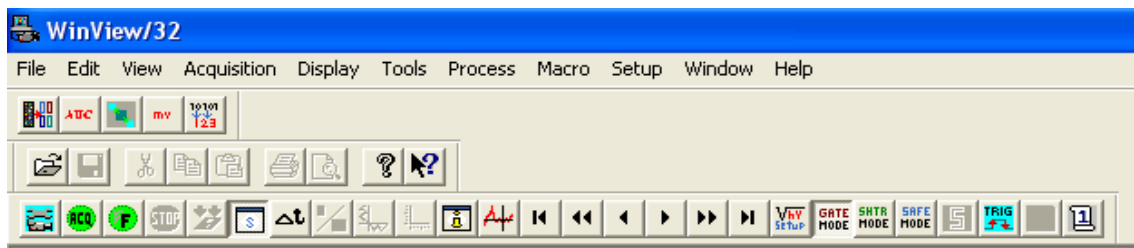
Fig. 22. Win-View 32 Image Software

This data can be used to determine flame species concentration as well as temperature and the method is described in later sections. See Appendix C for how to use Win-View 32 to analyze images. Fig. 23 is a raw PLIF image taken of a lifted hydrogen-air flame.

The white in the image is present due to the fluorescence of OH radicals. A Hencken burner is being used to produce the flame. This calibration method will provide an image intensity baseline of a laminar flame before PLIF images are taken of an unknown structure of flames inside the UCC.
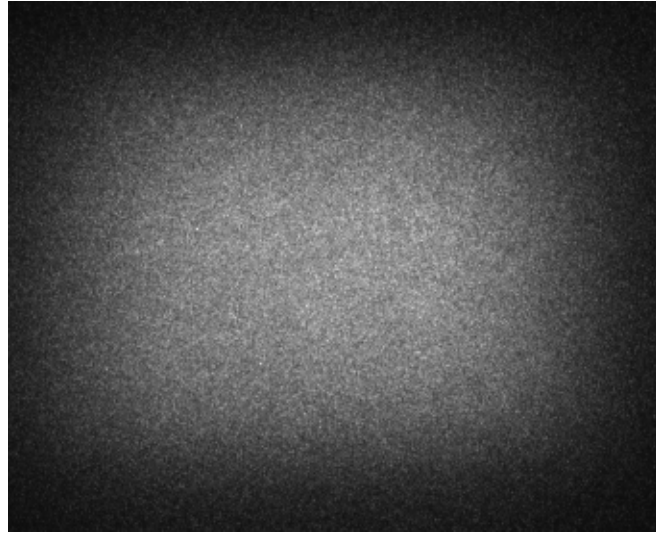
Fig. 23. Raw PLIF image of fluorescing OH radicals

Automatic Control of Optics

Motion controller software, ESP Utility Version 4.2, was used to move the laser sheet through the flame while keeping the camera focused. Made by Newport, the Universal Motion Controller/Driver, model ESP300 (see Fig. 24) is an integrated

Fig. 24. Newport Universal Motion Controller

driver and controller in one chassis. It can drive and control up to three axes of motion. For analysis of the flame produced by the Hencken burner, axis one and two were configured to control the camera and laser optic respectively. The laser optic (see Fig. 25) would move the laser sheet through the flame, and the motion controller on the camera would keep it focused as the distance changed between the camera and the laser sheet. See Appendix D for how to operate the motion controller.
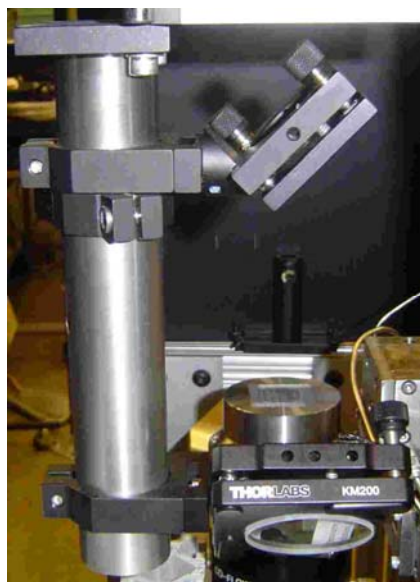
Fig. 25. Auto-positioned optics

Mass Flow Controller Calibration

Calibrating the mass controllers properly is the key to obtaining accurate results from PLIF measurements. It allows one to be sure they have the correct air to fuel mixture for the flame of study. MKS ALTA digital mass flow controllers were used to accurately control the flow of hydrogen, air, and nitrogen co-flow to the Hencken burner.

Fig. 26 shows the mass flow controllers. Located from left to right is a five slpm controller labeled "FUEL". It was not used for any measurements. Next is a 10 slpm controller also labeled "FUEL" used for hydrogen and will be used later with ethylene for igniting the combustor. There is also a 30 slpm controller labeled "ZERO AIR" and a 50 slpm controller labeled "CO-FLOW" used for a nitrogen coflow around the flame and a nitrogen purge for the fuel lines in the UCC.
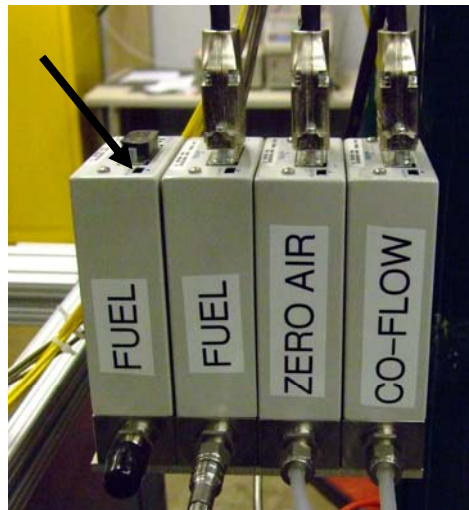
Fig. 26. MKS ALTA digital mass flow controllers

To calibrate the controllers correctly, they first had to be zeroed out. All flow was stopped going in and coming out of the controllers. Once an absolute no-flow condition was obtained, a zero reset button on top of each controller was pressed, see location depicted by the arrow in Fig. 26. This was necessary to ensure the mechanism electronically controlling the flow inside the controller was properly seated in the no-flow position. To accurately control the flow, an MKS 247D four channel power supply / readout seen in Fig. 27 was used to operate the mass flow controllers. Channels one, two,

and three control the hydrogen, zero air, and co-flow respectively. It also had to be adjusted for a no-flow condition. With everything still in a no flow condition, the readout needs to be adjusted to read all zeros. For example, to adjust channel two, turn the display channel dial to 2 as seen in Fig. 27. Using a small screwdriver, turn the screw located under Z on the panel until the display reads all zeros.

Fig. 27. MKS 247D four channel power supply/readout

Now both the panel and the controller are calibrated for a no flow condition. However, it is important to note when pressure is applied to the controllers, they will allow a small amount of flow through resulting in a small numerical indication on the panel. It is common for this to be as high as 0.7 to 0.9 in some cases.

Flow through the controllers must be calibrated next. The MKS 247D panel reads in either slpm or percentages. It gives a more accurate reading when operated in terms of percentages and is currently set up this way. For example, 51.5 on the panel is 51.5%. The mass flow controllers must be calibrated to determine how flow rate correlates with flow percentage. This was done using a BIOS Definer 220-H flow meter, see Fig. 28.

Fig. 28. BIOS International Corporation Definer 220-H Flow Meter

To do the calibration, disconnect the desired gas line from the output side of the

controller and hook it up into the "pressure" connection of the flow meter. Set the

readout on the MKS 247D to a certain percentage and log the corresponding flow rate

from the BIOS flow meter. The meter can calculate an average flow rate after so many

readings. It was set up to take an average after every ten readings. Before recording

averages, it is important to adjust the reading on the digital control panel. For example, if

using a 10 slpm mass flow controller, set the digital control panel to read 50% and check

the reading on the flow controller. It should read five slpm of flow. If it does not, adjust

the digital control panel reading until it does. If there is a reading of 51.4% for example,

look on the back of the control panel and adjust the dial for that particular channel until a

reading of exactly 50.0% is obtained. The digital control panel is now ready to be used

for readings.

Hydrogen and ethylene gases were used for calibration through the mass flow

controllers. Hydrogen was used for PLIF measurements of the Hencken burner and is no

longer hooked up. Ethylene and air are now in use to ignite the UCC. Two averages

were recorded for every 10% of flow rate, and the average of those two was taken. As an

example of recorded data for the calibration of hydrogen flow see Table 4. Interpolations can now be made of every percentage based on the desired mass flow rate using a curve fit. Fig. 29 shows curve fits of data points from hydrogen, air, and ethylene. This is a necessary procedure in order to operate at different equivalence ratios. The calculation of the equivalence ratio for different fuels used is presented in the next section.

Table 4. Hydrogen percentage and flow rate data

Fuel (10SLPM)			
Percentage	Avg 1 (SLPM)	Avg 2 (SLPM)	Avg (SLPM)
10.00	1.0090	1.0090	1.0090
20.00	2.0350	2.0340	2.0345
30.00	3.0320	3.0320	3.0320
40.00	4.0410	4.0210	4.0310
50.00	5.0480	5.0480	5.0480
60.00	6.0510	6.0530	6.0520
70.00	7.0580	7.0560	7.0570
80.00	8.0560	8.0570	8.0565
90.00	9.0390	9.0410	9.0400
100.00	10.0230	10.0430	10.0330
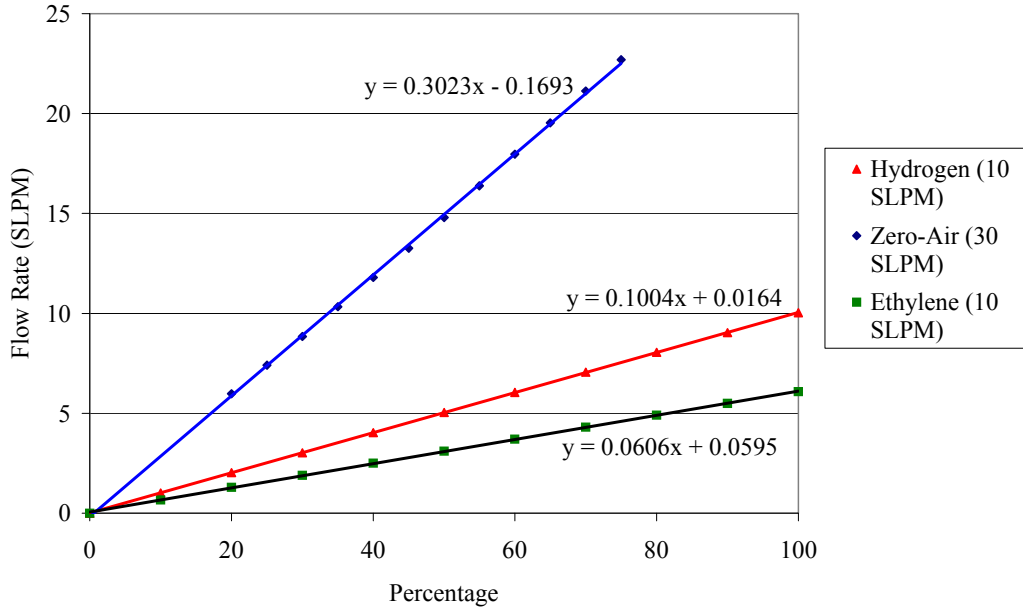
Fig. 29. Mass flow meter calibration data

Equivalence Ratio Calculations

Equivalence ratios (ϕ) were calculated for three different types of fuel and air

mixtures. For the Hencken burner operation, a ϕ for Hydrogen-air was calculated. To

ignite and operate the UCC, a ϕ was calculated for Ethylene-air and JP-8 respectively.

The equivalence ratio was varied for many of the experiments using PLIF as well as

lighting and operating the UCC.

The equation for perfect combustion of a hydrogen-air flame representing an
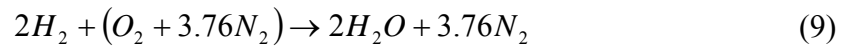
equivalence ratio of one is given by the following:

$$2H_2 + (O_2 + 3.76N_2) \rightarrow 2H_2O + 3.76N_2 \tag{9}$$

Using this equation, the stoichiometric air to fuel ratio can be found using equation (4) as

follows:

$$(A/F)_{STOIC} = \frac{4.76}{2} = 2.38$$

If air is held constant at 15.45 slpm, equation (5) on page 25 can be used to solve for

different amounts of fuel flow while varying the equivalence ratio as follows:

$$\phi = \frac{2.38}{\left(\dfrac{15.45}{F}\right)}$$

Data calculated in this way can be found in Table 5.

Table 5. Hydrogen-air flame equivalence ratio data

ϕ	Fuel (SLPM)
0.3	1.95
0.4	2.60
0.5	3.25
0.6	3.90
0.7	4.54
0.8	5.19
0.9	5.84
1	6.49
1.1	7.14
1.2	7.79
1.3	8.44
1.4	9.09

The equation for perfect combustion of a ethylene-air flame representing an
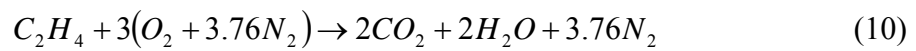
equivalence ratio of one is given by the following:

$$C_2H_4 + 3(O_2 + 3.76N_2) \rightarrow 2CO_2 + 2H_2O + 3.76N_2 \tag{10}$$

Using this equation, the stoichiometric air to fuel ratio can be found using equation (4) as

follows:

$$(A/F)_{STOIC} = \frac{14.28}{1}$$

If air is held constant at 25 slpm, equation (5) on page 25 can be used to solve for

different amounts of fuel flow while varying the equivalence ratio as follows:

$$\phi = \frac{14.28}{\left(\dfrac{25}{F}\right)}$$

Data calculated in this way can be found in Table 6.

Table 6. Ethylene-air flame equivalence ratio data

ϕ	Fuel (SLPM)
0.5	0.88
0.6	1.05
0.7	1.23
0.8	1.40
0.9	1.58
1	1.75
1.1	1.93
1.2	2.10
1.3	2.28
1.4	2.45
1.5	2.63
1.6	2.80
1.7	2.98
1.8	3.15
1.9	3.33
2	3.50

Calculating the equivalence ratio for JP-8 and air is done the same way. The equation for

perfect combustion of JP-8, a kerosene ($C_{12}H_{23}$) based fuel, and air flame representing an
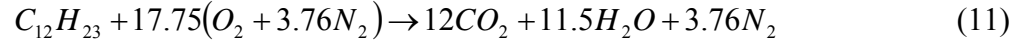
equivalence ratio of one is given by the following:

$$C_{12}H_{23} + 17.75(O_2 + 3.76N_2) \rightarrow 12CO_2 + 11.5H_2O + 3.76N_2 \qquad (11)$$

Using this equation, the stoichiometric air to fuel ratio can be found using equation (4) as follows:

$$(A/F)_{STOIC} = \frac{4.76(17.75)}{1}\left(\frac{28.89}{167}\right) = 14.616$$

As an example, fuel is held constant at 35.7 ml/min, which is 0.0267 kg/min. This conversion is made using 749 kg/m^3, the density of n-dodecane (Ref. 18), a JP-8 equivalent. Equation (5) on page 25 can be used to solve for different amounts of air flow while varying the equivalence ratio as follows:

$$\phi = \frac{14.616}{\left(\dfrac{A}{35.7}\right)}$$

Data calculated in this way can be found in Table 7. These equivalence ratios were only calculated for air flow in the cavity.

Table 7. JP-8 and air equivalence ratio data

φ	Air (kg/min)
0.5	0.780
0.6	0.650
0.7	0.557
0.8	0.488
0.9	0.434
1.0	0.390
1.1	0.355
1.2	0.325
1.3	0.300
1.4	0.279
1.5	0.260
1.6	0.244
1.7	0.230
1.8	0.217
1.9	0.205
2.0	0.195

Theoretical Equilibrium Data

A combustion equilibrium solver known as STANJAN (Ref. 36) was used to calculate theoretical equilibrium data for a hydrogen-air flame. The data is produced from coded adiabatic combustion equilibrium calculations. See Appendix B for how to use STANJAN to obtain theoretical data. An equilibrium temperature, also known as an adiabatic flame temperature, and OH species concentrations were determined for a range of equivalence ratios at atmospheric pressure and temperature. To vary the equivalence ratio, moles of hydrogen were varied while moles of air were held constant. This theoretical data was used as a basis for comparison to data gathered from OH PLIF of a flame produced by a Hencken burner. It was used to validate the laser system in the COAL lab.

LIFBASE is a free spectral simulation database used to obtain electronic transition data for diatomic molecules (Ref. 27). It can do either absorption or emission simulation. For this research, the absorption simulation was used to collect data on the OH radical in the (A-X) transition system where A is the excited state and X is the ground state. More specifically, spectral lines from the rotational transitions of the OH (A-X) (1-0) band were used. Fig. 30, a screen shot from LIFBASE, shows some of the many lines representing absorption wavelengths in Angstroms ($\overset{o}{A}$) of the OH radical.
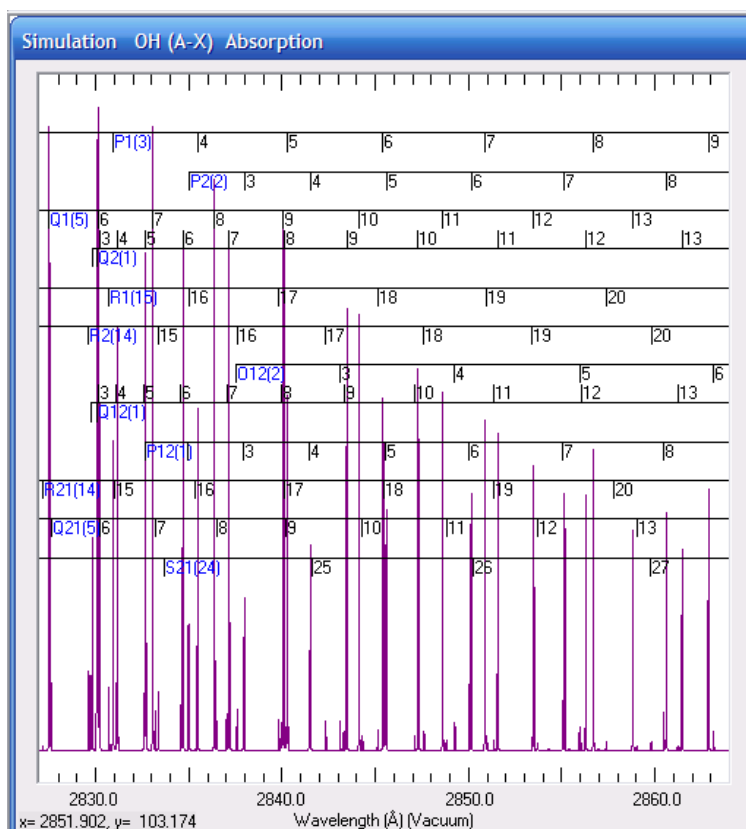
Fig. 30. Rotational transitions of the OH (A-X) (1-0) band from LIFBASE

The higher the peak, the stronger the signal will be. The height of the peak is a function of temperature. The lines in Fig. 30 are normalized in signal strength with the magnitude of the tallest line equal to 100. Generally, a temperature insensitive line is compared to a temperature sensitive line. It is the ratio of their peaks as well as a wavelength scan of the lines used to determine temperature. These methods are explained in later sections. A description of how to use LIFBASE can be found in Koether's thesis (Ref. 3).

3.3   *Hencken Burner Operation*

The Hencken burner is simple to operate and the following explanation goes along with the checklist in Appendix A. This checklist is updated from the original created by Koether (Ref. 3). The Hencken burner was set up to operate manually without the use of lab-view in the computer control station. However, there are solenoid valves installed and controlled through lab-view to turn fuel flow off and on to the mass flow controllers, see Fig. 26. These are currently not in use and therefore the burner is operated in the following manner. The first thing to do is to turn on the MKS-247 control panel, see Fig. 27. It needs approximately 30 minutes to warm up. In addition, it powers the mass flow controllers. These also have a 30-minute warm up time. This time is needed for accuracy of the controllers. For a comprehensive list of specifications on the panel and the controllers, as well as how to operate them, see Koether's thesis (Ref. 3). The next thing to do for warm-up considerations is to start the laser system. It needs about 15 minutes to warm-up. See Appendix A for laser start-up procedures, also found on the computer at the laser control station. Once the digital control panel and the laser are warming up, go to the tank farm located just outside of Lab 258 and open the

regulators on the tanks of the desired gases. Occasionally, it is a good idea to check the lines from the regulator to the mass flow controller for leaks. Checking for leaks is especially important when a precise and steady amount of gas flowing through the lines is needed. Currently, the Hencken burner is burning a hydrogen-air flame. In the tank farm, turn on the fuel (hydrogen), air, and nitrogen. Nitrogen is the co-flow for the flame. Its use is explained by Koether (Ref 3). Once the desired tank farm bottles are opened, then open the valves in the lines for fuel, air, and nitrogen on the wall behind the MOKON machine. Proceed with the checklist for setting the set points for different equivalence ratios. As a caution to prevent equipment damage, ensure there is positive pressure to the mass flow controllers before turning the toggle switch for flow to the on position illuminating the green light. If the toggle switch is on for more than two minutes with no pressure, the mass flow controllers can be severely damaged. Please proceed with the checklist in Appendix A for lighting the flame.

To shut down the Hencken burner, turn the toggle switch for fuel, air, and nitrogen on the MKS 247 digital control panel to off. The green lights will go out, and this will extinguish the flame. After shutting off the tanks in the tank farm, the lines will still be pressurized. It is possible to bleed the lines using the following procedure. With the tanks shut off and the valves in the lines behind the MOKON machine still open, turn the toggle switch on the digital control to "On" for a brief period. With the correct channel selected for the display, the number will start to decrease as pressure is decreased from the line. It is important to use caution when doing this. Leaving the toggle switch open (green light on) for too long with no pressure will severely damage the mass flow

controllers. So use caution when bleeding the lines. When done, follow the rest of the

checklist in Appendix A for Hencken burner shut down.

3.4 *Laser Diagnostics*

Experimental Set-Up

The AFIT COAL lab is a state-of-the-art facility for combustion research because

of the capability to perform laser diagnostics. The laser system consists of a Quanta-Ray

PIV-Series dual pulsed Nd:YAG laser made by Spectra-Physics and a Continuum

ND6000 dye laser. A Schott CG-WG-295 colored glass filter was used to block out light

from the laser so only the OH fluorescent signal could be recorded. An ICCD camera

made by Princeton Instruments was used to capture the OH signal. A Hencken burner

was used to produce a laminar premixed hydrogen-air flame with a nitrogen coflow. All

components are discussed previously. The configuration of the laser system, the beam

path used to analyze the Hencken burner flame, laser system operation, and detailed

description of the laser are located in Koether's thesis (Ref. 3).

MKS ALTA digital mass flow controllers seen in Fig. 26 were used to control the

amount of hydrogen, air, and nitrogen coflow going in to the Hencken burner. Hydrogen

was varied from 2 - 9 slpm and air was held constant at 15.43 slpm in order to produce

flames ranging from 0.3 - 1.4 in equivalence ratio. The nitrogen coflow was set to 22

slpm and held constant throughout. The mass flow controllers had accuracies of $\pm$ 1% of

the set-point for 20 - 100% flow.

OH Concentration Measurements

Measurements were taken of a laminar flame using PLIF to validate the laser system in the AFIT COAL lab. OH concentration measurements were made with a laser beam in the form of a sheet shot through the center of the hydrogen-air flame. The location of the beam was varied from the surface of the burner to five centimeters above it. The laser was tuned to 284.005 nm which is the wavelength for the Q1(9) line in the (1,0) band of the OH (A-X) electronic transition system. This particular line was chosen because of the strength of the signal it produces. This causes the OH radicals to fluoresce. The theory behind the fluorescence is covered in Chapter 2.2. Basically the more intense the fluorescence the greater the concentration of OH in the flame. The aperture on the camera lens was adjusted to let less light in to ensure the camera was never saturated with too high of an intensity. This also ensured the most proportionality of intensity to the amount of concentration aside from quenching effects. Fig. 31 shows how the amount of intensity varies as a function of aperture setting when intensity is plotted as a function of equivalence ratio. Camera aperture settings, also known as *f*-stops, are denoted by f3, and f4 in the graph legend. Error bars show standard deviation from the mean at each point. The standard deviation was lower for the higher *f*-stop value. This is a result of less light being allowed into the camera. Therefore the signal to noise ratio is decreased.
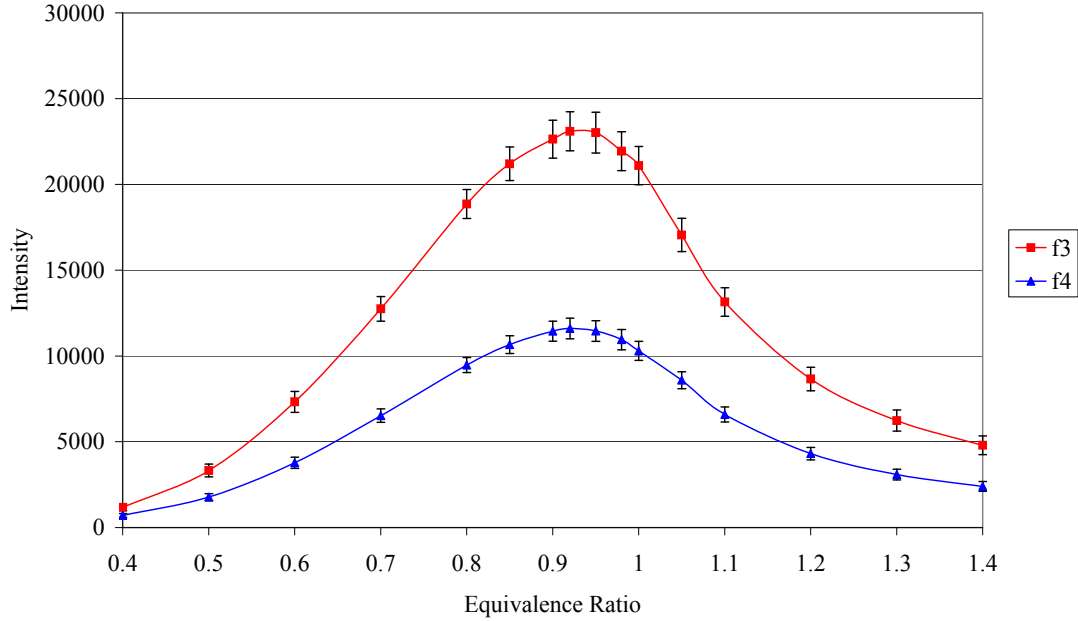
Fig. 31. Intensity versus equivalence ratio as a function of aperture setting

This was especially important while taking measurements with different wavelengths for temperature measurements, a method discussed in later sections. Intensities were recorded from image analysis described previously. The results are discussed in Chapter 4.1 along with corrections made to the PLIF signal due to quenching.

Quenching

The theory behind quenching was discussed in Chapter 2.6. Now a description of how to adjust the PLIF signal due to quenching effects will be given. A great summary of Tamura's analytical model (Ref. 25) can be found in Koether's thesis (Ref. 3) and is the same quenching rate correction method used on the data in Chapter 4.1. It will be reproduced here for ease of reference.

An equilibrium solver such as STANJAN must be used to determine pressure, adiabatic flame temperature, and mole fractions of the products of combustion. The procedure for this is given in Appendix A. Parameters of different colliding species for quenching rate are given in Table 8 for quenching rate corrections.

Table 8. Quenching rate parameters (Ref. 25)

Colliding Species	$\sigma_{Q(INF)}$ (Angstroms)^2	ε/k (K)	Quenching Rate Coefficent m^3/s
CH_4	11.0	320	$(5.07\times10^{-19})(\sigma_Q)(T^{0.5})$
H	14.5	84	$(15.0\times10^{-19})(\sigma_Q)(T^{0.5})$
O	0.0	0	$(0\times10^{-19})(\sigma_Q)(T^{0.5})$
N	0.0	0	$(0\times10^{-19})(\sigma_Q)(T^{0.5})$
H_2	4.5	224	$(10.88\times10^{-19})(\sigma_Q)(T^{0.5})$
OH	20.0	384	$(4.99\times10^{-19})(\sigma_Q)(T^{0.5})$
CO	12.0	397	$(4.47\times10^{-19})(\sigma_Q)(T^{0.5})$
NO	0.0	0	$(0\times10^{-19})(\sigma_Q)(T^{0.5})$
O_2	8.0	243	$(4.37\times10^{-19})(\sigma_Q)(T^{0.5})$
H_2O	20.0	434	$(4.92\times10^{-19})(\sigma_Q)(T^{0.5})$
CO_2	11.0	488	$(4.16\times10^{-19})(\sigma_Q)(T^{0.5})$
N_2	0.4	624	$(4.47\times10^{-19})(\sigma_Q)(T^{0.5})$

Also needed are a few constants. The spontaneous emissions constant for OH is A = 1.45×10^6 s^{-1} and Boltzman's constant is $k = 1.38065 \times 10^{-23} \dfrac{m^2 kg}{s^2 K}$. OH LIF efficiency must now be calculated in the following manner. The temperature dependence of the cross-sections for each molecule must be calculated using the following equation:

$$\sigma_Q = \sigma_{Q(INF)} e^{\left(\frac{\varepsilon}{kT}\right)} \tag{12}$$

Next, the equations in Table 8 were used to calculate the quenching rate coefficients for each molecule. Then use the following equation to calculate number density for each species:

$$\textit{Species Number Density} = \textit{(mol fraction of the species)}\left(\frac{P}{kT}\right) \tag{13}$$

Now calculate the quenching rate for each species using the following equation:

$$Q_{each\_species} = \textit{(Species Number Density)(quenching rate coefficient)} \tag{14}$$

Then get a total quenching rate by adding the quenching rates for each molecule:

$$Q_{TOTAL} = \sum Q_{each\_species} \tag{15}$$

Finally, LIF efficiency can be calculated in the following manner:

$$\textit{LIF Efficiency} = \frac{A}{\left(A + Q_{TOTAL}\right)} \tag{16}$$

This LIF efficiency number is used to correct the signal of the experimental data and is discussed in Chapter 4.1.

OH PLIF Thermometry

OH PLIF thermometry is a unique method of measuring flame temperatures without disturbing the natural flow of the flame. Temperature was determined using both a ratio of intensities and performing a spectral analysis. The theory behind PLIF thermometry is covered in Chapter 2.6. The actual procedure will be described here. Each spectral line with its particular wavelengths used for the temperature measurements can be found in Table 9. Essentially a thermometer was made by tuning the laser to these particular wavelengths and recording an OH intensity.

Table 9. Spectral lines and respective wavelengths

Line	Wavelength (nm)
P1(7)	570.18
Q2(11)	570.32
R2(8)	563.45
R2(5)	563.48
Q1(14)	572.91
Q1(5)	565.50
R2(13)	565.28
P1(2)	565.33
Q1(9)	568.01
Q2(8)	568.02
P1(5)	568.06

To measure temperature using a ratio of intensities, a ratio of peaks from LIFBASE was used. The magnitude of the peaks will vary according to temperature. A LIFBASE simulation was ran for an expected range of flame temperatures. For example, magnitudes of peaks from a temperature insensitive line like Q1(14) and a temperature sensitive line like Q1(5) for a range of temperatures were recorded. The ratios of the magnitude of these peaks were plotted as a function of temperature. In a sense, this becomes a thermometer. Intensities from the laser tuned to the wavelength of these lines are then recorded. They are then divided by the power from the laser to make sure they are only a function of wavelength. The ratios of these intensities are then compared to the ratio of peaks from LIFBASE to determine a temperature. Measurements were taken of a flame ranging from 0.5-1.3 in equivalence ratio.

Spectral analysis was used to measure temperature by using a spectral line from LIFBASE at a particular wavelength. Each line in LIFBASE has a peak for a particular wavelength, a specified shape, and produces a particular full-width half-maximum (FWHM) value for different temperatures, see Fig. 32**.**
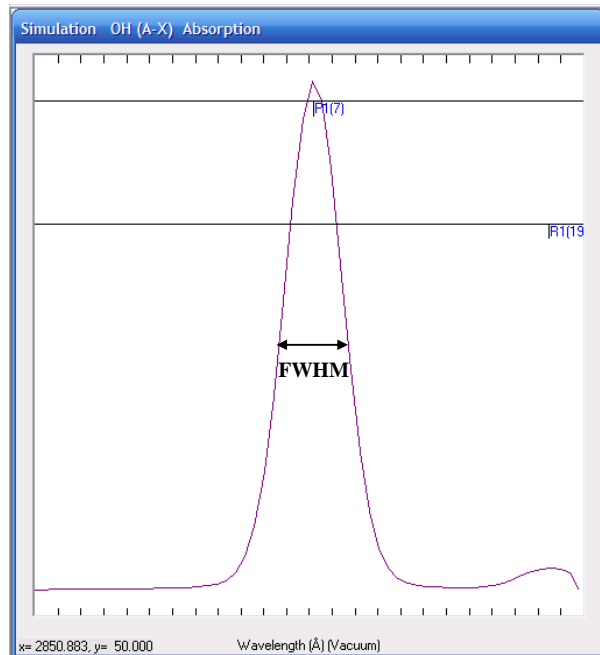
Fig. 32. Picture of FWHM location

FWHM is the width of the curve in wavelength at half the maximum intensity of the curve. It is determined in the following manner. Pick the point half way up the line. On either side of the line, drop down to the particular wavelengths and subtract them. This is the FWHM value, and it will vary with temperature. Perform a LIFBASE simulation for a particular line and wavelength at an expected range of temperatures, and record the FWHM value. Plot these as a function of temperature. In a sense, this becomes another thermometer. Using the laser, a scan around this particular wavelength where the peak exists is performed. For example, the laser is tuned to scan around 572.910 nm, a range from 572.903 - 572.921 nm and intensities are recorded at each wavelength. Recorded intensities are plotted as a function of wavelength and the FWHM value is determined in the same manner. This value is then compared to the FWHM values as a function of

66

temperature plotted from LIFBASE to determine a temperature. Measurements were taken using each of the lines in Table 9 for equivalence ratios of 0.7 and 1.0.

3.5   UCC Operation

Operation of the small-scale UCC in the COAL lab was made possible by many previous AFIT students. Before graduating, Koether had configured and tested most lab components such as the combustor air rig, heaters, emissions analyzer, and exhaust system. The description and operation of these components is covered in detail (Ref. 3) and will not be covered again. Only the fuel pump had not been completely tested.

The fuel pump is a dual syringe pump model 1000 D made by ISCO, see Fig. 33. It had sat in the lab for almost two years after being installed by a previous AFIT student (Ref. 37). It is capable of delivering up to 5.67 ml/s at 1.38 x 10^7 Pascal (Pa) with an accuracy of 25.38 nl precision.

Fig. 33. ISCO dual syringe fuel pump (Ref. 3)

There were some things to work out before smooth operation was obtained. Some electrical connectors in the back had to be reconnected and the pump was initially controlled locally. Once operating correctly it was configured to operate remotely through Lab-View.

The pump has two modes of operation. It will operate in either constant flow mode or constant pressure mode. For example, if operating in constant pressure mode, it would only give the flow needed to operate at that pressure. If operating in constant flow mode, it would only give the pressure required for that flow. However, when supplying fuel to the atomizer nozzle in the combustor, a constant flow is needed at a certain pressure. Fuel flow has to be fixed at a constant value to operate at a desired equivalence ratio and the pressure-atomizing nozzles used in the combustor, Goodrich model 46817-33, require 2.07×10^6 Pa (300 pounds per square inch (psi)), (factory specified) to correctly atomize the fuel. It was determined, however, much lower pressures through the nozzles such as 2.07×10^5 - 3.44×10^5 Pa (30 - 50 psi) are sufficient. The pressures were measured at the pump while in constant flow mode and could have actually been different at the nozzle as there was no way to measure pressure in the fuel lines.

Pump syringe A and B were operated in constant flow mode delivering fuel in milliliters per minute to the combustor. Data was recorded to show the pressure difference between the syringes. Syringe A produced a steady rise in pressure for each increase in flow rate with only minor fluctuations of $\pm 13.79 \times 10^3$ Pa (± 2 psi). Syringe B operated at a lower pressure and at higher values fluctuated at $\pm 96.52 \times 10^3$ Pa (± 14 psi).

It is possible the line for syringe B has a larger orifice in it. Pressure differences are

shown as a function of flow rate for both pump syringes, see Fig. 34.
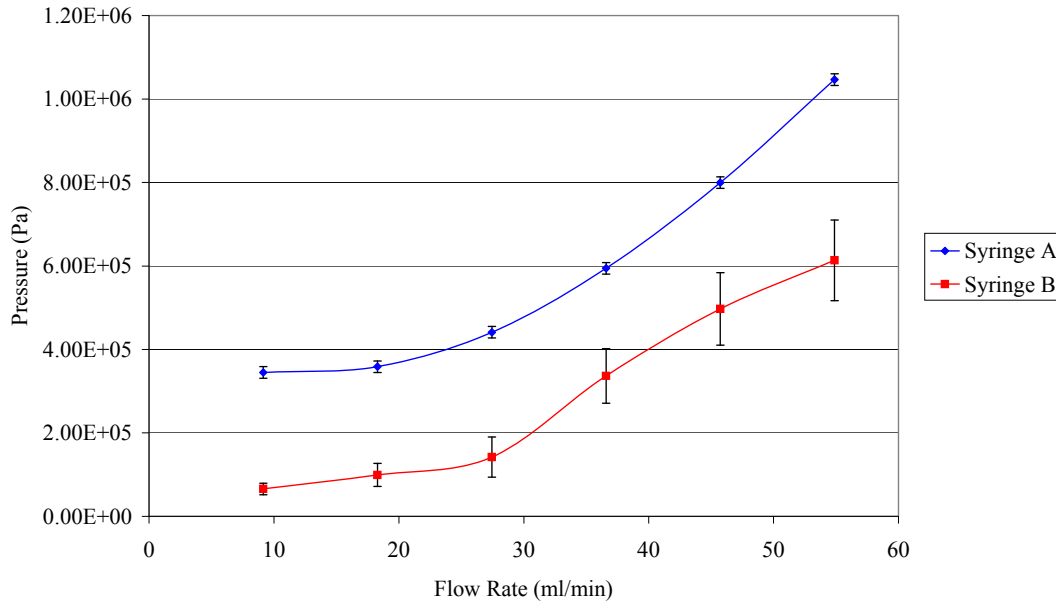
Fig. 34. Fuel pump operation – pressure versus constant flow rate

Lighting Procedure

The following is meant to supplement the step-by-step procedure for starting the

UCC found in Appendix A. For safety reasons, at least two persons should perform this

procedure. Adequate hearing protection should be available. First it is necessary to

perform the lab equipment start-up procedure in Appendix A. Once the equipment is

operating correctly, turn on the main and secondary air. Start out at 1 kg/min in the main

and 0.5 kg/min in the secondary. This is necessary to reduce fluctuations as it approaches

a steady state condition. Gradually increase them to between 80 and 90 percent of their

maximum values. This is necessary for the heaters to reach a steady state condition.

Using low air flow for starting conditions and bringing the heaters up to operating conditions will almost always cause one or both heaters to over heat. It was determined heating the air flow helped the JP-8 to light better and reduced pooling. Once the heaters reach a steady state condition, bring the air flow down to starting conditions. The most successful starts were with the main air set at 1.3 kg/min and 0.3 kg/min in the secondary. The main heater was set at 400 degrees Fahrenheit (°F) and the secondary heater was set at 300 °F.

A slightly fuel-rich mixture (equivalence ratio of 1.4) of ethylene and air was used to ignite the JP-8 inside the combustor. An equivalence ratio of 1.0 was being used until the temperature of the ethylene dropped to around 32 F as a result of the ethylene supply tank being located outside. A range of equivalence ratios for ethylene and air can ignite the JP-8 based on temperature of the ethylene and will be the focus of further study in future research.

The fuel pump was operated in constant pressure mode for starting. This ensured the fuel nozzles received enough pressure to properly atomize the fuel for a good light when the combustor was cold. Good results were achieved by letting the pressure build in the line by leaving the manual fuel valve closed until the pressure displayed on the VI reached the desired value. Pressures of $2.07x10^5 - 4.14x10^5$ Pa (30 to 60 psi) providing approximately 35 ml/min of fuel were used. This resulted in a highly fuel-rich condition for starting, an equivalence ratio over 2.0.

Once lit, the amount of fuel being delivered was immediately decreased by changing the fuel pump to constant flow mode to deliver 20 ml/min of fuel. The secondary air was increased to 0.7 in increments of 0.1 for the cavity and 1.5 for the

main. This had to be done quickly but steadily to keep the combustor from pooling up with fuel or flaming out. This brought the equivalence ratio back down to a lean operating condition.

Emissions Collection

A Testo 350 portable emissions analyzer is used to measure emissions from the UCC, see Fig. 35. It comes equipped with an emissions probe that can withstand temperatures up to 1000 ºF. It is capable of measuring numerous emissions parameters. Unburned hydrocarbons (UHC) can be measured with an accuracy of less than 400 parts per million (ppm). Carbon monoxide (CO) and nitrous oxide (NO_X) can be measured with an accuracy of less than five ppm. Carbon dioxide (CO_2) is measured with non-dispersive infrared technology to an accuracy of $\pm\ 0.3\%$. These pollutants were used to calculate an emissions index and combustion efficiency using equations six and seven respectively found in Chapter 2.4.

Fig. 35. Testo 350 portable emissions analyzer

Fig. 36 shows the UCC in operation with the emissions probe coming in from the left side. It was used to measure emissions from the main exhaust as shown here. In this position, it is approximately one inch from the exhaust plane. The results of emissions analysis are discussed in Chapter 4.2.
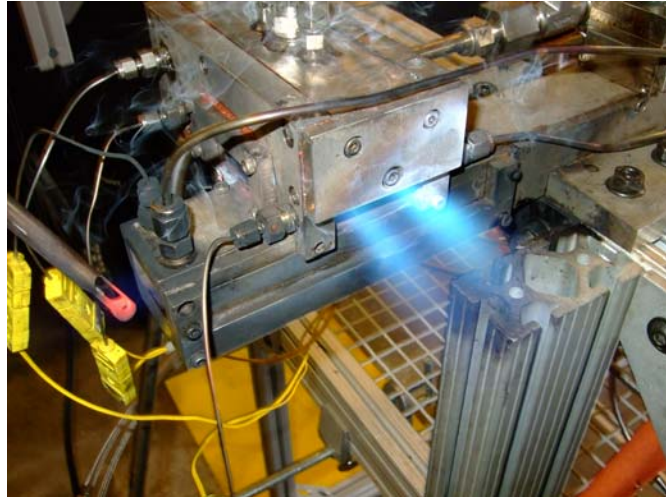
Fig. 36. UCC in operation with Testo 350 emissions probe in main vane exhaust

IV. Results and Analysis

4.1 OH PLIF Results

The laser in the AFIT COAL lab was validated by using PLIF to produce images of a laminar premixed hydrogen-air flame produced by a Hencken burner. Amounts of OH species concentration were determined as a function of equivalence ratio and height above the burner. The amount of species concentration is proportional to intensity as discussed in Chapter 2.6. Therefore, the intensities gathered from image analysis were compared to theoretical data obtained using STANJAN for accuracy. Numerous images were gathered and are discussed.

Theoretical Equilibrium Data

STANJAN, described in Chapter 3.2, was used to obtain theoretical concentration amounts of OH and adiabatic flame temperature as a function of equivalence ratio (ϕ), see Figures 37 and 38. Since most measurements are taken assuming atmospheric pressure to be 1 atmosphere (atm), pressure was varied from 1 atm to 0.97 atm to better represent conditions in the lab. On average this resulted in only a 1% difference for both temperature and OH concentration. Therefore, the influence on the data due to atmospheric pressure was not considered to be a factor. OH concentration was the highest for $\phi = 0.95$ and adiabatic flame temperature was found to be the highest for $\phi = 1.1$. Both of these conditions assume complete combustion. Experimental data gathered in the lab was compared to this data to determine the accuracy of results.
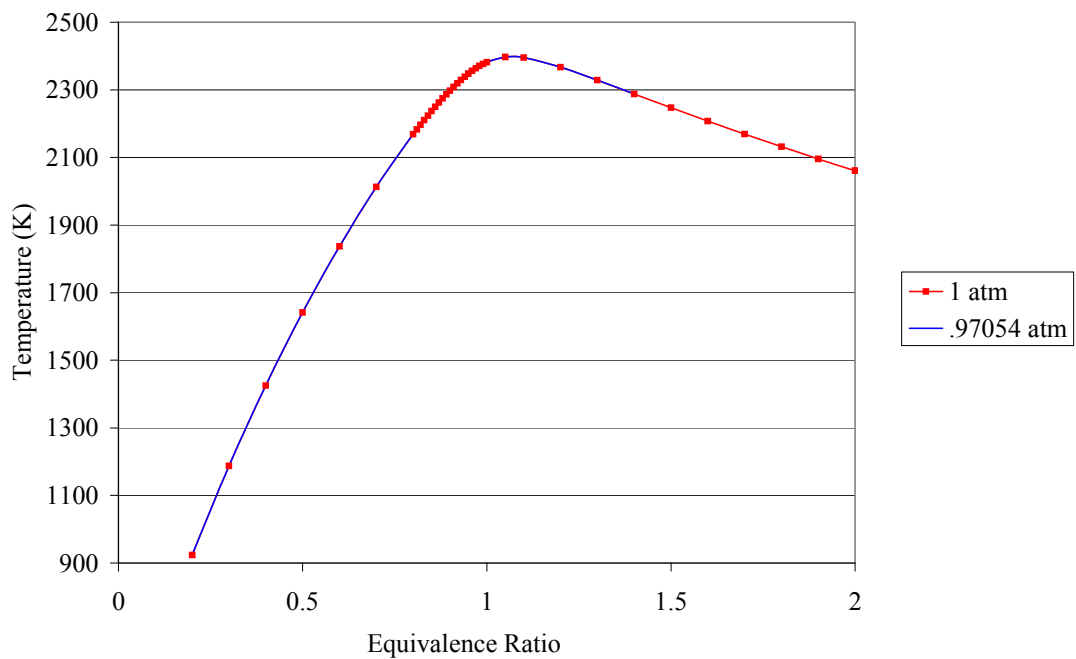
Fig. 37. Theoretical equilibrium data - temperature vs. equivalence ratio

OH Species Concentration
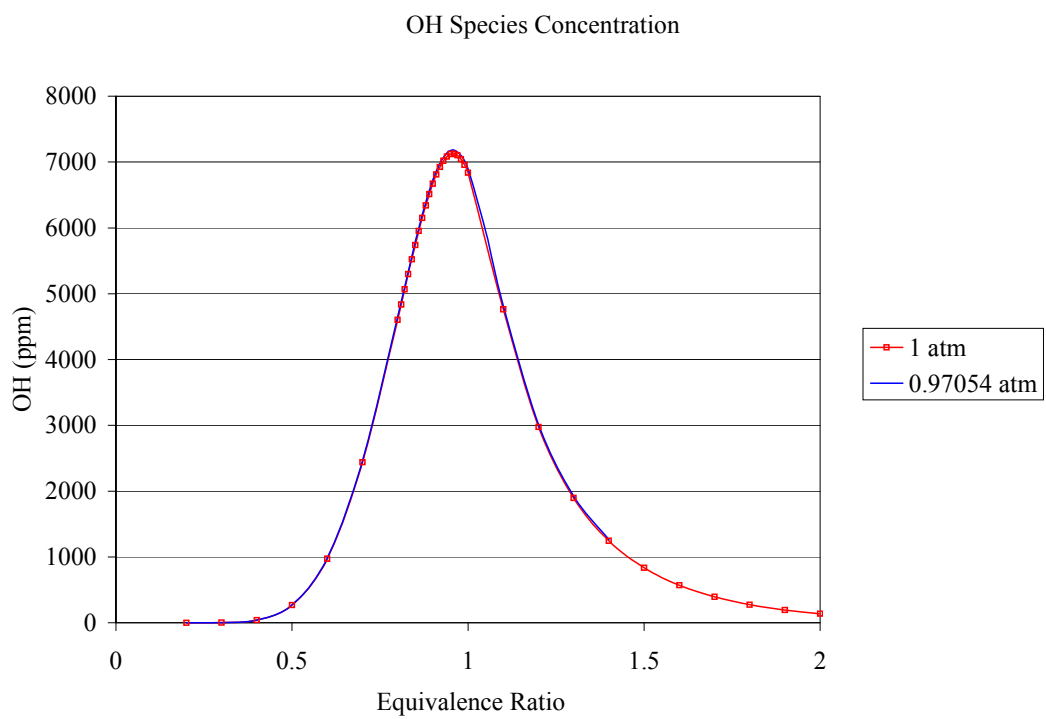
Fig. 38. Theoretical equilibrium data - OH concentration vs. equivalence ratio

Concentration Measurements

Numerous PLIF images were taken at a range of equivalence ratios from the burner surface to approximately 5 cm above. For all concentration measurements, the fluorescing area of OH radicals was produced by a 1.3 cm wide laser sheet tuned to 284.005 nm. Fig. 39 shows this area produced by the laser sheet running from right to left.
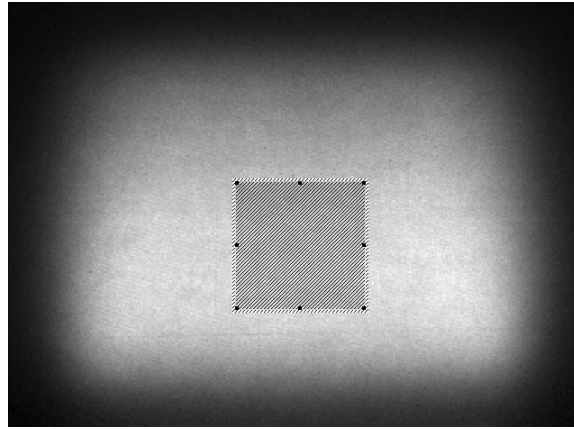
Fig. 39. Interrogation area of PLIF Image

In every instance the interrogation region of the image was 100 x 100 pixels or 49 mm^2. The average intensity and standard deviation of this region for 50 images was calculated using Win-View 32 imaging software described previously. This particular region in the area was selected because the highest intensity is found here. This was verified to reduce errors in data analysis by taking an image of a flame at equivalence ratios of 0.8, 0.9, and 1.0. Analysis was performed on the square interrogation region. It was further divided up into five equal rectangular sections; the first rectangular section located at the bottom and the fifth located at the top with the second, third, and fourth in the middle numbered from bottom to top. Location three produces the highest average intensity because even

though the laser beam is spread into a sheet, properties of the optics used to route the beam cause the most intense part of it to remain in the middle. This is displayed in Fig. 40 where the middle point for each line is at the peak intensity.
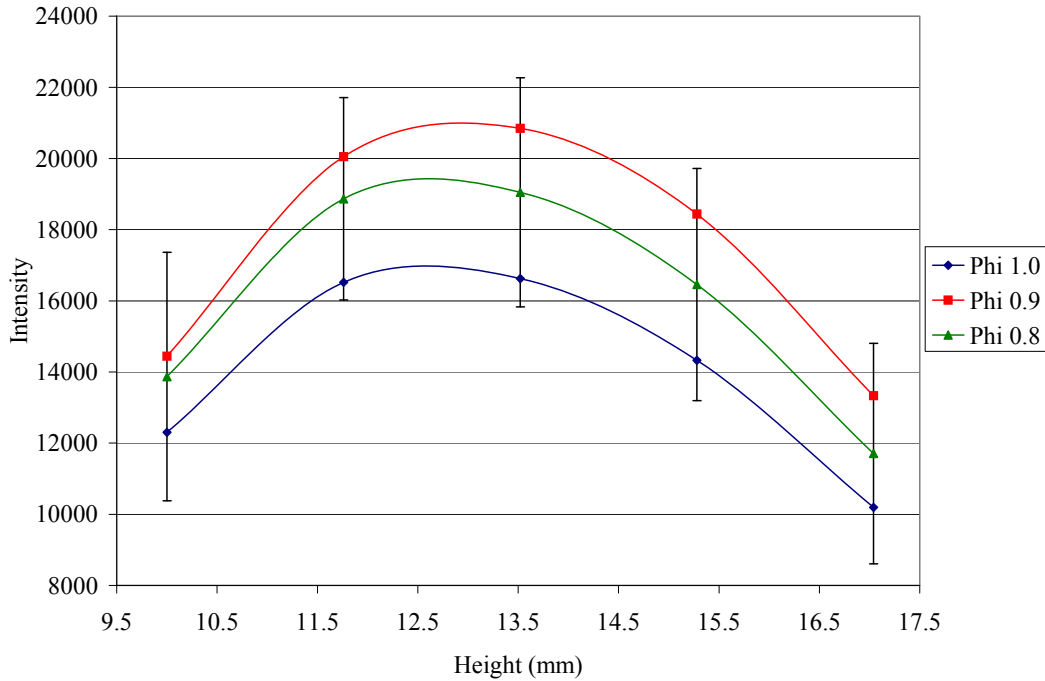
Fig. 40. Average intensity vs. height inside interrogation area

Error bars were only added to the line for $\phi = 0.8$ to refrain from cluttering the graph. This line has the smallest variance of the three. The percent error ranged from as high as 22% at the surface to as low as 7% in the middle to 17% at the highest location measured. The larger percent error is most likely due to areas near the edge of the laser beam where the signal is not as concentrated. The line for $\phi = 1$ is highest in variance because the largest amounts of OH concentration are produced at this equivalence ratio, therefore the signal is the strongest.

Numerous images were gathered while validating the laser system to determine the area of greatest intensity above the burner surface. Three sets of data taken at different locations above the burner were averaged together to plot species concentrations versus equivalence ratio. Fig. 41 shows raw intensities as a function of equivalence ratio at these different locations. Intensity is highest at the surface. This is most likely due to noise in the signal from the shiny surface of the burner. As a result, the largest variance occurs here.
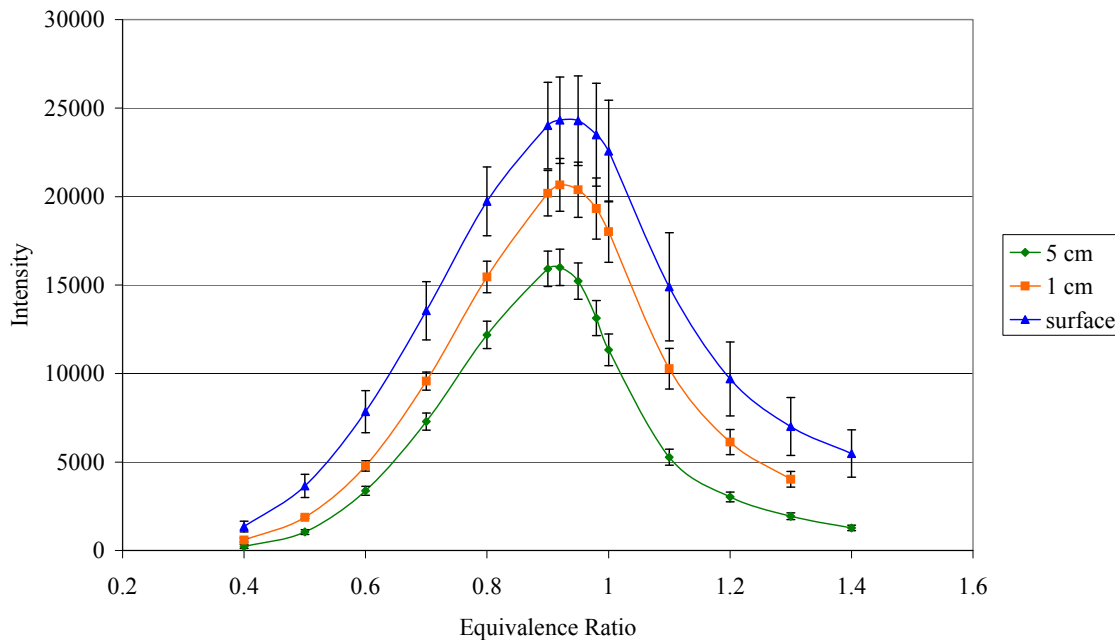
Fig. 41. Raw intensities at different locations above the burner

The greatest amount of OH is produced at $\phi = 0.95$ based on theoretical results. This means the highest intensity should have been at $\phi = 0.95$ also, but this result was not achieved. The highest intensity was actually achieved at $\phi = 0.92$ at every one of the three locations. As a result, every curve produced from data at each location is shifted to

the left of the blue theoretical curve. This is a shift of approximately 3.15% in the peak

of each curve. This shift can be seen in Fig. 42 for data taken at the surface of the burner.
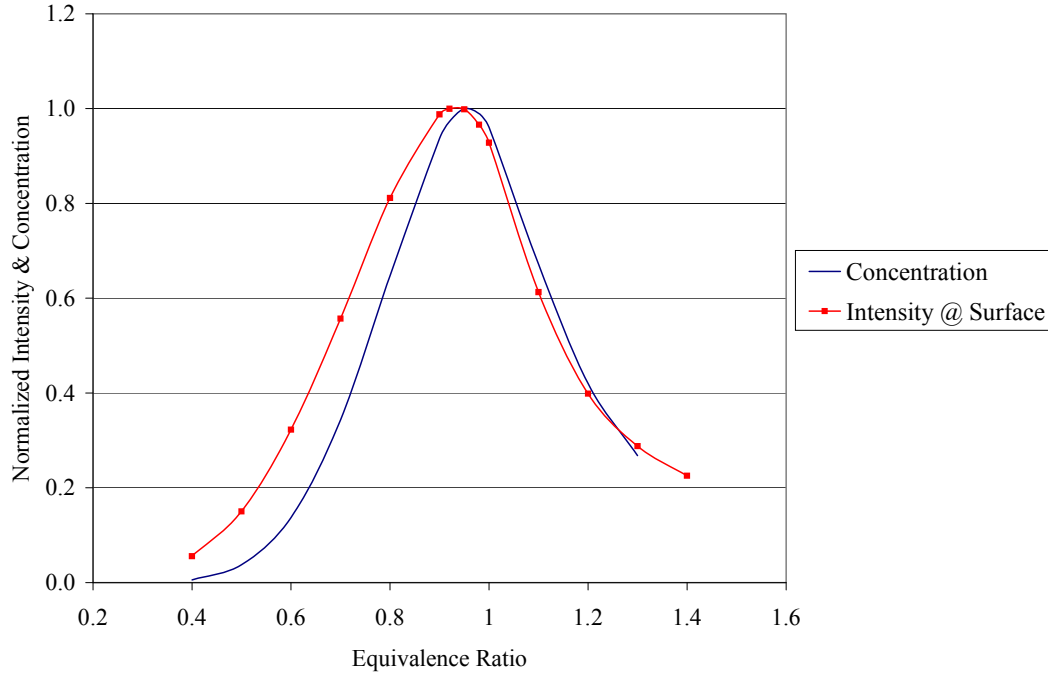
Fig. 42. Uncorrected data at the surface of the burner

Normalized experimental data is plotted with normalized theoretical OH concentration

data. This shift is most likely due to noise in the signal from the shiny surface of the

burner, location dependence of OH, fluctuations in air-to-fuel ratio from the mass flow

controllers, and quenching. Analytical corrections must be made to the data for

quenching and this procedure is described in the following paragraph.

Quenching and the theory behind it was discussed in Chapter 2.6. The procedure

to calculate LIF efficiencies due to quenching was used here. These numbers were then

used in the following equation to obtain a corrected intensity:

$$Corrected\ Intensity = \frac{Average\ Intensity}{LIF\ Efficiency} \qquad (17)$$

The corrected intensity for each equivalence ratio was then normalized and plotted against theoretical data in each figure below. These corrections made only a slight difference at most locations. The amount of quenching correction is obviously dependent on height above the burner. Temperature and mixing of the flame change with height and these are significant parameters used to calculate LIF efficiencies for quenching corrections. Uncorrected and corrected normalized intensities are compared to theoretical data, see Figures 43 - 45.
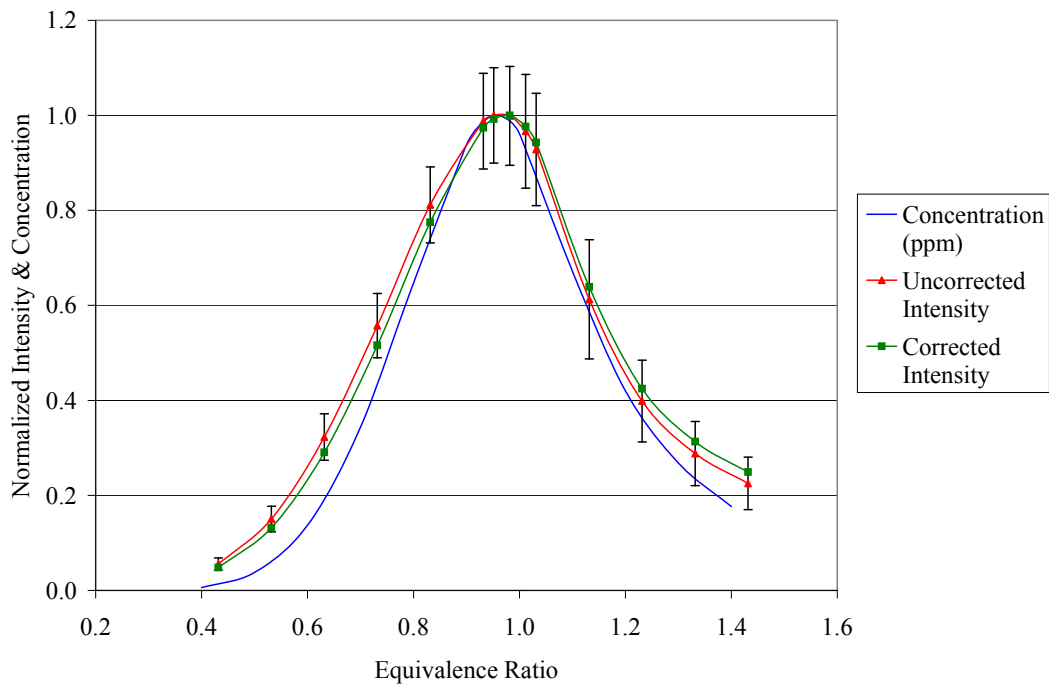
Fig. 43. OH intensities from surface and equilibrium OH concentration
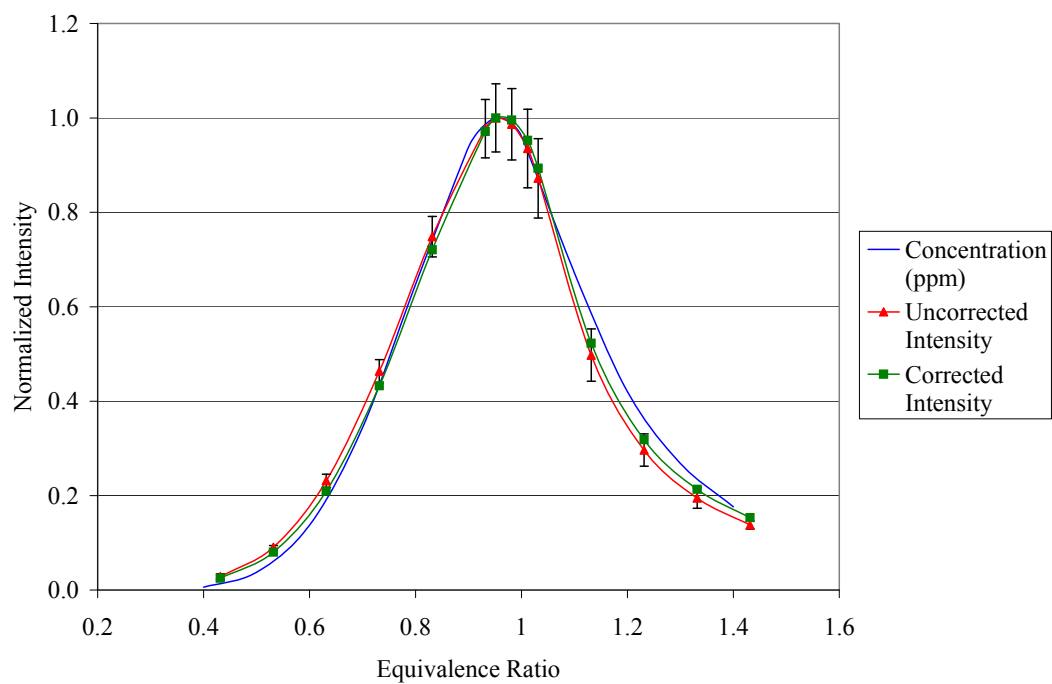
Fig. 44. OH intensities from 1 cm and equilibrium OH concentration
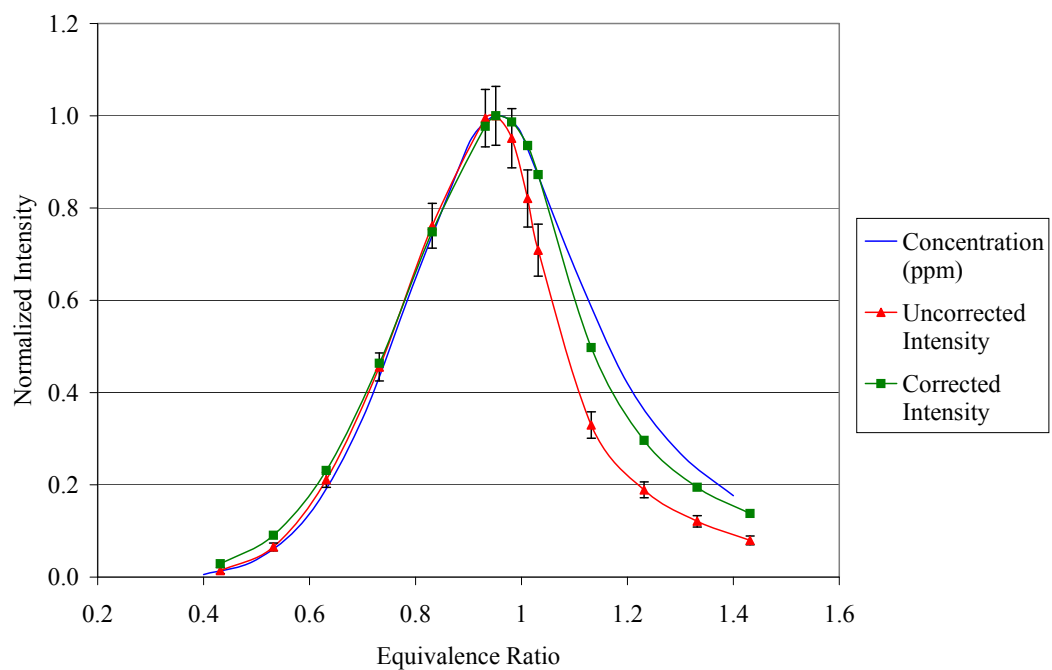
Fig. 45. OH intensities from 5 cm and equilibrium OH concentration

STANJAN produces theoretical data based on equilibrium and adiabatic conditions. This results in decreased amounts of species concentrations than would be expected in an actual flame. It is possible the flame is not at equilibrium at the surface and could explain why the data is shifted and higher than expected in Fig. 43. In addition, there is the possibility of a slight error in the air-to-fuel ratio as mentioned previously. Also at the surface, the temperature is not adiabatic. There are heat losses to the surface by radiation and conduction. At one centimeter above the surface, the experimental data curves match theoretical the best, see Fig. 44. There still exists some slight error here. By one centimeter above the burner surface, the flame should be at equilibrium, so there is an even greater possibility of a an error in equivalence ratio caused by the mass flow controllers. The temperature is still not adiabatic due to heat loss as well as mixing of the coflow. In this area, the flame begins to experience a cooling effect by the nitrogen used to keep the flame laminar. Error due to quenching effects also becomes a factor since quenching has been shown to be a function of height above the burner. The biggest quenching correction occurs at five cm above the burner surface as seen in Fig. 45. Here the temperature is definitely at adiabatic equilibrium and mixing of the coflow is occurring. Quantifying this uncertainty, we can correct the curves by shifting the equivalence ratios to match expected peaks. The error bars in each figure show the variance is the largest at the surface and the smallest at five cm. This follows the trend of higher fluctuations in the signal with higher intensity, as well as noise due to the shiny surface of the burner. There are also fluctuations due to laser power. The variance suggests an average 5% uncertainty in these measured values depending on equivalence ratio and height above the burner.

In order to show how flame properties vary as a function of height above the burner surface, normalized intensity is plotted versus φ for two locations above the surface. At one centimeter above the surface there is more OH concentration for fuel-rich conditions than at five centimeters.
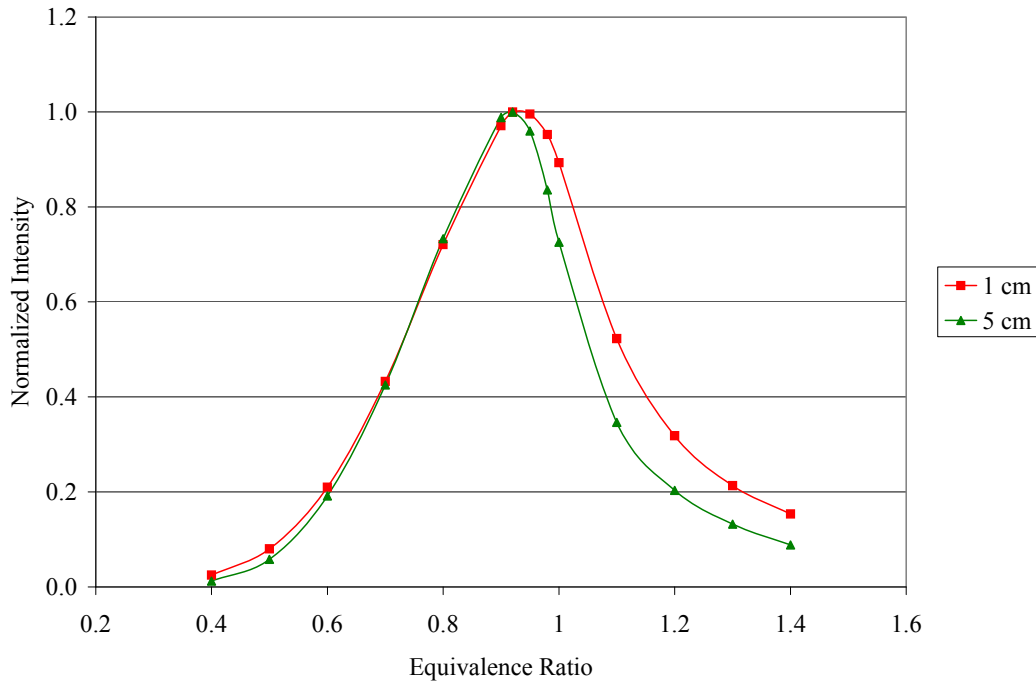
Fig. 46. Normalized intensity versus equivalence ratio

The reason for this is at five cm, there is less OH being produced. Quantitatively, there is as much as 42% less. OH is a flame marker for combustion, and this decreased OH amount is near the end of the flame at this five cm location. Here the flame is mostly at equilibrium.

PLIF Thermometry – Ratio of Intensities

Eleven different spectral lines and their respective wavelengths shown in Table 9 were used to gather intensities at one centimeter above the burner surface. Seven different pairs of the lines were used for computing ratios. As discussed previously, LIFBASE simulations were ran to gather different peak magnitudes of these lines over a range of temperatures. The ratio of these peaks seen in Table 10 are what essentially was used as a thermometer. They were plotted as a function of temperature.

Table 10. LIFBASE ratios of peak magnitudes

Temp	R2(8)/Q2(11)	R2(13)/P1(2)	P1(7)/Q2(11)	R2(5)/Q2(11)	Q1(14)/Q1(5)	Q2(8)/Q1(9)	P1(5)/Q1(9)
1000	1.7091	0.0377	2.9444	2.9252	0.0246	1.1199	1.5573
1100	1.4855	0.0579	2.4211	2.3114	0.0382	1.1329	1.3423
1200	1.3162	0.0827	2.0776	1.8896	0.0543	1.0952	1.1941
1300	1.2119	0.1098	1.8089	1.6112	0.0733	1.0670	1.0781
1400	1.0880	0.1439	1.6217	1.3570	0.0975	1.0496	0.9774
1500	1.0156	0.1792	1.4717	1.2127	0.1179	1.0355	0.9204
1600	0.9629	0.2185	1.3370	1.0969	0.1426	1.0071	0.8516
1700	0.8964	0.2596	1.2455	0.9805	0.1711	0.9993	0.8065
1800	0.8597	0.3000	1.1725	0.9053	0.2000	0.9850	0.7585
1900	0.8172	0.3530	1.0976	0.8335	0.2295	0.9636	0.7278
2000	0.7820	0.3918	1.0609	0.7764	0.2582	0.9727	0.7085
2100	0.7581	0.4383	0.9986	0.7266	0.2875	0.9495	0.6742
2200	0.7265	0.4908	0.9617	0.6827	0.3259	0.9433	0.6477
2300	0.7116	0.5340	0.9124	0.6513	0.3535	0.9303	0.6288
2400	0.6892	0.5802	0.8869	0.6217	0.3845	0.9406	0.6177
2500	0.6772	0.6234	0.8552	0.6038	0.4126	0.9209	0.5908

Curve fit equations were then applied to each set of data points. The ratios of intensities from Table 11 were used in these equations to calculate a temperature. The intensities used in these calculations were all divided by the laser power to ensure they were only a function of wavelength and not power fluctuations in the laser.

Table 11. Ratios of intensities from experimental data

φ	R2(8)/Q2(11)	R2(13)/P1(2)	P1(7)/Q2(11)	R2(5)/Q2(11)	Q1(14)/Q1(5)	Q2(8)/Q1(9)	P1(5)/Q1(9)
0.5	1.1977	0.1902	1.9438	1.4860	0.1017	1.1731	1.2085
0.6	1.0439	0.2530	1.7383	1.2011	0.1620	1.0450	1.0310
0.7	0.9473	0.3241	1.5815	1.0713	0.2188	1.0335	0.9374
0.8	0.8937	0.3904	1.4624	0.9341	0.2641	1.0362	0.8898
0.9	0.8290	0.4582	1.3667	0.8431	0.3047	1.0726	0.8697
0.95	0.7965	0.4748	1.3235	0.8122	0.3199	1.1671	0.9174
1	0.7893	0.4943	1.3193	0.7968	0.3136	1.3646	1.0584
1.1	0.8178	0.4902	1.3139	0.8120	0.3040	1.9461	1.4972
1.2	0.8246	0.4853	1.3133	0.8217	0.2909	2.1731	1.6767
1.3	0.8194	0.4852	1.3253	0.8171	0.2755	2.1798	1.6569

Temperatures were calculated for every pair of the lines in Table 11 for a range of equivalence ratios. Errors occurred while recording data using the Q1(9) line and as a result the data was discarded. Some line pairs produced temperatures closer to equilibrium than others. Experimental temperatures followed the trend of equilibrium temperatures very well when plotted versus equivalence ratio as seen in Fig. 47.
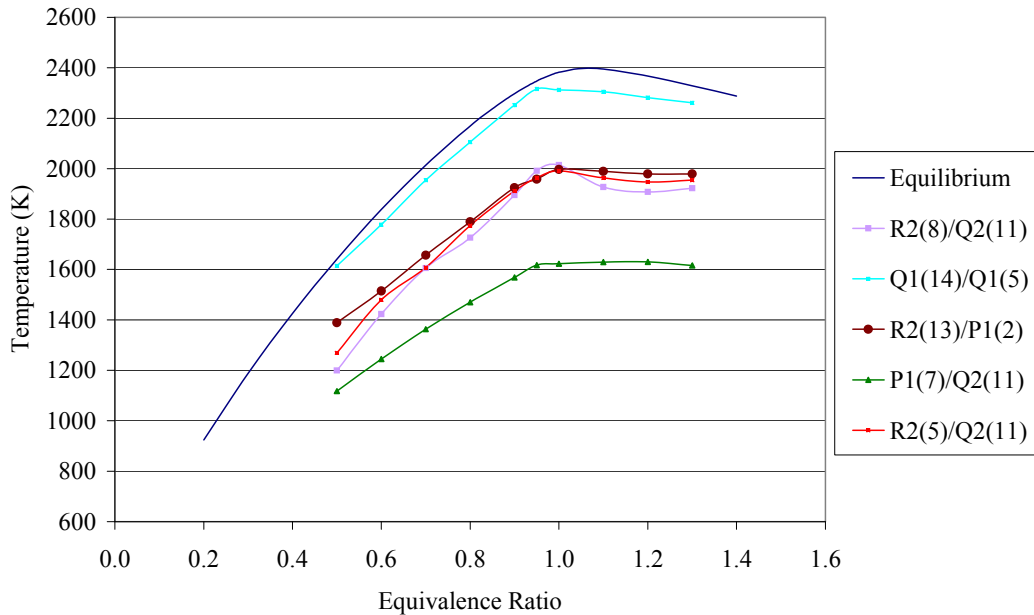
Fig. 47. Theoretical and experimental flame temperatures

All of the line pairs followed the trend predicted by STANJAN. The Q1(14)/Q1(5) line pair provided results closest to equilibrium out of all the pairs. R2(13)/P1(2) provided the next closest results to equilibrium. This is assumed due to the larger wavelength separation of the rotational transition, J numbers 14 - 5 and 13 - 2, the more accurate the measurement. The agreement of the three line pairs with the R2 line show a strong temperature dependence on the R2 line and suggest the temperature of the flame of the Hencken burner is approximately 300 K to 400 K less than equilibrium at the 1 cm location for the experimental hydrogen-air flow rate used. The Q lines are generally stronger and give a better signal to noise ratio. As a result the Q1(14)/Q1(5) line pair was picked for comparison to equilibrium data and the Hancock lines (Ref. 30) in Table 12 below.

Table 12. Summarized temperature results from ratio of intensities

φ	Equilibrium	Exp Data Average	Exp Data % Difference	Hancock	Hancock % Difference	Q1(14)/Q1(5)	Q1(14)/Q1(5) % Difference
0.5	1642	1288	21.5%	1655	0.8%	1464	10.8%
0.6	1837	1466	20.2%	1840	0.1%	1665	9.4%
0.7	2014	1617	19.7%	2040	1.3%	1854	7.9%
0.8	2169	1753	19.2%	2145	1.1%	2005	7.5%
0.9	2298	1888	17.8%	2260	1.6%	2141	6.8%
0.95	2347	1944	17.2%	2300	2.0%	2191	6.7%
1	2382	1959	17.7%	2350	1.3%	2170	8.9%
1.1	2395	1929	19.4%	2375	0.8%	2138	10.7%
1.2	2367	1912	19.2%	2350	0.7%	2095	11.5%
1.3	2328	1903	18.3%	2310	0.8%	2043	12.2%

The averages of all experimental temperatures calculated were as much as 21.5% lower than equilibrium. The Q1(14)/Q1(5) line pair produced the lowest difference (7-21%) when compared with equilibrium data. The percent difference of the temperatures found using nitrogen CARS on a hydrogen-air flame by Hancock et. al (Ref. 30) as compared with equilibrium predictions was much smaller. Experimental data in the current work

were taken lower in the flame as compared with the Hancock data because the mass flow controllers used in the lab were not capable of reaching flow rates necessary to keep the flame stable. While this may lead to slight differences in temperature, it should also be noted the higher flow rates used by Hancock would lead to reduced heat losses due to radiation and conduction. These heat losses could be reasonably assumed to reduce temperatures by 100 K from equilibrium values. Under this assumption, the Q1(14)/Q1(5) could be used to accurately measure temperature within 2.5% of equilibrium depending on equivalence ratio and height above the burner surface.

In order to quantify this accuracy without an assumption, an analysis was performed on the Q1(14)/Q1(5) line pair. Using the standard deviation of the average intensity, two separate ratios were made. One gives the absolute lowest value the temperature could be and the other the absolute highest value. Once these temperatures were obtained they were subtracted from the original temperature obtained, to produce error bars. The original temperature was plotted again with error bars using these plus and minus values and compared to theoretical temperatures, see Fig. 48.
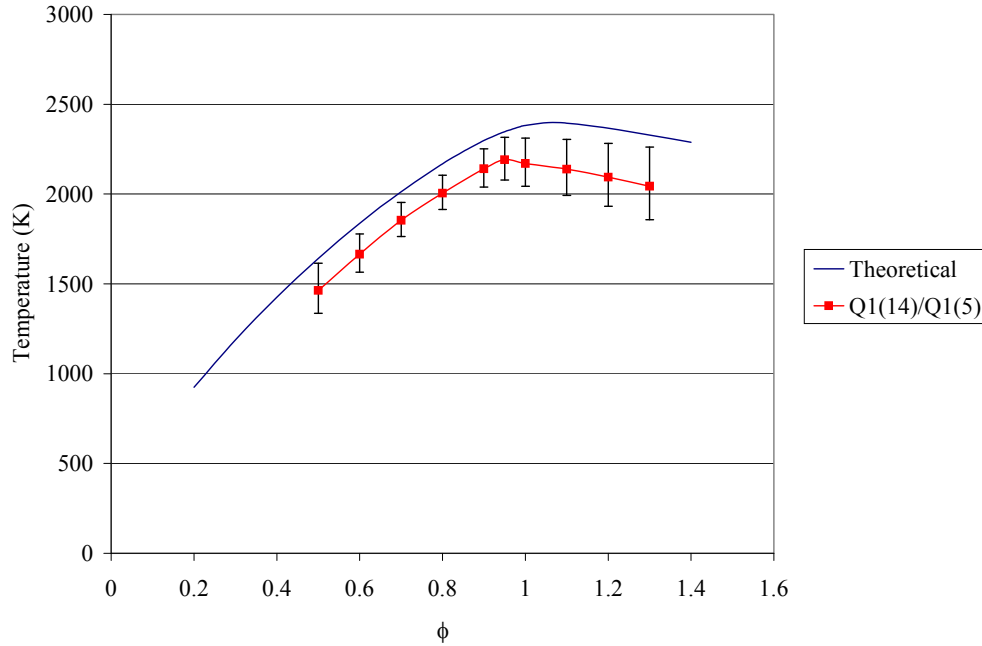
Fig. 48. Experimental compared to theoretical temperature

On the high side, the temperature is within a percent difference of as little as 1%. Notice the experimental line does not peak where the theoretical line does. As stated previously, theoretical data is produced at adiabatic conditions. The Hencken burner flame is not adiabatic, therefore the difference in peaks is due to heat losses of the flame such as radiation and conduction. There is also an entrainment of coflow. In other words there is a mixing of cooler air decreasing the temperature of the flame.

Qualitatively this method could be used to determine methods of hot and cold regions. Fig. 49 is the ratio of two raw PLIF images captured using the Q1(14) and Q1(5) line. It is produced using Win-View 32 software.
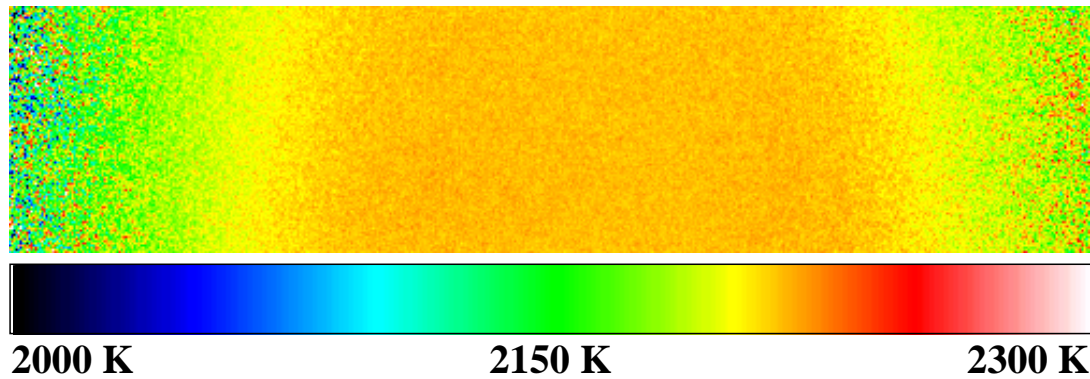
Fig. 49. 2-D temperature map of a laminar flame

A laser sheet was placed through the center of a laminar hydrogen-air flame at an equivalence ratio of 1.0. In this picture, the laser sheet runs from right to left. The images are divided, and their corresponding pixel values have been divided to produce different ratios. Colors have been assigned depending on the value of the ratio. Orange has been assigned to the highest values showing the hottest area of the flame in the middle. Light green has been assigned to the lowest values showing the "cooler" areas at the outside edge of the flame. The Hencken burner flame has a temperature of approximately 2200 K in this location. This is an excellent tool for non-intrusively measuring flame temperature.

PLIF Thermometry – Spectral Analysis

Temperatures were calculated by performing a spectral analysis, also known as a wavelength scan, of each of the lines listed in Table 9. Temperatures of a hydrogen-air flame were measured at two different equivalence ratios, $\phi = 0.7$ and $\phi = 1.0$. Performing this method accurately requires accounting for collisional and Doppler broadening of the

line. This affects the FWHM value. Affects on the ratio of intensity method to obtain

temperature are minimal, since only the peak of the line matters. Both collisional and

Doppler broadening are combined to give the Voigt FWHM, which gives a theoretical

shape of the line (Ref. 38). Fig. 50 is the result of a Voigt line width calculation by

Olivero and Longbothum (Ref. 38).
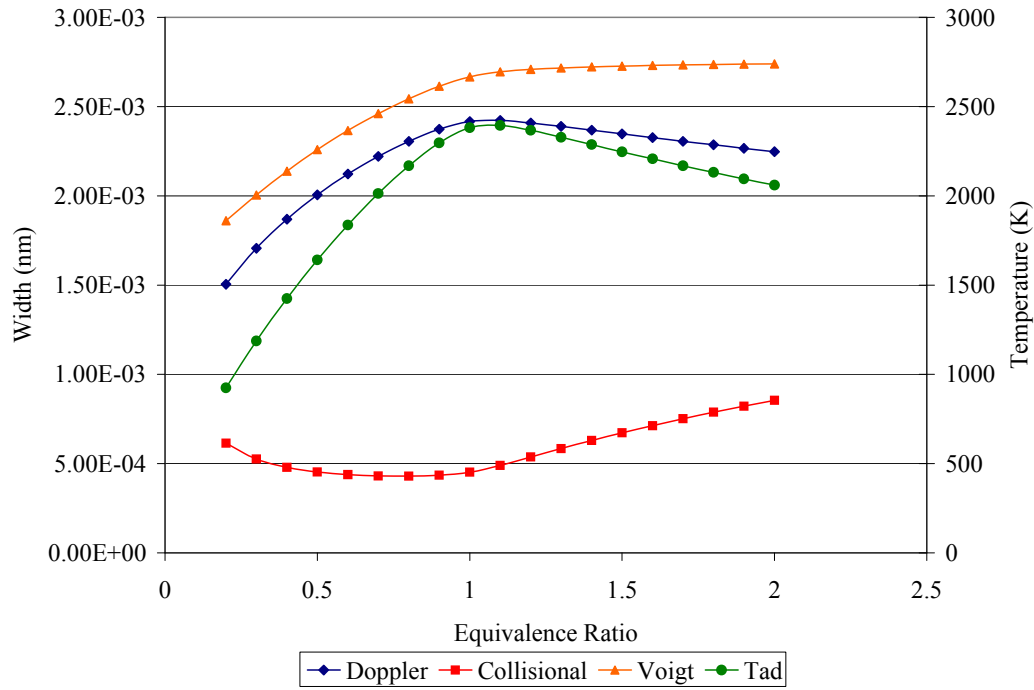
Fig. 50. Collisional and Doppler broadening (Ref. 38)

This particular case is for the P1(7) line at 570.1764 nm. When calculating a FWHM

value to determine a temperature, broadening affects the width of the line. As

temperature increases, the line broadens until $\phi = 1$. Collisional and Doppler broadening

are inversely proportional to one another and the combination of the two affects line

width shape. As a result, if the effects are not taken into consideration, very inaccurate

temperature readings can be produced.

A LIFBASE simulation including Doppler and collisional broadening assumptions was ran on each of the lines at a range of temperatures to determine a theoretical FWHM value. These values were compared to experimental FWHM values obtained from performing a laser scan around the wavelength of a particular line. Temperatures calculated varied between 12% above and 27% below adiabatic flame temperature. The reason for this variance was determined to be a matter of resolution. The dye laser used for the scans is supposed to have a line width resolution of 0.05 cm^{-1} or 0.00162 nm at 570 nm. However, the actual data obtained from the laser proved otherwise. LIFBASE simulations were ran with two different resolutions, one producing a line with an increased resolution from laser specifications and one producing a line with a lower resolution found by matching the experimental data, see Fig. 51.
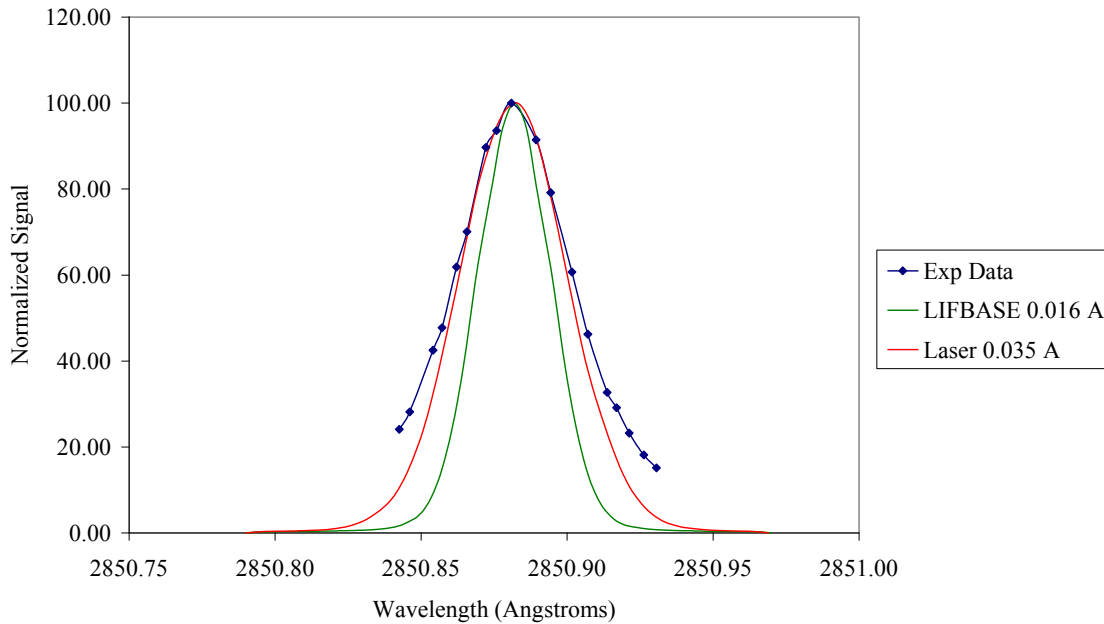
Fig. 51. Line width resolution comparison

It was determined the laser has a lower resolution of approximately $0.0035 \overset{o}{A}$, much

worse than the expected resolution of $0.0016 \overset{o}{A}$. Unfortunately, the dye laser cannot

resolve the OH line width with high precision. In other words, the laser wavelength

distribution is too broad to detect the OH line shape with a great deal of accuracy. For

example, the experimental FWHM value obtained from the P1(7) line at $\phi = 0.7$, plotted

in blue in Error! Reference source not found. above, is 0.047 nm in width. However, the

FWHM value for OH line width at this equivalence ratio is 0.00246 nm. In this case, the

data would produce an extremely high and inaccurate temperature. As a result,

temperature measurements were not made by performing wavelength scans and will only

be made using line ratios as discussed earlier.

4.2   UCC Characterization

Starting Conditions

Characterizing the combustor consisted of first learning how to start it before an

operational regime could be determined. It had never been started before so this was a

process of trial and error, and consisted of developing settings for three main systems to

include heater, ignition, and fuel. A specific starting condition for each system was given

in Chapter 3.5, but here a range of conditions will be discussed.

The main and secondary Gaumer electric air heaters played a major role in getting

the combustor to light. Some of the first flames inside the combustor were most likely

due to the inside getting saturated with fuel. The problem was the fuel was being sprayed

into a cold combustor. To alleviate this problem, each heater was turned on to heat the

air. The main and secondary heater will heat the air for the combustor to almost 450 ºF

(Ref. 3). Caution must be taken to keep the secondary heater from overheating while operating at lower air flow rates required for starting. For good starting conditions, the main and secondary heaters were operated at 300 - 400 ºF and 200 - 300 ºF respectively. This reduced pooling and helped the fuel to ignite faster.

A good ignition system was, of course, very important to get the combustor lit. It consisted of an ethylene-air mixture flowing past an electrical arc produced by a spark plug making a torch. Equivalence ratios were calculated for the mixture and are listed in Chapter 3.2. At first, a fuel-lean mixture was used to light the combustor. However, the ethylene tank is located outside and once it got colder , a fuel-rich mixture was needed to produce a good torch. As the ethylene became colder, more activation energy was needed to ignite at the same equivalence ratio. Air was held constant at 25 slpm and the amount of ethylene was increased from 1.4 slpm to 2.5 slpm, a ϕ range of 0.8 to 1.4. In conclusion, the equivalence ratio needed to light the combustor increased with decreasing temperature of the ethylene.

The main components of the fuel system consist of a fuel pump and nozzles. Optimal fuel pump operation was required to deliver the correct amount of fuel through the nozzles for the right fuel-air mixture. As described in Chapter 3.2, the fuel pump has two modes of operation, constant pressure and constant flow. The fuel nozzles need a pressure above 2.07×10^5 Pa (30 psi) to provide a proper fuel spray for lighting, otherwise pooling will occur. As a result, the fuel pump is operated in constant pressure mode delivering3.45×10^5 Pa (50 psi) for starting. Since each syringe on the fuel pump gives a different flow rate for the same pressure, care must be taken to ensure the flow rate does not exceed 35 ml/min. A good range is 25 - 35 ml/min. The main air flow should be set

at 1.3 kg/min and the secondary air flow at 0.13 kg/min. This will result in an

equivalence ratio of approximately 3.0, an extremely fuel-rich condition. This is needed

to get the combustor lit when it is relatively cold even though the air is heated. The

calculations for ϕ were described in Chapter 3.2, and it is important to note only the

secondary air flow creating the fuel-air mixture inside the cavity is considered. Once lit,

the fuel pump is immediately changed to constant flow mode to more accurately control

the flow of fuel coming into the combustor. Also described in Chapter 3.5, a fuel flow of

20 ml/min is set with the secondary air flow immediately but steadily increased to 0.7

kg/min to keep the flame from blowing out and obtain a stable operating fuel-lean

condition.   Table 13 displays optimal starting conditions for quick reference.

Table 13. Starting conditions for UCC

Condition	Lighting	After Light
Ethylene (slpm)	2.45	OFF
Air (slpm)	25	OFF
Main Heater (ºF)	300 - 400	300 - 400
Secondary Heater (ºF)	200 - 300	200 - 300
Main Flow (kg/min)	1.3	1.3
Secondary Flow (kg/min)	0.13	0.7
Fuel Pump Mode	Const Press	Const Flow
Fuel Flow (ml/min)	25 - 35	20
Cavity ϕ	2.5 - 3.0	0.3

Operational Regime

Several operating conditions were experimented with to determine areas of fuel-

lean, fuel-rich, low emission, and efficient operation. Each condition is given a number

for ease of reference in the following discussion. The combustor rig is fitted with

pressure transducers and thermocouples. Thermodynamic properties such as temperature

and pressure were recorded for every operating condition using experimental data automatically generated in Lab-View. The temperature data is used to plot temperature profiles of the combustor for different operating conditions. Fig. 52 is a drawing of the combustor and shows main vane and cavity air flow direction as well as locations of various pressure transducers and thermocouples.
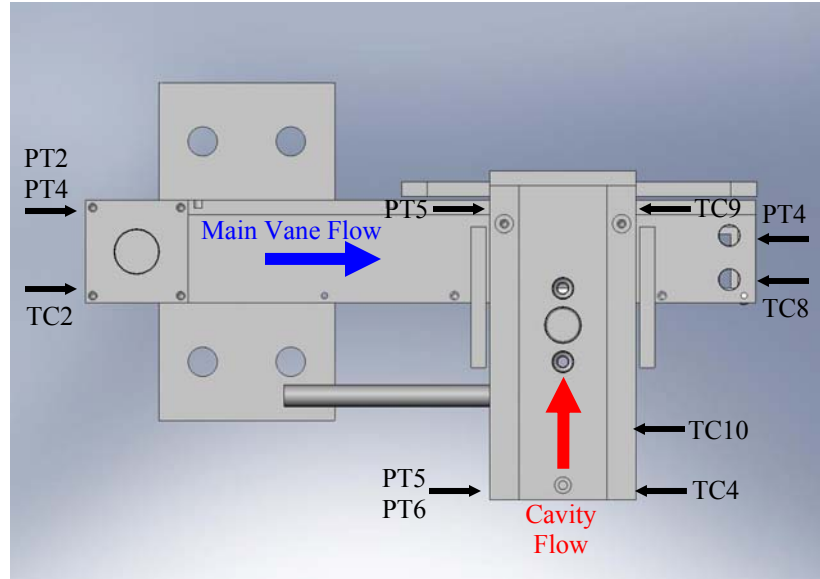
Fig. 52. Drawing of UCC sectional rig using Solid Works

In addition to thermodynamic properties, notes were taken on the external properties of combustor operation such as flame size, shape, and color. Appendix E contains a listing to include a name and location of each pressure transducer and thermocouple number.

Combustion efficiency was calculated using two methods. The first method used temperature data in addition to mass flow rates of air and fuel to calculate combustion efficiency in terms of enthalpy added to the flow, see equation 8. The results are presented in this section. The second method used emissions data from the main vane

exhaust to calculate combustor efficiency, see equation 7. These results are located in the following section titled emissions analysis.

Conditions 1 and 2 consisted of operating with various fuel-air mixtures through the combustor by performing equivalence ratio sweeps holding either fuel flow or air flow constant. The fuel pump was operated in constant flow mode to ensure accuracy of fuel-air mixtures. The equivalence ratio calculations for JP-8 and air found in section 3.2 considered only the fuel-air mixture inside the cavity.

For condition 1, fuel was held constant at 35.7 ml/min (.0267 kg/min) while air flow was varied giving a ϕ sweep of 0.445 - 1.4. As mentioned previously, the equivalence ratio was only a function of air flow in the cavity, but in this condition the main vane air flow was also varied to hold the main vane to cavity air ratio constant at approximately 3.5. Additional conditions were ran with various main vane to cavity air ratios and will be discussed in detail later. Fig. 53 shows the amount of main vane and cavity air flow for each ϕ. The airflow was controlled very precisely within ± 0.015 kg/min and ± 0.025 kg/min of the requested amount of main and cavity flow respectively.
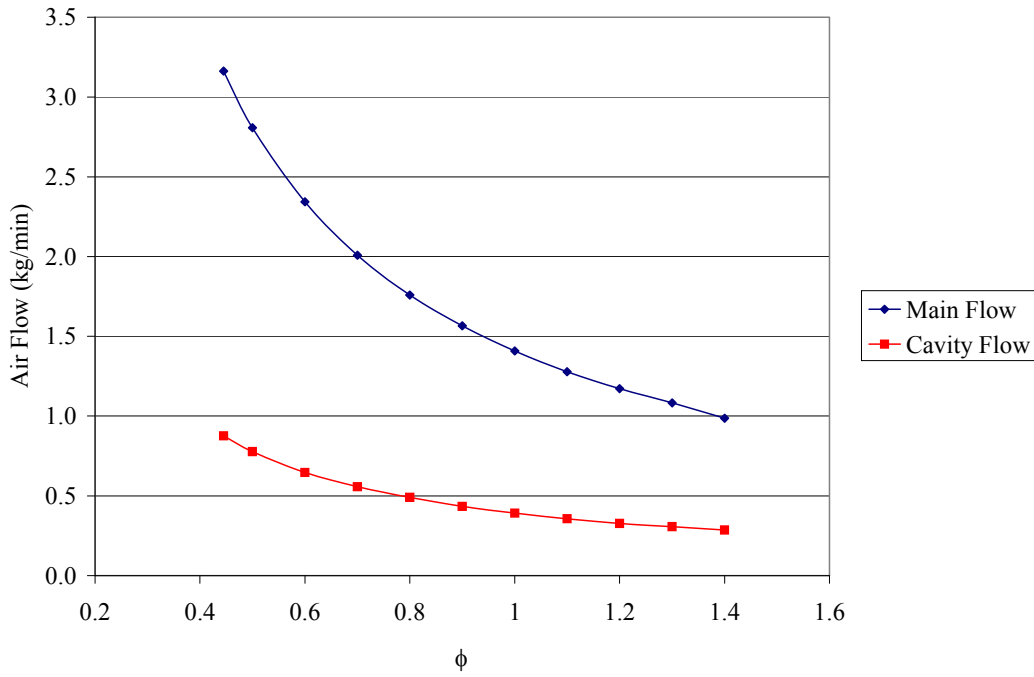
Fig. 53. UCC air flow vs. equivalence ratio (operating condition 1)

The combustor operated well in condition 1. A temperature profile was produced and the highest temperature recorded was at the main flow exit at $\phi = 1.4$. As expected the temperature at the main flow and cavity inlet changed the least. At the exit, the temperature changed the most, increasing with equivalence ratio. The data from these measurements and the amount of temperature increase from inlet to exit is shown in Fig. 54.
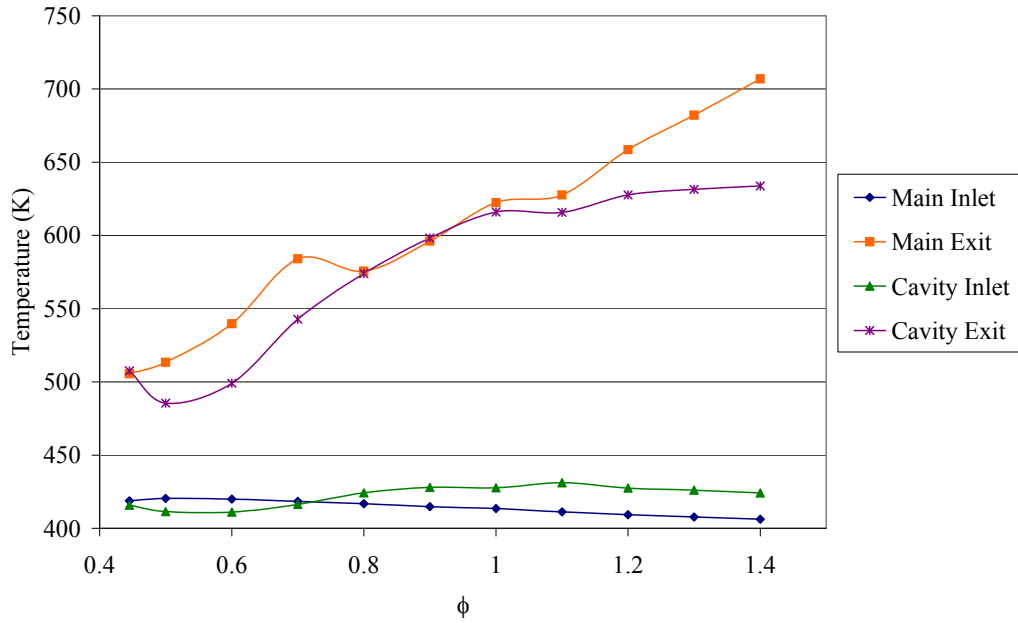
Fig. 54. UCC experimental temperature profile (operating condition 1)

A small blue flame, representative of a fuel-lean mixture, protruded out the cavity exit for $\phi = 0.445$. As the fuel mixture approached stoichiometric conditions, the blue flame increased in size and became orange in color. Fig. 55 shows pictures of the flames at fuel-lean and stoichiometric conditions respectively.
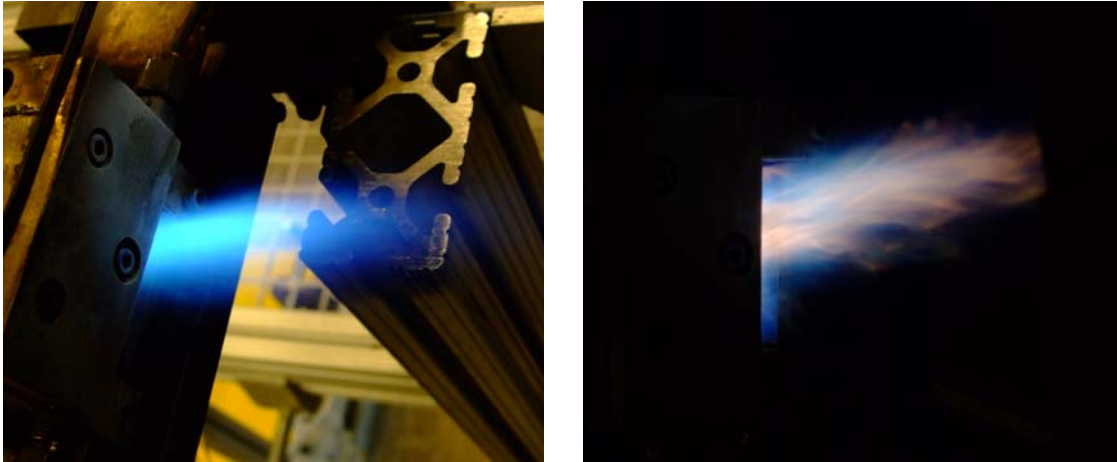
Fig. 55. Combustor flames at cavity exit, ϕ = 0.445 and 1.0

As the fuel mixture became increasingly fuel-rich, the flame increased in sized. The color became an orange-yellow mix at a ϕ of 1.4, see Fig. 56. At this point the combustor was shut down due to the increased amount of exhaust exceeding the limits of the ventilation system in the lab.
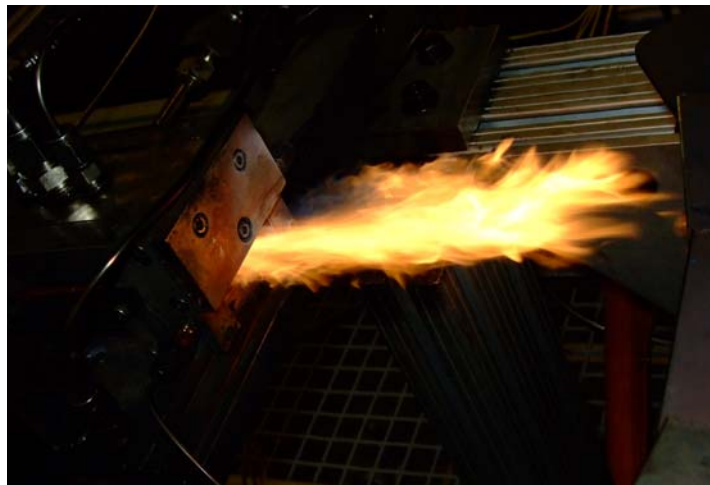
Fig. 56. UCC fuel-rich flame (fuel constant at 0.0267 kg/min)

The highest combustion efficiency for this condition, using mass flow rates and temperature change across the combustor, was only 36 %. This is shown in Table 14, a summary of operating condition 1. A summary of all other operating conditions can be found in Appendix F.

Table 14. Condition 1 experimental data (fuel flow constant)

ϕ_{cav}	ϕ_{Tot}	Main Flow (kg/min)	Cavity Flow (kg/min)	MF/CF	$\Delta P/P_{cavity}$ (%)	ΔT_{Main} (K)	ΔT_{cavity} (K)	η_b (%)
0.445	0.10	3.16	0.88	3.61	4.41	87	92	32.45
0.5	0.11	2.81	0.78	3.61	3.66	93	74	29.08
0.6	0.13	2.34	0.65	3.62	2.79	120	88	30.65
0.7	0.15	2.01	0.56	3.61	2.15	166	126	36.28
0.8	0.17	1.76	0.49	3.59	1.66	159	150	32.05
0.9	0.20	1.57	0.43	3.61	1.41	181	170	32.47
1	0.22	1.41	0.39	3.60	1.17	209	188	33.33
1.1	0.24	1.28	0.36	3.59	0.98	216	185	31.10
1.2	0.26	1.17	0.33	3.59	0.87	249	200	32.39
1.3	0.28	1.08	0.31	3.53	0.80	274	205	32.58
1.4	0.31	0.99	0.29	3.45	0.67	301	210	32.26

The overall equivalence ratio is denoted as ϕ_{Tot} for air flow in both the main vane and cavity. The highest amount of pressure loss for this condition was a little over 4% and decreased with increasing ϕ. This is very low since overall pressure loss is usually between 4 - 10%. Pressure loss for the main vane was not calculated for any condition due to a faulty pressure transducer.

For operating condition 2, main vane air flow and cavity flow were held constant at 0.7 kg/min and 1.1 kg/min respectively while fuel flow was varied giving a ϕ sweep of 0.1 - 1.1. The ratio of main vane flow to cavity flow was held constant at approximately 1.6. At $\phi = 0.1$ the combustor would flame out. This is at a fuel flow of 0.0048 kg/min. To remain lit, the fuel flow had to be increased to 0.00748 kg/min a ϕ of 0.156. This turned out to be a very valuable data point. It was the lowest amount of fuel flow for

which the combustor would remain lit. Fig. 57 shows fuel flow in kg/min as a function of ϕ.
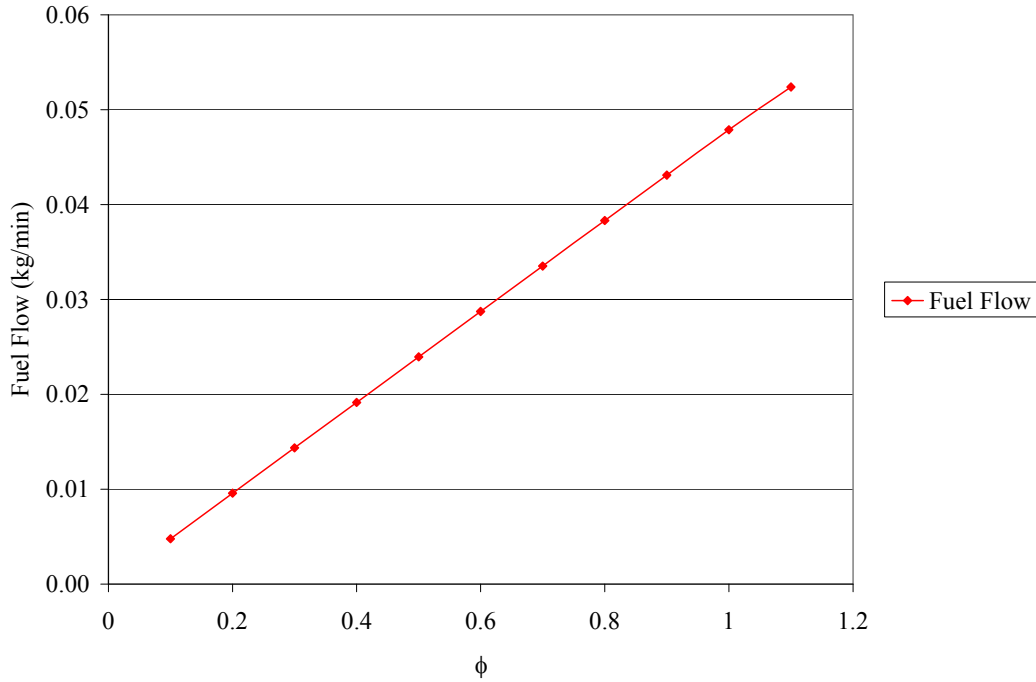
Fig. 57. UCC fuel flow (operating condition 2)

Notes about the flame at the cavity exit were recorded for each fuel flow rate. The flame was completely contained inside the cavity until a ϕ of 0.4 was reached. At $\phi = 1.0$ a large blue flame could be seen coming out of the cavity exit and two small blue flames could be seen coming from the main flow exit, see Fig. 58.
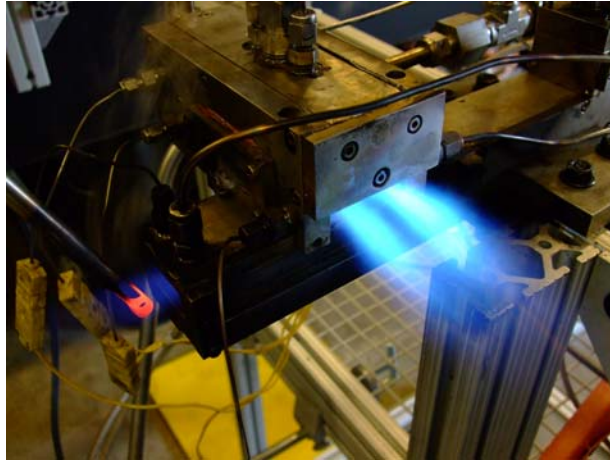
Fig. 58. UCC "dual vortex" flame at stoichiometric conditions

The flame in the picture shows a very promising result. It is the result of a trapped vortex inside the cavity. This is due to air from the main vane flowing in the axial direction meeting air injected into the cavity. In this case there appears to be two vortices. This creates increased mixing of the fuel. It is unclear what actually caused this type of flame since enough operating conditions were not evaluated to rule out the specific cause. However, if the air flow inside the cavity behaves in such a way if conditions are just right and the fuel mixture is rich enough, this second vortex will promote increased burning of the fuel. This will mean the combustor is operating as it should. Additional operating conditions will need to be evaluated to determine the root cause of this desired condition. Shortly after this picture was taken the combustor was shut down. The temperature profile for this condition is shown in Fig. 59.
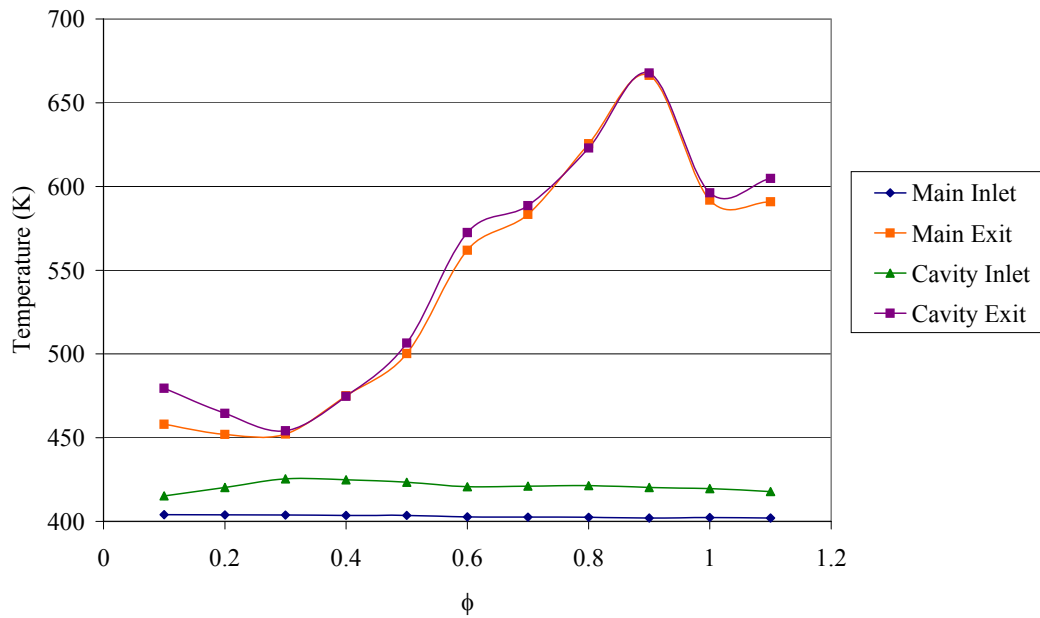
Fig. 59. UCC experimental temperature profile (operating condition 2)

The highest efficiency for this condition was over 55 %. The efficiencies increased and decreased as a function of equivalence ratio. It is possible the fluctuations are due to changes in temperature from inlet to exit. Since there was no change in air flow and the fuel pump was operated in constant flow mode for this condition, this could have been a result of the fuel being improperly atomized. A summary of operating condition 2 can be found in Table 23 located in Appendix F.

The next five conditions consisted of performing equivalence ratio sweeps of $\phi = 0.4 - 1.4$ while varying the ratio of cavity air to main air and amount of fuel flow. A matrix of test events was created to evaluate the combustor at each different operating condition. Three air ratio settings and three fuel flow rate settings were chosen for a total

of nine conditions, see Table 15. The previous operating conditions 1 and 2 are included

in the table.

Table 15. Main & cavity air ratios tested for UCC operational regime

Test Event Matrix		
Event	Main Air / Cavity Air	Fuel (kg/min)
Minimum	3.5	0.0075
Medium	10	0.0187
Maximum	15	0.0299
Condition		
1	3.5	0.0267
2	1.6	0.0088 - 0.0524
3	3.5	0.0075
4	3.5	0.0299
5	10	0.0187
6	15	0.0075
*	15	0.0299
7	15	0.0112

* Exceeds limits of system

Five conditions, encompassing minimums and maximums, were picked to examine the

operating regime of the combustor based on something other than holding fuel or air flow

constant. In Table 15, condition 7 fuel flow was changed to 0.0112 kg/min because the

required air flow to support the combustor at 0.0299 kg/min would have exceeded the

main air flow system limits of 7.0 kg/min. This table is reproduced in Appendix F and G

for ease of reference with the data located there.

Data was not collected for condition 3. Fuel was held constant at .0075 kg/min

(10 ml/min) and the main air flow range was 0.957 - 0.273 kg/min with the cavity air

flow range equal to 0.273 - 0.078 kg/min. This fuel and air flow rate was too low to keep

the combustor lit and the corresponding equivalence ratio sweep of 0.4 - 1.4 could not be performed.

The combustor exhibited stable operation using condition 4. The main air flow range was 3.826 - 1.093 kg/min and the cavity air flow range was 1.093 - 0.312 kg/min creating a main to cavity air ratio of 3.5. Fuel was held constant at 0.0299 kg/min and airflow was varied creating a ϕ range of 0.4 - 1.4 in the cavity. The flame at the cavity exit displayed similar features of other conditions but a dual vortex flame was never produced. It was blue for a fuel-lean mixture and mostly yellow for a fuel-rich mixture. Fig. 60 shows three pictures of the combustor operating in condition 4 at a ϕ of 0.7, 1.0, and 1.6 from left to right.
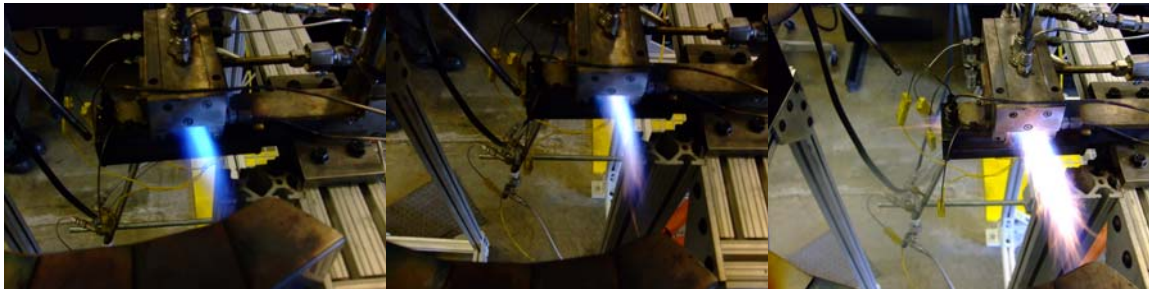
Fig. 60. UCC flames, ϕ = 0.7, 1.0, and 1.6 (air ratio = 3.5, fuel = 0.0299 kg/min, airflow varied)

Flames started to come out of the main flow exit at about ϕ = 1.6 as seen in the far right picture. This meant at fuel rich conditions, not all of the fuel being injected was combusted in the vortex cavity and therefore burned in the main flow channel. This is not optimal because combustion needs to remain inside the cavity for the most efficient extraction of the chemical energy. This was a rare result and will be discussed further in

the following section. The combustor was operated up to $\phi = 1.8$ where a temperature of 836 K was reached in the main vane exit. Fig. 61 shows the temperature profile of operating condition 4.
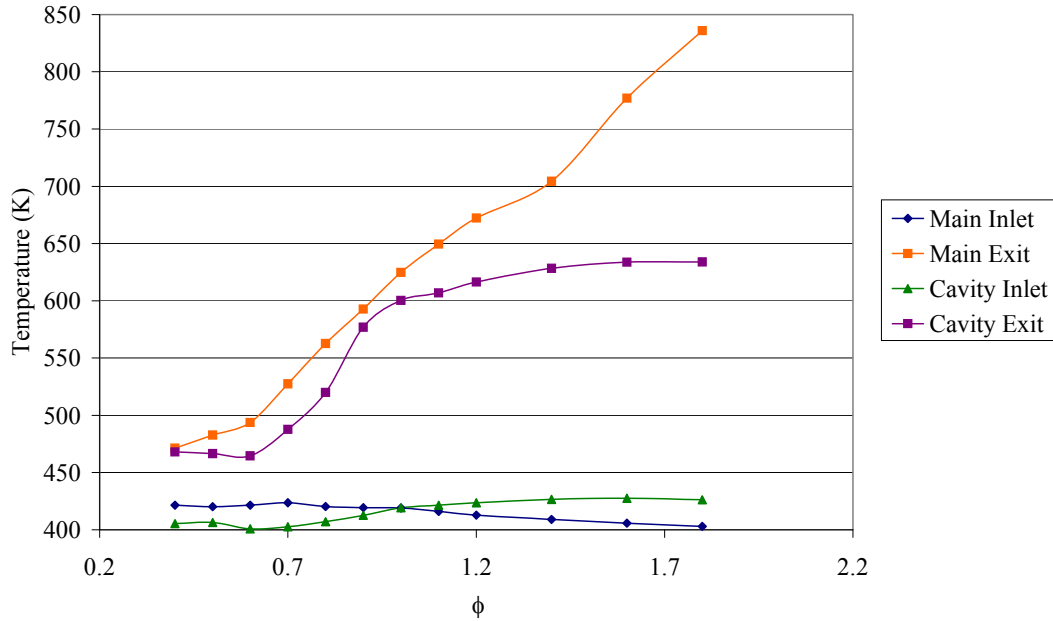
Fig. 61. UCC experimental temperature profile (operating condition 4)

The unique feature about this profile is it shows the largest temperature increase for any condition. Also uncharacteristic, is the cavity exit temperature becoming constant and the main vane temperature continuing to increase. Even though the temperature continues to increase, the efficiencies eventually reach a peak. This is possibly due to improper atomization of the fuel as in previous conditions. Table 19, located in Appendix F, summarizes operating condition 4 of the combustor.

In condition 5, the main air flow range was 6.785 - 1.241 kg/min and the cavity air flow range was 0.686 - 0.118 kg/min while fuel was held constant at 0.0299 kg/min.

This created a ϕ range of a little less than 0.4 to 2.2 in the cavity, and an overall ϕ range of 0.04 to 0.2. Operation for this condition was very stable with a fuel-lean mixture. The flame was completely contained inside the cavity until $\phi = 0.7$. Fig. 62 shows a picture of the inside of the cavity at $\phi = 0.6$. It appears unfocused due to the camera being in direct line with the exhaust but gives a good indication of the flame vortices inside.

Fig. 62. Picture of flame inside UCC cavity

This could possibly be a good condition to place optics inside the cavity and record images of the flame structure. At $\phi = 0.8$ a small blue flame began to protrude out of the cavity exit. This condition was used up to $\phi = 2.3$ where the mixture became extremely fuel-rich, and the fuel began to pool. The test was obviously stopped at this point and it is not recommended to operate this fuel-rich again. The highest temperature reached for this condition was 568 K at the main vane exit. The temperature profile can be seen in Fig. 63.
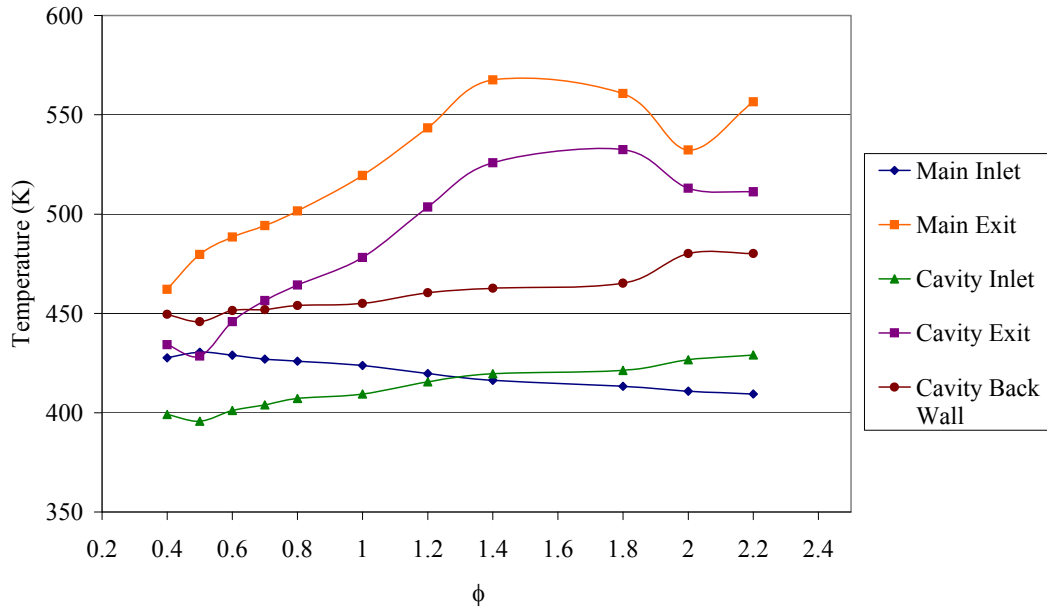
Fig. 63. UCC experimental temperature profile (operating condition 5)

This temperature profile shows the temperature of the back wall of the cavity in addition to the inlet and exit temperatures. The temperature of the cavity back wall was 460 K for $\phi = 1.2$. At this same ϕ an infrared image was taken of the back wall, see Fig. 64.
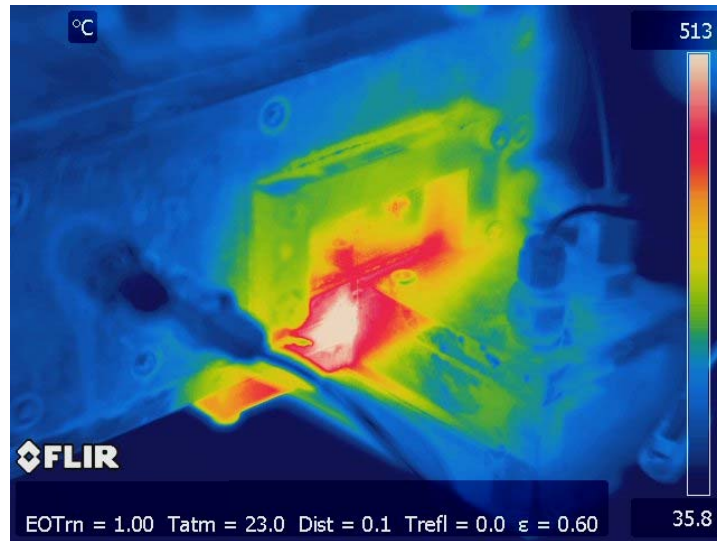
Fig. 64. Infrared image of UCC

107

This image was taken with a FLIR SC640 high definition infrared camera with a ± 2 degree Celsius (ºC) accuracy. This is an additional way of characterizing the temperature distribution of the UCC and is a close approximation. The cavity back wall is approximately 200 ºC (473.15 K) by the scale in this image.   This is within 2.8% of the cavity back wall temperature measured with a thermocouple. As a result, the thermocouple data can be used to anchor the temperatures produced by the infrared camera. In addition, the hottest area of the image appears to be at the cavity vane interaction point. This is a positive result. Increased mixing appears to taking place in this area. This supports a UCC objective to determine if the main vane can retrieve optimal mass extraction from the cavity. A summary of operating condition 5 is given in Table 20 located in Appendix F.

For condition 6, the main air flow range was 4.1-1.367 kg/min and the cavity air flow range was 0.273-0.091 kg/min while fuel was held constant at 0.00748 kg/min. This created a ϕ range of 0.4 to 1.2 in the cavity and an overall ϕ range of 0.2 to 0.73. Operation was similar to condition 5 at $\phi < 1$ but became unstable after $\phi > 1$. The problem was the air and fuel flow were too low here to sustain stable operation. The temperature profile created with condition 6 did not vary as much with equivalence ratio as the previous conditions, see Fig. 65.
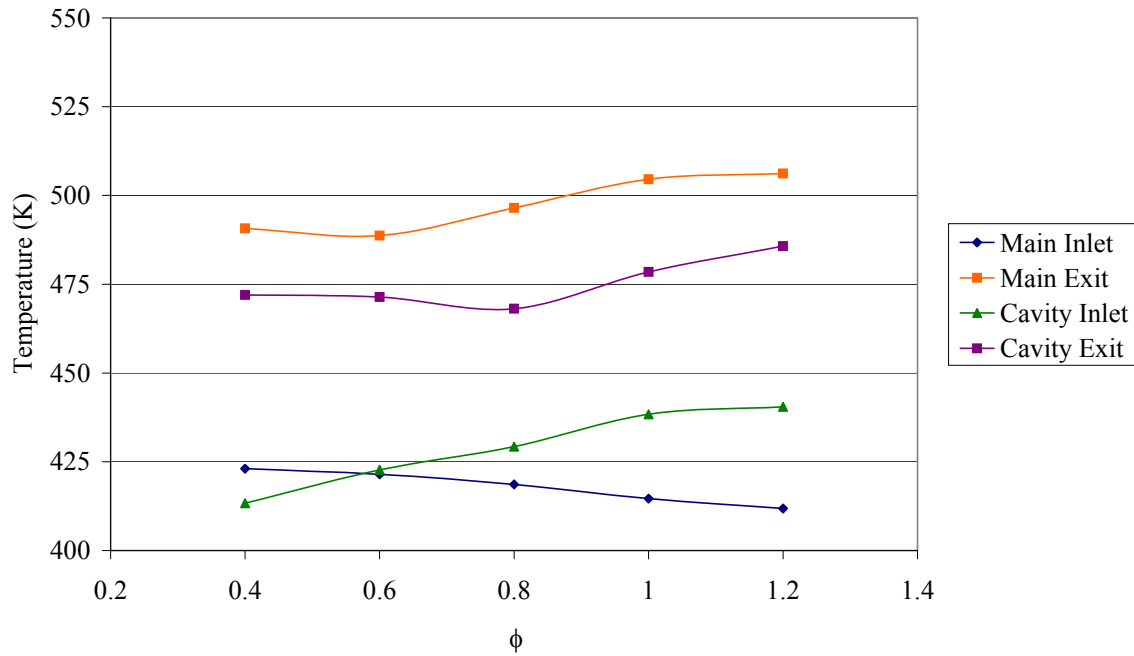
Fig. 65. UCC experimental temperature profile (operating condition 6)

The main vane exit temperature remained within 6% of the cavity exit temperature. This relationship shows heated mass flow is being drawn out of the cavity. Condition 6 produced one of the highest efficiencies recorded in terms of mass flow. This was a fuel-lean condition with the highest air ratio of the experiment. A summary of operating condition 6 is given in Table 21 located in Appendix F.

Condition 7 was the last test event for air ratio and fuel flow. Operation at this condition was possibly the best. The main air flow range was 6.15 - 1.757 kg/min and the cavity air flow range was 0.41 - 0.117 kg/min while fuel was held constant at 0.0112 kg/min. This created a ϕ range of 0.4 to 1.4 in the cavity and an overall ϕ range of 0.03 to 0.09. Operation was similar to condition 5 and was stable over the range of equivalence ratios. The cavity flame remained inside until $\phi > 1$. This is another

possible operating condition that could be used to take optical measurements inside the cavity. The temperature profile created with condition 7 can be found in Fig. 66.
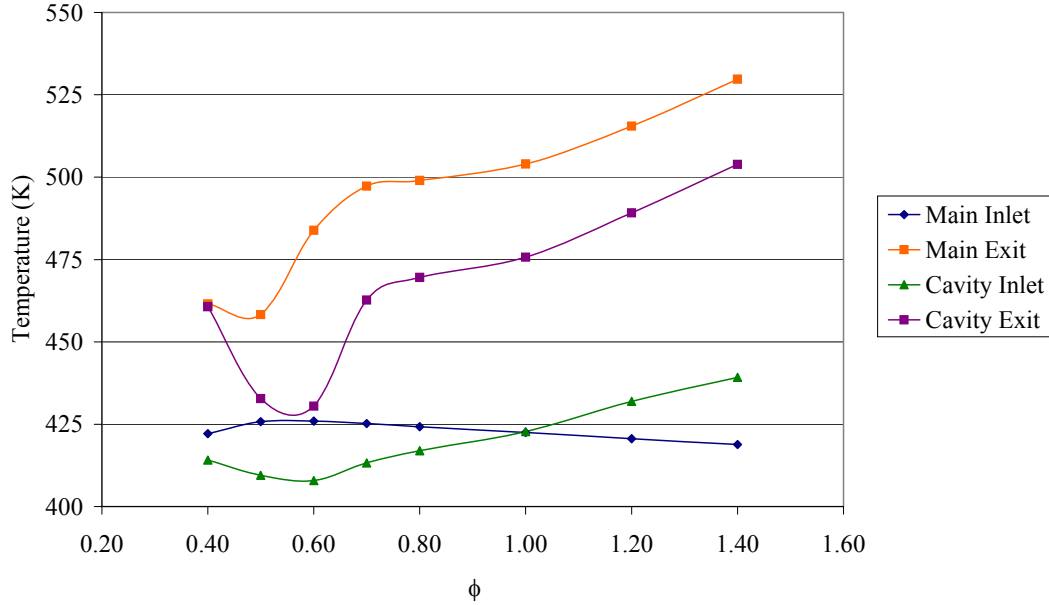
Fig. 66. UCC experimental temperature profile (operating condition 7)

This temperature profile is similar to the one for condition 6 because both conditions have the same main to cavity air ratio. The combustor efficiency is comparable to condition 6 also. Table 22 summarizes operating condition 7 and is located in Appendix F.

The next operating conditions are from the CFD analysis done by Moenter (Ref. 16). The conditions are labeled ATM 1 and 2 for atmospheric 1 and 2. For both conditions the air ratio was 4.5, $\phi = 1.6$, and $\phi_{tot} = 0.29$. ATM 1 required cavity and main air flow to be 0.243 kg/min and 1.099 kg/min respectively while fuel flow was at 0.0267 kg/min (35.7 ml/min). ATM 2 required cavity and main air flow to be 0.195

kg/min and 0.879 kg/min respectively while fuel flow was at 0.0214 kg/min (28.61 ml/min). Both conditions were extremely fuel-rich. Operating the combustor at these conditions caused fuel to pool up and catch fire, resulting in flames coming out of unsealed areas. Basically the air flow was too low to put such an amount of fuel through the combustor. As a result, each condition was operated only a few times to obtain pressure, temperature, and emissions data. The experimental temperature data can be seen for both conditions in Table 16.

Table 16. ATM 1 and ATM 2 experimental data

Condition	ϕ	ϕ_{Tot}	Main Flow (kg/min)	Cavity Flow (kg/min)	MF/CF	$\Delta P/P_{cavity}$ (%)	ΔT_{Main} (K)	ΔT_{cavity} (K)	η_b (%)
ATM 1	1.6	0.29	1.099	0.243	4.5	0.51	313	175	34.44
ATM 2	1.6	0.29	0.876	0.195	4.5	0.39	261	150	29.09

The main vane temperature is the highest in each condition and is characteristic of fuel-rich conditions where the temperatures are elevated at higher equivalence ratios.

Extremely valuable data was collected from every operating condition. Combustor efficiencies calculated using mass flow rates and temperature data were much lower than those calculated with emissions data as will be seen in the following section. Summarizing the operating regime of the UCC, it will flame out at low fuel and air flows of about 0.0075 kg/min and 0.13 kg/min respectively resulting in cavity equivalence ratios of less than 0.4. It is too fuel rich at cavity equivalence ratios of 1.6 and above. The best envelope of operation is any fuel flow from 0.0187 kg/min to 0.0267 kg/min, and any air flow from 0.7 kg/min to 1.4 kg/min producing a cavity equivalence ratio of 0.4 to 1.4. In conclusion, an operating regime has been determined for the UCC.

Emissions Analysis

Emissions data was recorded at atmospheric pressure using a portable emissions analyzer described in section 3.5. Measurements were taken with the emissions probe placed one inch from the main vane exhaust plane. Pollutant emissions of concern in combustion design such as unburned hydrocarbons (UHC), carbon monoxide (CO), and nitrous oxide (NO_x) are presented in terms of EI. Combustor efficiency is calculated using this data.

Emissions data was not recorded for conditions 1 and 3. Emissions data was collected over a range of equivalence ratios for each operating condition. Similarities among certain conditions, like equal air ratio, were plotted showing produced emissions for changing fuel flow. Operating condition 6 and 7 were used here because both these conditions use a main to cavity air ratio of 15 and the fuel flow rate is different between the two. This is shown in Figures 67 - 69.
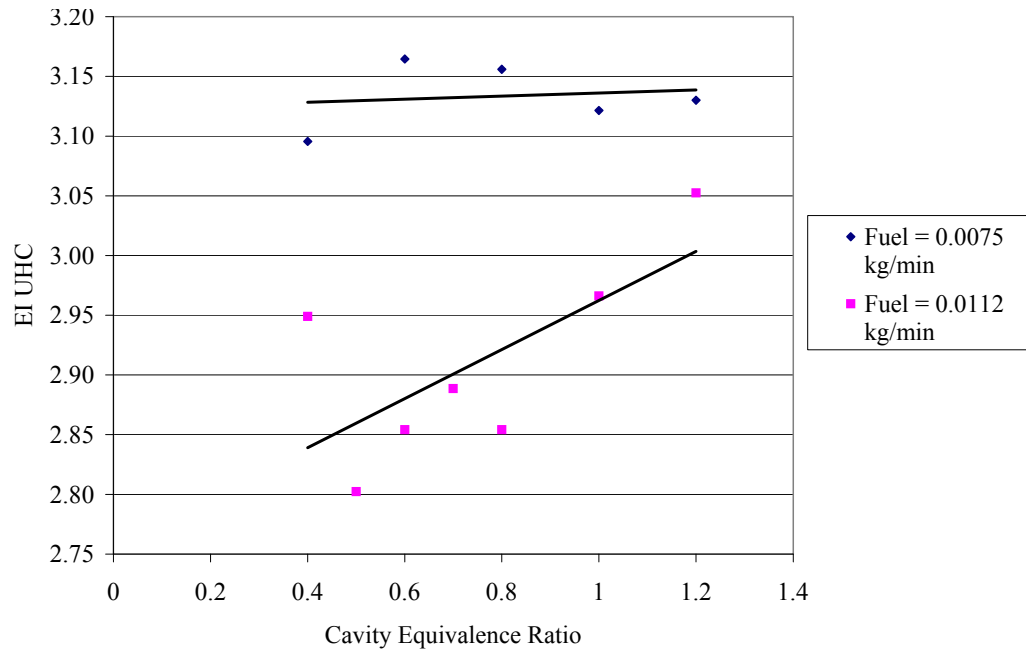
Fig. 67. UCC UHC emissions for $\dot{m}_{main}/\dot{m}_{cav} = 15$
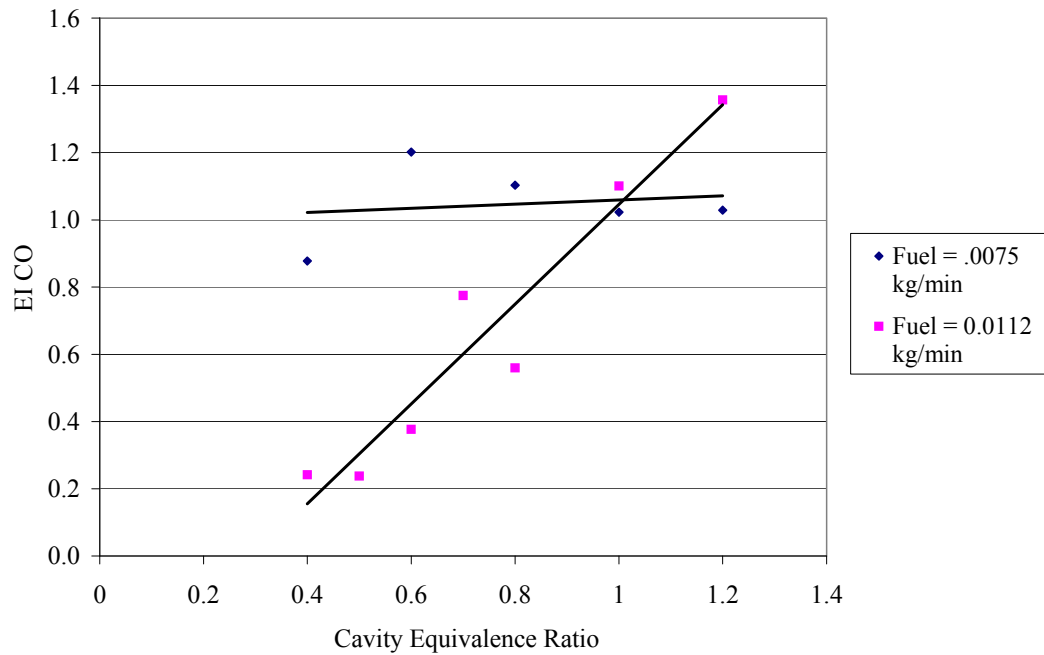
Fig. 68. UCC CO emissions for $\dot{m}_{main}/\dot{m}_{cav} = 15$
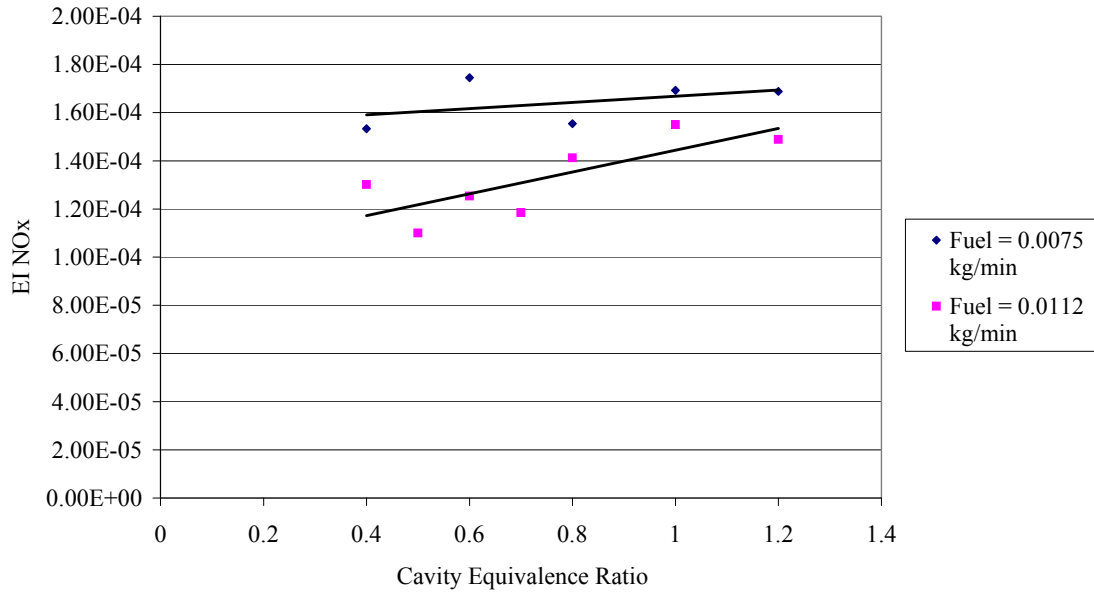
Fig. 69. UCC NO_X emissions for $\dot{m}_{main}/\dot{m}_{cav} = 15$

UHC emissions are the result of incomplete combustion to include inadequate burning rates, poor fuel atomization, and decreased residence time. As seen in Fig. 67, more UHC is produced for increased fuel flow. The higher fuel flow rate shows a more constant increase. The fluctuation in the lower fuel flow rate is most likely due to accuracy error. The most contrasting relation is shown for CO emissions in Fig. 68. For different fuel flows, the data intersects at $\phi = 1$. The lower fuel rate produces an increased amount of CO with increasing equivalence ratio at a faster pace over the higher fuel rate. This is shown by the greater slope in the data. Emissions of NO_X remain mostly constant for both fuel rates.

Emissions data was also plotted for similarities among certain conditions such as approximately equal fuel flow with different air ratios. Operating condition 5 and 7 were used because both these conditions use a similar fuel flow rate of 0.0187 kg/min and

0.0112 kg/min with an air ratio of 10 and 15 respectively. These plots are created to show how emissions change as fuel is held mostly constant and main to cavity air ratio is increased. This is shown in Figures 70 - 72.
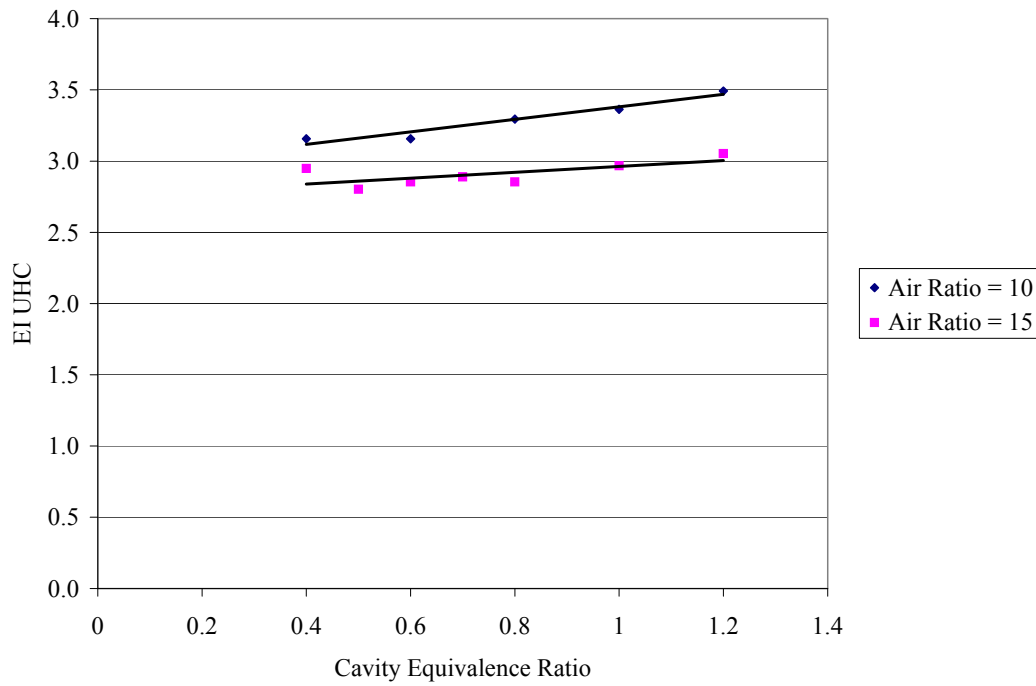
Fig. 70. UCC UHC emissions for approximately equal fuel flow
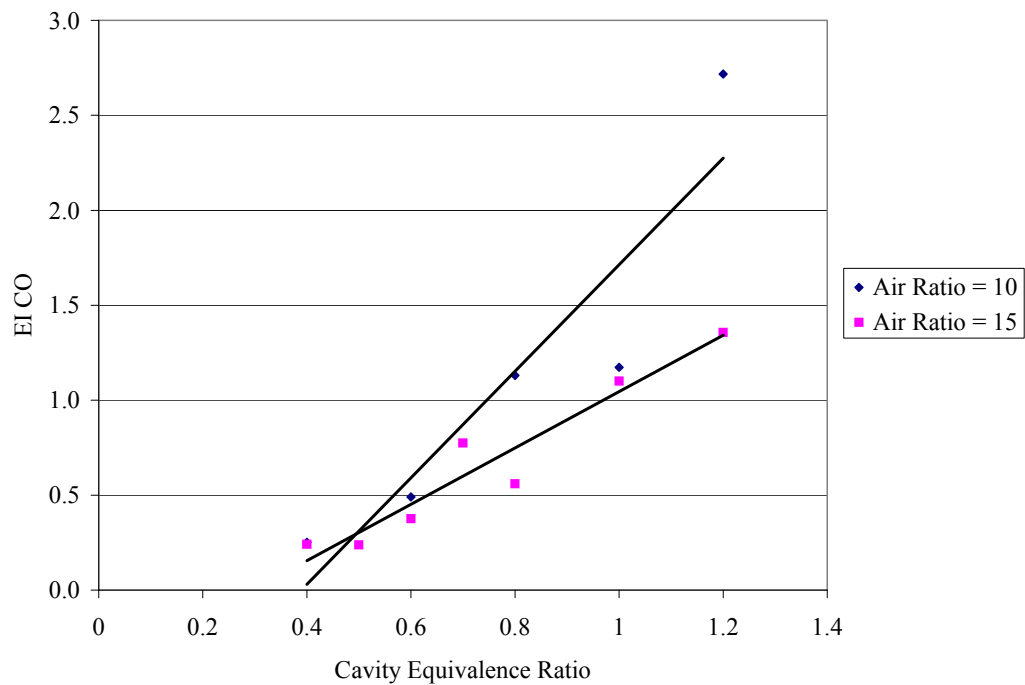
Fig. 71. UCC CO emissions for approximately equal fuel flow
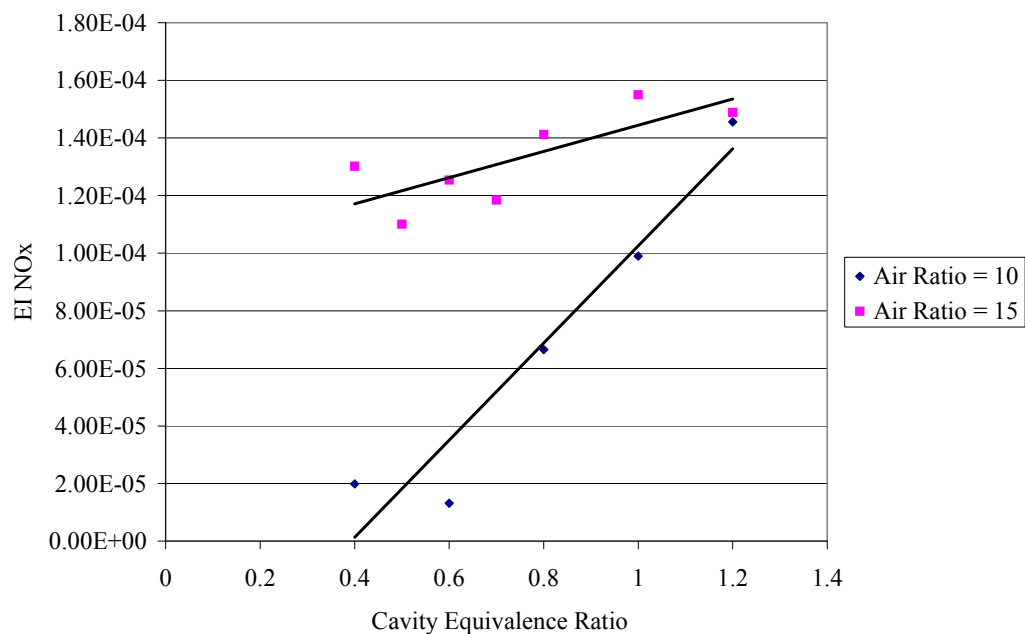
Fig. 72. UCC NO$_X$ emissions for approximately equal fuel flow

116

UHC is mostly constant with changing air ratio. It is reasonable a little more is produced with the small increase in fuel flow. The biggest change in emissions as a function of air ratio are shown by CO and NO_X. A higher air ratio produces the most CO and lowest amount of NO_X.

Along with emissions data, verification of incomplete combustion is provided in how the emissions measurements were taken. The emissions probe, seen in Fig. 36, was placed one inch from the main vane exhaust plane down stream of where the bulk of the burning occurred. Most importantly, the main flow was below this area of burning and therefore carried only trace particles of combustion along with it. Evidence of decreased emissions produced at this measurement location is proven by increased efficiencies of over 98%. The emissions index of UHC and CO were used to calculate combustor efficiency using equation 7. As the quantity of these emissions is increased, efficiency decreases. For increasing equivalence ratio, both UHC and CO increased. This means as the fuel mixture becomes increasing rich, less is burned efficiently. These trends are displayed in Fig. 85 found in Appendix G. Efficiency data was also plotted for both previous scenarios where either fuel or air ratio was held constant. This is shown in Figures 73 and 74.
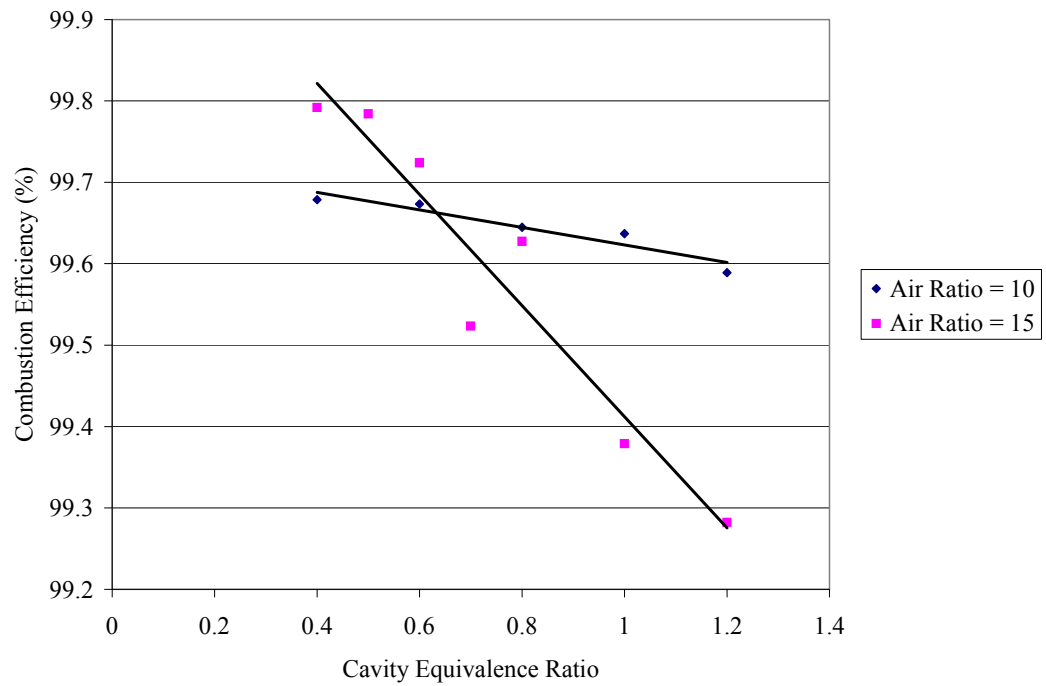
Fig. 73. UCC efficiency as a function approximately constant fuel flow
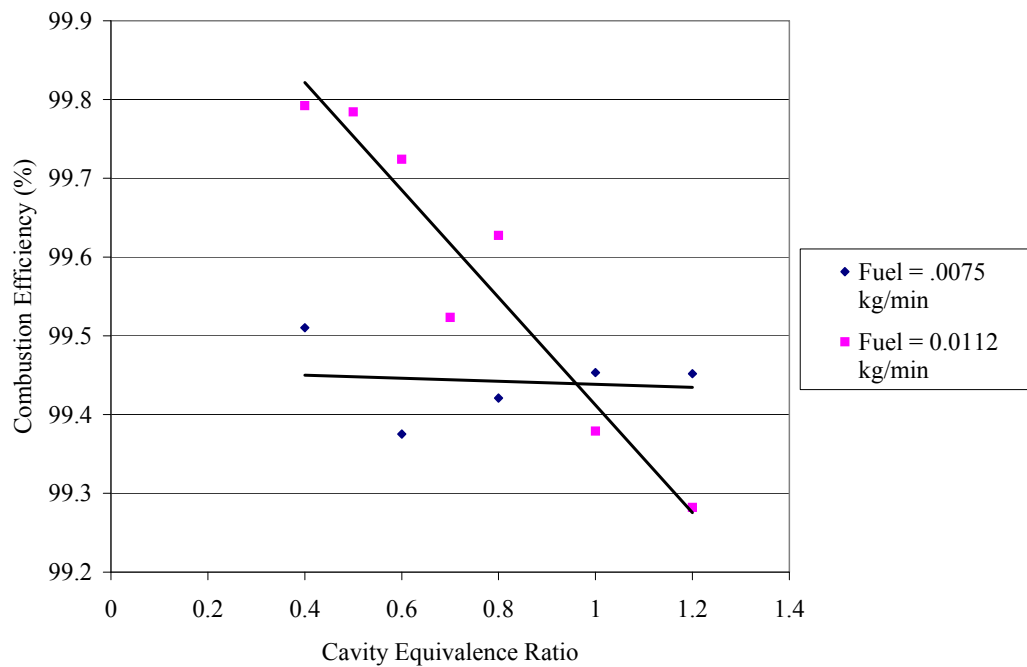
Fig. 74. UCC efficiency with $\dot{m}_{main}/\dot{m}_{cav} = 15$

118

For the sake of brevity, additional emissions data can be found in Appendix G. Emissions index versus cavity equivalence ratio and temperature are plotted there. Tables of raw emissions data for different operating conditions are also placed in Appendix G. Figures should be referenced for the following discussion. Most of the emissions were produced at lower temperatures as seen in Figures 82 – 84. This also provides evidence of inadequate burning. CO is a byproduct of incomplete combustion and is more prevalent in fuel-lean mixtures as seen in Fig. 80. NO_X emissions are high for long residence times and Fig. 81 shows only trace amounts. Every operating condition produced fewer emissions on the fuel-rich side of stoichiometric. It is a possibility condition 6 produced more emissions because the air ratio of 15, higher than any other condition, pulled more combustion products out of the cavity. This further proves most of the combustion process is occurring inside the trapped vortex cavity and a majority of emissions produced are exiting out of the cavity exhaust. Visual evidence of this provided by the large flames at the cavity exit and none at the main vane exit. As a result of this information, it can be reasonably assumed the combustor is operating as it should. Further research is needed and this information gives reasonable relative values to use when comparing with the curved section combustor in later experiments.

The last set of emissions data came from operating the combustor at Moenter's (Ref. 16) conditions, ATM 1 and ATM 2. Experimental data turned out to be drastically different from CFD data as seen in Table 17.

Table 17. CFD emissions & efficiency data compared with experimental results

Condition	CO (ppm)	NO$_x$ (ppm)	UHC (ppm)	% O$_2$	% CO$_2$	η_b (%)
EXP ATM1	1577.90	7.00	1740.00	18.84	2.08	99.88
CFD ATM 1	2586.95	102.81	1.35	16.23	2.85	99.12
EXP ATM2	208.00	1.30	790.00	20.87	0.51	99.92
CFD ATM 2	1665.53	42.43	0.72	16.01	3.05	99.45

The biggest difference occurs in readings CO and UHC. Calculated efficiencies were very comparable to efficiencies obtained with CFD, however, the actual operation of the combustor was very inefficient. It was very fuel-rich when operated at these conditions and fuel could be seen dripping out of the combustor during operation. When using Moentor's emissions data from ATM 1 and ATM 2 to calculate efficiencies using the ARP equations used in this research, efficiencies of 94.96% and 88.78% were calculated. Various reasons are assumed to be the caused of such differences in data. It is very possible the theoretical CFD data was calculated using different versions of the ARP equations to calculate emissions index. Also, the data from the Testo 350 portable emissions analyzer has questionable accuracy when recording minimal data points. It is possible that enough data points were not recorded during the experiment. There also remains the possibility the experimental data is much different than theoretically predicted CFD analysis. In conclusion, further experimentation is needed both in the CFD analysis and experimental operation of the UCC in order to produce an accurate theoretical code for the combustors actual operation and performance.

V. Conclusions and Recommendations

5.1 Laser Diagnostics

The AFIT COAL lab is now configured to begin laser diagnostic testing on the UCC. The laser system has been validated with the use of a laminar flame produced by a Hencken burner and is set-up to do OH PLIF. The process of operating the laser to collect accurate data has been fine tuned. Concentration and temperature measurements have been taken and the accuracy proven with comparisons to theoretical data and past research. It is recommended to use line ratios instead of spectral analysis for temperature measurements until the problem of laser resolution can be resolved. The best lines to use for PLIF thermometry are the Q1(14) and Q1(5) lines at a wavelength of 572.913 nm and 565.5008 nm respectively. Quantifiable, non-intrusive laser diagnostics can now be performed on the inside of the UCC where an unknown flame structure exists.

5.2 UCC Operation

Data collected while operating the UCC has proven it is possible to achieve every goal set in place by the current UCC research objectives. Nothing proves this more than the combustion efficiency calculated from the main vane exhaust and overall mass balance. Efficiencies of over 98% were discovered at the main vane exhaust and efficiencies of up to only 55% were discovered overall. This shows fewer emissions are exiting the main vane exhaust and possibly more are being exited out of the cavity exhaust. As a result, less mass than expected is being pulled out of the cavity. This enables the UCC to operate effectively but with some variation from a full annular combustor. Unburned products are being left inside the cavity to be further burned. In an

annular UCC, the cavity would not have an exhaust and these products would be left to recirculate inside the cavity for increased burning and enhanced combustion efficiency. It should be noted, however, with this flat cavity, there is no centripetal acceleration to cause a pressure gradient to transport hot gasses towards the center, or in this case the main flow. Also, the decreased efficiencies calculated using overall mass balance could possibly be the result of the fuel not getting atomized correctly. If this happens not all of the fuel will burn and it will get blown out of the cavity exhaust. This is very possible considering the biggest temperature difference across the cavity was only around 400 K. It is recommended to flow fuel through the fuel nozzles at 2.07×10^6 Pa (300 psi), a factory recommended setting, and study the operation of the combustor. However, as discussed previously, the fuel pump has only two modes, constant pressure and constant fuel flow. When operating in constant pressure it is going to output a flow rate to support 2.07×10^6 Pa (300 psi). This will pump entirely too much fuel to the combustor. Alternative fuel nozzles should be considered for future research.

Characterization of the UCC is now complete. All major components used to control the UCC such as Lab-View and the fuel and air supply systems have been thoroughly evaluated. An operational procedure has been documented. An optimal starting procedure and a verified operating regime have been discovered. Operating condition 2 is the best in terms of stable operation. It is recommended to use either condition 5 and 7 for taking optical measurements of the flame inside the cavity. In conclusion, safe and controlled operation of the UCC has been proven, and the COAL lab is now ready to support state-of-the-art research in combustion diagnostics.

5.3   *Future Work*

A few modifications to the lab need to be completed. The ventilation system needs to be upgraded to properly vent the amount of exhaust the combustor produces. An electric pneumatic valve operated through lab view should be installed to replace the manual fuel shut-off valve on the pole near the combustor for safety reasons. Once these modifications are complete the lab will be ready to resume combustion diagnostics.

The first thing to do when operating the combustor again is to install the quartz windows and determine if they crack due to thermal expansion. Next will be to determine which operating condition least affects the optical clarity of the window with combustion products. A few operating conditions have been recommended, but before taking optical measurements of the inside of the combustor, another experiment with the Hencken burner should be performed. A higher combined air and fuel flow rate of at least 70 slpm should be used to see if temperatures get closer to theoretical data. The reason is the more the flow rate, the higher the flame will be lifted off of the burner surface, and the closer the flame will be to adiabatic (no heat loss). If the flame is lifted higher, then less heat will be conducted to the burner surface and the more adiabatic the flame will be.

Once the experiment with the Hencken burner is complete, PLIF can be performed on the inside of the combustor. Areas of burning can be located and temperature measurements can be made. To determine flow structure, such as trapped vortex flow, PIV should be used. It can either be done alone or simultaneously with PLIF. The ability to perform these laser diagnostic techniques is the key to understanding the complex flame structure inside the UCC.

APPENDIX A: COAL Lab Operation Procedures

Lab Equipment Start-Up:
1. Turn ON valve feeding black air tank for instrument air
2. Turn ON computer
   a. Open Lab-View
   b. Open "Combustion **Lab – Anderson Alex and Terry** Final.vi"
3. Ensure power strip ON in back of computer cabinet (powers the DC supply, SCXI 1100 and DAQ Pad 6508)
4. Turn ON DAQ pad
5. Press "Run" on "Combustion Lab – Anderson Final.vi"
   a. Listen for fuel pumps to turn on (takes 5 sec)
6. Ensure pressure in control valve to IPT^2 reads 20-40psi and control valve to other equipment reads80-90psi
7. Turn on "Equip" switch
8. **CAUTION** – On wall by lab entrance turn lab ventilation OFF (in case of fire this will ensure smoke will not get transmitted to other parts of the building setting off fire alarms)

Hencken Burner Start-Up (See section 3.3 for step-by-step explanation.)
1. Power up MKS-247D digital control panel (give 30 minute warm-up time) Turn "Power" Toggle Switch "ON"
2. Turn on Fuel, Air, and Nitrogen in tank farm (open regulators on tanks – see direction to turn on knob)
3. Leave tank farm unlocked for emergency shutdown procedures and to perform hourly checks
4. Open valves for Fuel, Air, and Nitrogen on wall behind MOKON machine
5. Check lines from regulator to mass flow controllers for leaks (periodically)
6. Set desired mass flow rates on MKS-247D digital control panel
   a. Turn "Display Channel" Rotary Switch to desired channel
      i. Channel 1- Fuel
      ii. Channel 2- Air
      iii. Channel 3- CO-Flow (Nitrogen)
   b. Push Toggle Switch Up and Hold "Set Pt." for each channel
   c. Turn screw to desired percentage
   d. Release Toggle Switch
   e. Desired Equivalence Ratios for Hydrogen can be found in "Equivalence Ratios for H2.xls" on desktop
7. Turn On "Fan" switch at Computer Control Station
8. **CAUTION:** Before performing steps 9, 10, and 12 ensure there is positive pressure to the controllers (check steps 2 and 4)
9. Turn Toggle Switch "On" Channel 2-Air on digital control panel (green light will illuminate) and let stabilize
10. Turn Toggle Switch "On" Channel 1-Fuel on digital control panel (green light will illuminate) and let stabilize

11. Light Flame
12. Once lit, turn Toggle Switch "On" Channel 3-CO-Flow on digital control panel (green light will illuminate)
13. Equivalence ratios may be changed during operation by turning the screw for fuel or air on the MKS-247D digital control panel

Hencken Burner Shutdown:
1. Turn "Off" Toggle Switch for fuel, air, and nitrogen in this order (green lights will go out) on MKS-247D digital control panel
2. Flame will extinguish
3. Close valves for Fuel, Air, and Nitrogen on wall behind MOKON machine
4. Turn fuel, air, and nitrogen off out in tank farm by closing regulators – see direction to turn on knob
5. Lock tank farm door when all bottles are closed
6. Power Down MKS-247D digital control panel – Turn "Power" Toggle Switch "Off"
7. Turn off fan
8. Put cover on top of burner to keep dirt out

UCC Start-Up Procedure
1. Perform all steps in "Lab Equipment Start-Up" above – ensure step 8: lab ventilation off
2. Turn on all required bottles in the tank farm
3. Leave tank farm unlocked for emergency shutdown procedures and to perform hourly checks
4. Open manual ball valves(red handles) on main and secondary rig air lines – located on wall behind laser control station
5. Turn ON main and secondary Gaumer heater circuit breakers
    a. Turn the black lever to ON
    b. Turn the green button CW to ON
6. Turn ON the "Fan" switch to turn on the exhaust
7. Set the desired main and secondary air flow rates on the Lab-View control screen (range for main: 0 – 7 kg/min; range for secondary: 0 – 2 kg/min)
8. Turn ON the main and secondary air lines on the control screen
    a. It will take a few seconds for the air to reach a steady state condition
    b. Adjust knobs located on top right of computer control station to increase or decrease the demand for air
9. Once air is on, set the desired air line heater temperatures on the control screen
    a. It will take approximately 30 minutes for the rig to heat up
    b. **CAUTION** – air flow at lower rates can cause over-temp on heaters – use higher air flow until heaters stabilize
    c. If over-temp should happen increase air flow and decrease heater temperature setting on control screen
    d. Only after over-temp condition no longer exist will the yellow light go out by pushing reset button on circuit breaker panel door

10. Turn ON MOKON oil machine (If taking emissions measurements with California Analytical Instruments gas analyzer)
    a. Check fluid level
    b. Make sure bypass valve is open – black handle
    c. Open chiller lines and ensure they are operating – place orange handles on lines on wall behind MOKON machine in vertical position
    d. Turn Power ON – red dial on MOKON machine front panel
    e. Press and Hold the "Start" button for 10 seconds – then purge
    f. Set temperature to 350°F
    g. Check and make sure discharge pressure is below 40 psi
    h. Close the bypass valve to allow the oil to reach the probe
    i. Hold down the "Purge" button for a couple minutes to get the air out of the lines
    j. Make sure pressure does not get too high
    k. It takes about 15 minutes for the probe to heat up
11. Turn on California Analytical Instruments gas analyzer
    a. Check the VI reading matches the analyzer output
    b. Make sure emissions temperature is set to 340°F at control station
    c. Make sure emissions temperature control is set to 350°F at gas analyzer
    d. Make sure emissions filter is set to 200°F at gas analyzer
    e. Make sure pressure, temperature, and humidistat readings are reasonable
12. Open valves for C_2H_8 and Air on wall behind MOKON machine
13. Set desired mass flow rates on MKS-247D digital control panel
    a. Turn "ON" controller – toggle switch on
    b. Turn "Display Channel" Rotary Switch to desired channel
        i. Channel 1- Fuel
        ii. Channel 2- Air
    c. Push Toggle Switch Up and Hold "Set Pt." for each channel
    d. Turn screw to desired percentage
    e. Release toggle switch
    f. Desired Equivalence Ratios for Ethylene can be found in "Equivalence Ratios for H2.xls" on desktop
14. Turn ON the "Fuel Pump" switch at the VI
15. Refill both pumps A and B
    a. Select "Refill" on the VI
    b. Click "Stopped, Press to Run" on the VI
    c. When finished click "Running, Press to Stop" on the VI
16. Decide whether to use pump A or B – pumps operate individually
17. Select "Constant Pressure" or "Constant Flow" on the pump
18. Set the desired JP-8 fuel flow rates in pressure or flow
19. Turn ON the "Fuel Valve" on the VI
20. To ensure an initial fuel spray out of the nozzles when starting fuel flow prime the line with pressure
    a. Ensure the manual fuel line valve at the combustor stand is still CLOSED
    b. Click "Stopped, Press to Run" on the VI

  c. Let the pressure build – seen on the fuel panel VI – 50 psi is good enough

  d. Click "Running, Press to Stop" on the VI

21. Ensure desired main and secondary air flow rates are set on the VI
22. Ensure desired fuel flow rate or pressure is set on the VI
23. Click ON "Ethylene and Air Valves" on VI (if operating through solenoids)
24. Turn Toggle Switch "On" Channel 2-Air on digital control panel (green light will illuminate) and let stabilize
25. Turn Toggle Switch "On" Channel 1-Fuel on digital control panel (green light will illuminate) and let stabilize
26. Turn on "Igniter" by pressing igniter button on control screen – sounds like pops similar to popcorn in a microwave
27. Open manual fuel line valve at combustor stand
28. Once lit, turn off "Igniter
29. **CAUTION – FAILURE TO LIGHT** – fuel will pool up inside and drip on the floor and possibly start a fire

  a. **IMMEDIATELY** – shut off Igniter and manual fuel valve at combustor stand and shut off JP-8 and ethylene fuel flow

  b. Re-evaluate conditions for lighting

30. Click "Stopped, Press to Run" on chosen fuel pump
31. Turn OFF "Ethylene and Air Valve" on VI
32. Turn OFF Channel 1 and Channel 2 toggle switches on MKS-247 digital control panel
33. Change air and fuel flow to desired settings
34. Click "Write" button on VI to save a file with UCC temperature and pressure data as well as other data from the front panel
35. Proceed with experiment

Good Start Conditions for UCC Operation

1. Set chosen pump to constant pressure

  a. Pressure should be above 50 psi for good spray of fuel out of nozzle

  b. Flow rate should be about 20 to 30 ml/min

2. Ensure both main and secondary heater temps are at least 300 degrees F
3. Set Main air flow to 1.3 kg/min
4. Set Secondary air flow to 0.3 kg/min
5. Once lit turn fuel pressure down to 30 psi – or switch to constant flow rate - 20 ml/min or lower
6. Increase secondary air flow to 0.6 kg/min
7. From this step adjust air and fuel flow rates accordingly to achieve different operating conditions

UCC Shutdown

1. Turn OFF Fuel Pumps
2. Turn OFF "Fuel Valve"
3. Set air line heater temperatures to 0

  a. It will take at least 30 mins for the heaters to cool down

b. Do NOT turn air or heaters off until below 150°F
4. Turn ON "Fuel Line Purge"
5. Once all fuel has been purged out of the system, turn OFF "Fuel Line Purge"
6. Turn ON "Probe Purge"
7. Once emission line is purged, turn OFF "Probe Purge"
8. Turn off California Analytical Instruments analyzer
9. Turn MOKON machine temperature to 0
    a. It will take at least 15 minutes for the MOKON machine to cool down
    b. Do NOT turn off machine until below 150°F
10. Once air temperatures for main and secondary line are below 150°F, click OFF main and secondary air lines
11. Manually turn OFF electric heater circuit breakers
12. Once MOKON machine is below 150°F turn OFF machine
    a. Close the chiller lines
    b. Turn Power OFF
13. Close the ethylene, air, and nitrogen valves at the wall behind the MOKON machine
14. Close all bottles in the tank farm
15. Turn OFF "Fan"
16. Proceed to "Lab Shutdown"

Hencken Flame Shutdown:
9. While operating - turn fuel, air, and nitrogen off out in tank farm
10. Turn off mass flow controller
11. Click off the "Fuel and Air Valve" and "Fuel Probe Purge" toggle switch in Lab-View control panel
12. Close valves for Fuel, Air, and Nitrogen on wall behind MOKON machine
13. Turn off fan
14. Proceed to "Lab shutdown"

Lab Shutdown:
1. Turn off "Equip" switch
2. Push "Stop" on Lab-view
3. Turn off DAQ pad
4. Turn off power strip in back of cabinet
5. Turn off air valve to black tank

APPENDIX B: Adiabatic Flame Temperature Calculation using STANJAN

The following procedure details how to use the combustion software STANJAN to calculate the adiabatic flame temperature. As an example, how to calculate the adiabatic flame temperature of a hydrogen air flame at an equivalence ratio of 1.0 is given.

Pressing return or the enter key gives an answer of "no."
Items in bold print are inputs required by the user.

Select a species data file or <return> if no file is desired.
Species data file? **COMB.SUD**

Getting species data file COMB.SUD   PLEASE WAIT!
C
C(S)
CH4
CO
CO2
C12H26
C3H8
H
HO
H2
H2O
H2O(L)
N
NC8H18
NO
NO2
N2
O
O2

Is this the file wanted? **Y**

Do you want to select REACTANTS or PRODUCTS (r/p)? **R**

Species data file: COMB.SUD

C	C(S)	CH4	CO	CO2	C12H26	C3H8	H
HO	H2	H2O	H2O(L)	N	NC8H18	NO	NO2
N2	O	O2					

REACTANTS selection: each PHASE is a homogeneous mixture of REACTANTS.

Type the species in phase 1, separated by commas or blanks; <return> = done.
  * = all gas species   # = all condensed species   ? = help!

H2 N2 O2 CO2 (use all caps, when finished press enter)

Species data file: COMB.SUD

C   C(S)   CH4   CO   CO2   C12H26 C3H8   H
HO   H2   H2O   H2O(L) N   NC8H18 NO   NO2
N2   O   O2

REACTANTS selection: each PHASE is a homogeneous mixture of REACTANTS.

Type the species in phase 2, separated by commas or blanks; <return> = done.
  * = all gas species   # = all condensed species   ? = help!

Do you want to CHECK the ATOMS in the molecules? **<return>**

Enter the mols of each SPECIES in phase 1 after its name:
 H2   : **2** (for phi of 1)
 N2   : **3.76**
 O2   : **1**
 CO2   : **.0016**

This is the CURRENT SETUP:

Reactant phase 1: mols
    H2   2.00000E+00
    N2   3.76000E+00
    O2   1.00000E+00
    CO2   1.60000E-03

Do you want to CHANGE the SETUP?**<return>**

Enter P (atm): **1**

Enter T (K): **298**

The sound speed can be calculated, but then the calculations take longer.

Do you want the SOUND SPEED?**<return>**

Do you want to SAVE the run OUTPUT in a file?**<return>**

Do you want to MONITOR the run (probably not)?**<return>**

Working; PLEASE WAIT!
OUTPUT READY

Use ctrl-s to stop/start the screen display.

Do you want to see the JANNAF data used?

On IBM-PC, use <ctrl-PrtSc> to start printer (optional).

Computed properties

atoms	population
C	1.60000000E-03
H	4.00000000E+00
O	2.00320000E+00
N	7.52000000E+00

Reactants at P = 1.000E+00 atmospheres

species	mol fraction in the phase	mol fraction in mixture	mass fraction in mixture	mols*

phase 1: molal mass = 20.917 kg/kmol T = 298.00 K

H2	.29579E+00	.29579E+00	.28508E-01	2.00000E+00
N2	.55608E+00	.55608E+00	.74474E+00	3.76000E+00
O2	.14789E+00	.14789E+00	.22625E+00	1.00000E+00
CO2	.23663E-03	.23663E-03	.49788E-03	1.60000E-03

Calculations made using frozen composition.

* Species mols for the atom populations in mols.

Mixture properties: molal mass = 20.917 kg/kmol
  P = 1.0133E+05 Pa   V = 1.1690E+00 m**3/kg
  U =-1.2308E+05 J/kg   H =-4.6284E+03 J/kg   S = 8.7750E+03 J/kg-K

Made   0 (T,P) iterations;   0 equilibrium iterations; v 3.96 IBM-PC

On IBM-PC, use <ctrl-PrtSc> to stop printer (optional).

This is the CURRENT SETUP:

Reactant phase 1:   mols
    H2   2.00000E+00

```
      N2        3.76000E+00
      O2        1.00000E+00
      CO2       1.60000E-03
Do you want to CHANGE the SETUP? Y

Change options:
  0  No changes; ready to select run option.
  1  Select species from a DIFFERENT DATA FILE
  2  Select DIFFERENT SPECIES (same data file)
  3  Change REACTANT MOLS (same reactants)
  4  Quit STANJAN

Change option?  2

Do you want to select REACTANTS or PRODUCTS (r/p)? P

Species data file: COMB.SUD


 C      C(S)    CH4     CO      CO2     C12H26  C3H8    H
 HO     H2      H2O     H2O(L)  N       NC8H18  NO      NO2
 N2     O       O2


PRODUCTS selection: each PHASE is a homogeneous mixture of PRODUCTS.

Type the species in phase  1, separated by commas or blanks; <return> = done.
  * = all gas species   # = all condensed species   ? = help!
```

H O N H2 HO CO NO O2 H2O CO2 N2

Species data file: COMB.SUD

```
 C      C(S)    CH4     CO      CO2     C12H26  C3H8    H
 HO     H2      H2O     H2O(L)  N       NC8H18  NO      NO2
 N2     O       O2


PRODUCTS selection: each PHASE is a homogeneous mixture of PRODUCTS.

Type the species in phase  2, separated by commas or blanks; <return> = done.
  * = all gas species   # = all condensed species   ? = help!
```

Do you want to CHECK the ATOMS in the molecules?<**return**>

This is the CURRENT SETUP:

Atom   population

C   1.60000000E-03
H   4.00000000E+00
O   2.00320000E+00
N   7.52000000E+00

Product phase 1:
H   O   N   H2   HO   CO   NO   O2
H2O   CO2   N2

Do you want to CHANGE the SETUP?**\<return\>**

Run options:

  0 Abort and redo setup
  1 Specified T and P
  2 Specified T and V
  3 Specified T and S
  4 Specified P and V
  5 Specified P and H
  6 Specified P and S
  7 Specified V and U
  8 Specified V and H
  9 Specified V and S
 10 A matrix of specified P,T cases (LOTUS file option)
 11 P and H same as last run
 12 V and U same as last run
 13 Specified T, S same as last run
 14 Specified P, S same as last run
 15 Specified V, S same as last run
 16 Chapman-Jouguet detonation of last-run mixture
 17 One of the above at specified composition
 18 One of the above under specified linear constraints

Enter run option: **11**

Enter estimated T (K): **2000**

The sound speed can be calculated, but then the calculations take longer.

Do you want the SOUND SPEED?**\<return\>**

Do you want to SAVE the run OUTPUT in a file? **Y** (this will put the file in the same
directory STANJAN is located)

WARNING! Be sure a disk on which you want to write is in its drive
BEFORE you give the file name. If you get an error message attempting

to write, do NOT change disks because MS-DOS may destroy the new disk directory! Instead, Abort, or use ctrl-c to go to DOS and start over.

SAVE file name? **PHI 1** (name arbitrarily chosen)

Is this an existing file? **N**

Do you want to keep the data now in the file?<**return**>

Do you want to MONITOR the run (probably not)?<**return**>

Working; PLEASE WAIT!
Next time try the state iteration monitor!

OUTPUT READY

Use ctrl-s to stop/start the screen display.

Do you want to see the JANNAF data used?

On IBM-PC, use <ctrl-PrtSc> to start printer (optional).

Computed properties

Independent atom	population	element potential
C	1.60000000E-03	-26.2618
H	4.00000000E+00	-12.1080
O	2.00320000E+00	-17.3633
N	7.52000000E+00	-13.9866

Products at T =   2382.03 K   P = 1.000E+00 atmospheres

2382.03 K is the adiabatic flame temperature

species	mol fraction in the phase	mol fraction in mixture	mass fraction in mixture	mols*
phase 1: molal mass = 24.277 kg/kmol				
H	.17968E-02	.17968E-02	.74603E-04	1.04678E-02
O	.54188E-03	.54188E-03	.35713E-03	3.15683E-03
N	.73555E-07	.73555E-07	.42441E-07	4.28509E-07
H2	.15286E-01	.15286E-01	.12693E-02	8.90500E-02
HO	.68379E-02	.68379E-02	.47902E-02	3.98352E-02
CO	.58724E-04	.58724E-04	.67754E-04	3.42108E-04

NO	.26621E-02	.26621E-02	.32905E-02	1.55085E-02
O2	.48100E-02	.48100E-02	.63398E-02	2.80215E-02
H2O	.32370E+00	.32370E+00	.24022E+00	1.88580E+00
CO2	.21592E-03	.21592E-03	.39142E-03	1.25789E-03
N2	.64409E+00	.64409E+00	.74320E+00	3.75225E+00

* Species mols for the atom populations in mols.

Mixture properties: molal mass =   24.277 kg/kmol
  T = 2382.03 K   P = 1.0133E+05 Pa   V = 8.0511E+00 m**3/kg
  U =-8.2040E+05 J/kg   H =-4.6287E+03 J/kg   S = 1.1075E+04 J/kg-K

Made   6 (T,P) iterations;   27 equilibrium iterations; v 3.96 IBM-PC

On IBM-PC, use <ctrl-PrtSc> to stop printer (optional).

APPENDIX C: Image Analysis using Win-View 32 Software

1. Open Win-View 32 Software
2. Focus the camera
    a. Click the blue button lower left side (brings up experimental set-up), see Fig. 75
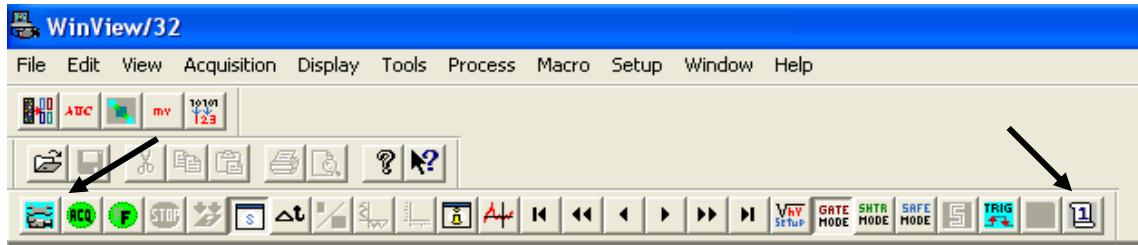

Fig. 75. Win-View 32 control panel

    b. Fig. 76 will appear and choose desired tab
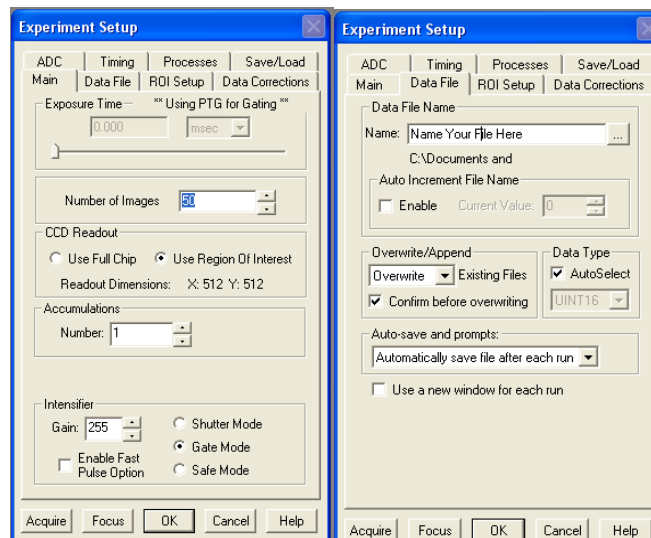
Fig. 76. Win-View 32 experimental setup tabs

    b. Set gain to 0
       c. Select shutter mode
       d. Push Focus
3. Take an image (take background first with laser sheet only, no flame) bring up experimental set-up again
    a. Set gain to 255
    b. Select Gate mode

c. Set desired Number of Images – 50 in this case
   d. Select data file tab – select file location and name it
   e. Go back to main tab
   f. Push Acquire
4. Average images
   a. Open an image to average
   b. Click the button lower right side (looks like paper with 1 on it)
   c. Average window comes up – check the box to average and click process
   d. Name the file
5. Subtract back ground from the averaged images
   a. Select Process - located where File, Edit, View, etc. are found, see Fig. 75
   b. Select Image Math, Fig. 77 will appear
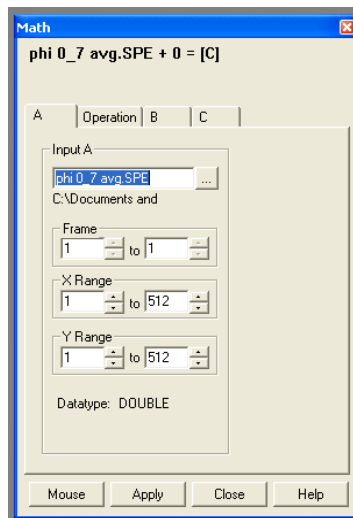
Fig. 77. Win-View 32 image math window

   c. Tab A – select the image to subtract background from
   d. Tab Operation – select subtraction
   e. Tab B – select the background to subtract
6. Get an average intensity
   a. Select Process on Fig. 75
   b. Select Statistics, Fig. 78 will appear
   c. Select area of interrogation – choose XRange and YRange
   d. Click OK – a window will come up giving average intensity and standard deviation for the particular area
   e. Record the intensity and standard deviation
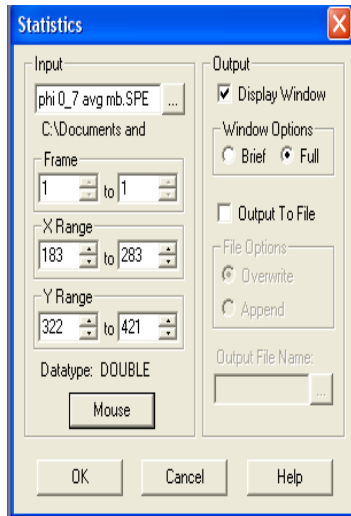
Fig. 78. Win-View 32 statistics window

APPENDIX D: Newport Universal Motion Controller Operation

1. Power ON controller
2. Turn ON buttons 1 and 2 for positions 1 and 2
3. Open ESP Utility software
4. Select Serial (RS232)
5. Click OPEN port
6. When asked if you want to reset controller – click NO
7. A window will appear stating:
   "ESP300 Detected on Tower 3"
   "Axis 1 Detected"
   "Axis 2 Detected"
   a. Click OK
8. Click Terminal – ASCII Command Terminal will open - issue commands here
   for movement
   a. 1pa1 moves the component (if on axis 1) 1 mm forward
   b. 1pa-1 moves the component 1 mm backward
   c. 2pa1 moves the component (if on axis 2) 1 mm left
   d. 2pa-1 moves the component 1 mm right

*left, right, forward, and backward will depend on how components are arranged

APPENDIX E: VI Output File Key

1. THC Output
2. NOX Output
3. CO_2 Output
4. CO Output
5. O_2 Output
6. THC Oven Temperature
7. Conv Temp
8. NOX Oven Temperature
9. Combustor Main Pressure (PT1)
10. Combustor Main Vane Inlet Pressure (PT2)
11. Main Temperature from FOX BOX
12. Main Flow from FOX BOX
13. Main Temperature from Heater
14. Combustor Main Vane Differential Pressure (PT4)
15. Secondary Flow Line Wall Inlet Pressure (PT3)
16. Combustor Cavity Inlet Pressure (PT6)
17. Secondary Temperature from FOX BOX
18. Secondary Flow from FOX BOX
19. Secondary Temperature from Heater
20. Combustor Cavity Differential Pressure (PT5)
21. Liquid Fuel Pressure (PT8)
22. Ambient Pressure (PT9)
23. Gas Fuel Pressure (PT7)
24. Gaseous Fuel Flow
25. Main Line Wall Inlet Temperature (TC1)
26. Combustor Main Vane Inlet Temperature (TC2)
27. Secondary Line Wall Inlet Temperature (TC3)
28. Combustor Cavity Inlet Temperature (TC4)
29. Liquid Fuel Temperature (TC5)
30. Oil Temperature at Combustor (TC6)
31. Gaseous Fuel Temperature (TC7)
32. Combustor Main Vane Exit Temperature (TC8)
33. Combustor Cavity Exit Temperature (TC9)
34. Combustor Cavity Back Wall Temperature (TC10)
35. Temperature
36. Humidity

APPENDIX F: Summary of UCC Operating Condition Data

Test Event Matrix		
Event	**Main Air / Cavity Air**	**Fuel (kg/min)**
Minimum	3.5	0.0075
Medium	10	0.0187
Maximum	15	0.0299
Condition		
1	3.5	0.0267
2	1.6	0.0088 - 0.0524
3	3.5	0.0075
4	3.5	0.0299
5	10	0.0187
6	15	0.0075
*	15	0.0299
7	15	0.0112

* Exceeds limits of system

Table 18. Condition 2 experimental data (air flow constant)

ϕ_{cav}	ϕ_{Tot}	Fuel Flow (kg/min)	$\Delta P/P_{cavity}$ (%)	ΔT_{Main} (K)	ΔT_{cavity} (K)	η_b (%)
0.10	0.04	0.0048	2.31	54	64	55.47
0.20	0.08	0.0096	2.29	48	44	23.23
0.30	0.12	0.0144	2.35	48	29	14.12
0.40	0.16	0.0192	2.52	71	50	15.78
0.50	0.19	0.0239	2.60	97	83	17.89
0.60	0.23	0.0287	2.70	159	152	24.72
0.70	0.27	0.0335	2.76	181	167	23.83
0.80	0.31	0.0383	2.83	223	202	25.39
0.90	0.35	0.0431	2.83	264	247	27.01
1.00	0.39	0.0479	2.79	189	177	17.89
1.10	0.43	0.0524	2.69	189	187	16.79

Table 19. Condition 4 experimental data

ϕ_{cav}	ϕ_{Tot}	Main Flow (kg/min)	Cavity Flow (kg/min)	$\Delta P/P_{cavity}$ (%)	ΔT_{Main} (K)	ΔT_{cavity} (K)	η_b (%)
0.4	0.09	3.80	1.09	4.22	50	63	21.83
0.5	0.11	3.03	0.87	5.78	63	60	20.43
0.6	0.13	2.54	0.73	3.03	72	64	19.40
0.7	0.16	2.18	0.62	2.45	104	85	23.14
0.8	0.25	1.18	0.54	1.90	142	113	19.34
0.9	0.20	1.70	0.49	1.69	174	164	30.67
1	0.22	1.53	0.44	1.44	206	181	32.11
1.1	0.25	1.39	0.40	1.22	233	185	32.34
1.2	0.27	1.26	0.36	1.05	260	193	32.31
1.4	0.30	1.12	0.32	0.88	295	202	32.17
1.6	0.36	0.95	0.27	0.66	371	206	32.99
1.8	0.40	0.85	0.24	0.55	433	208	33.78

Table 20. Condition 5 experimental data

ϕ_{cav}	ϕ_{Tot}	Main Flow (kg/min)	Cavity Flow (kg/min)	$\Delta P/P_{cavity}$ (%)	ΔT_{Main} (K)	ΔT_{cavity} (K)	η_b (%)
0.4	0.04	6.78	0.69	2.05	35	35	33.24
0.5	0.05	5.46	0.55	1.42	49	33	36.76
0.6	0.05	4.70	0.46	1.06	60	45	38.40
0.7	0.06	3.86	0.39	0.83	67	52	35.95
0.8	0.07	3.40	0.34	0.70	76	57	35.49
1	0.09	2.72	0.27	0.58	96	69	35.85
1.2	0.11	2.26	0.23	0.53	124	88	38.45
1.4	0.13	1.94	0.20	0.46	151	106	40.30
1.8	0.16	1.52	0.15	0.22	147	111	31.04
2	0.18	1.36	0.14	0.22	121	86	23.18
2.2	0.20	1.24	0.12	0.18	147	82	25.08

Table 21. Condition 6 experimental data

ϕ_{cav}	ϕ_{Tot}	Main Flow (kg/min)	Cavity Flow (kg/min)	$\Delta P/P_{cavity}$ (%)	ΔT_{Main} (K)	ΔT_{cavity} (K)	η_b (%)
0.4	0.20	4.05	0.27	0.28	68	59	91.34
0.6	0.25	2.72	0.22	0.23	67	49	61.27
0.8	0.39	2.04	0.14	0.11	78	39	52.08
1	0.48	1.60	0.11	0.10	90	40	47.30
1.2	0.73	1.37	0.07	0.06	94	45	42.46

Table 22. Condition 7 experimental data

ϕ_{cav}	ϕ_{Tot}	Main Flow (kg/min)	Cavity Flow (kg/min)	$\Delta P/P_{cavity}$ (%)	ΔT_{Main} (K)	ΔT_{cavity} (K)	η_b (%)
0.4	0.03	5.32	0.41	0.59	39	47	48.23
0.5	0.03	4.89	0.34	0.31	33	23	35.35
0.6	0.04	4.01	0.28	0.32	58	23	50.19
0.7	0.04	3.51	0.23	0.23	72	49	55.55
0.8	0.05	3.07	0.20	0.19	75	53	50.70
1	0.06	2.45	0.16	0.15	82	53	44.13
1.2	0.08	2.04	0.13	0.13	95	57	42.72
1.4	0.09	1.75	0.12	0.11	111	65	42.79

APPENDIX G: Additional UCC Emissions Data

Test Event Matrix		
Event	**Main Air / Cavity Air**	**Fuel (kg/min)**
Minimum	3.5	0.0075
Medium	10	0.0187
Maximum	15	0.0299
Condition		
1	3.5	0.0267
2	1.6	0.0088 - 0.0524
3	3.5	0.0075
4	3.5	0.0299
5	10	0.0187
6	15	0.0075
*	15	0.0299
7	15	0.0112

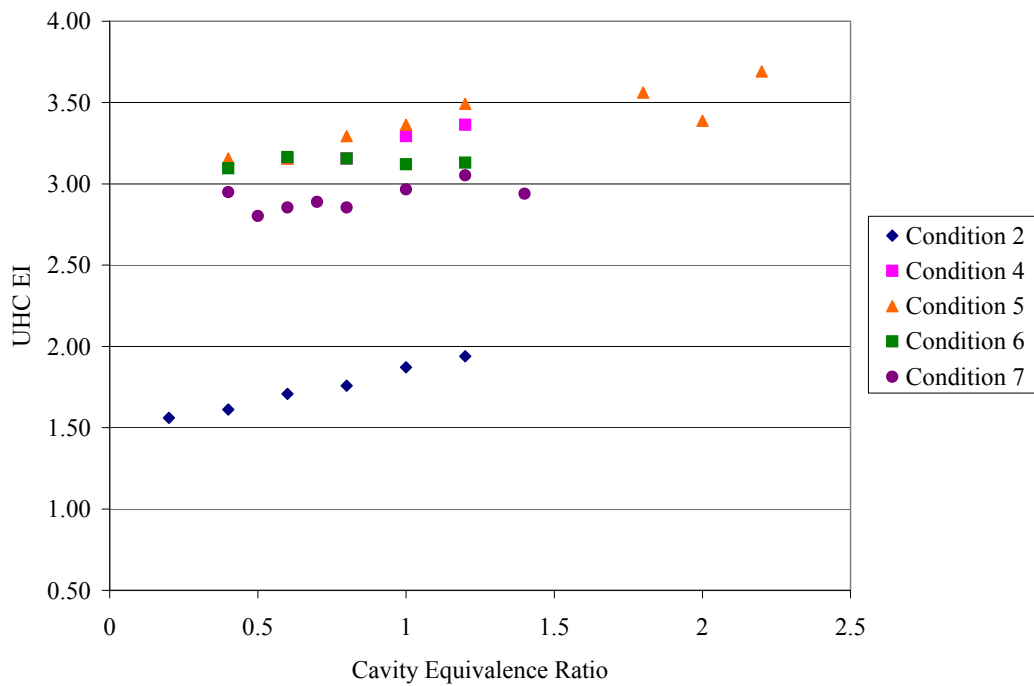* Exceeds limits of system

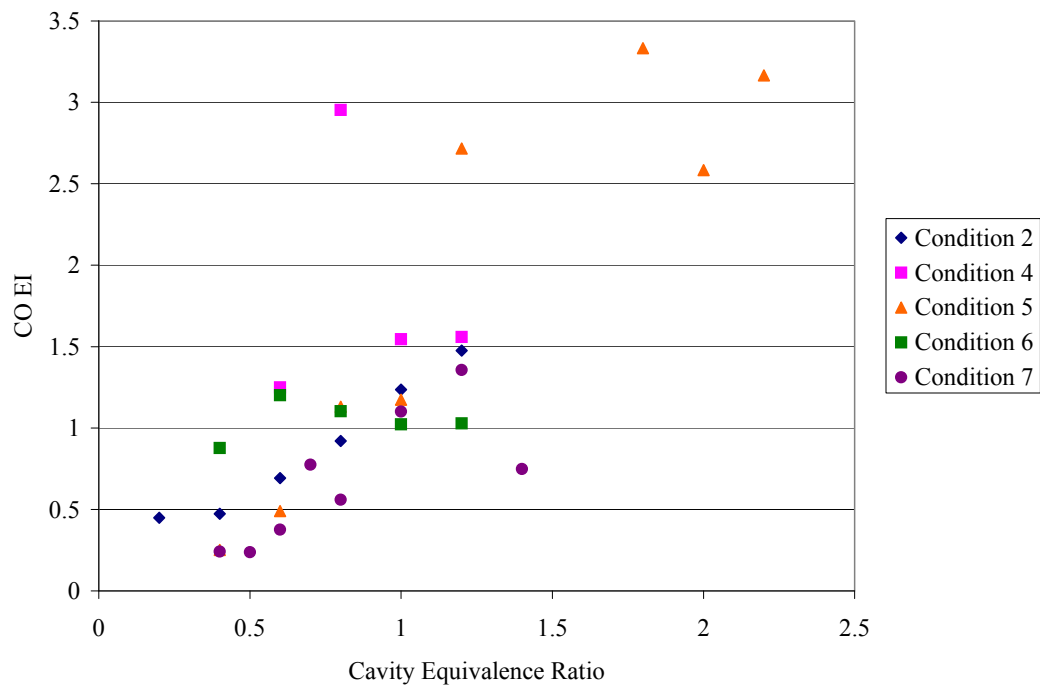Fig. 79. UCC UHC emissions versus cavity equivalence ratio

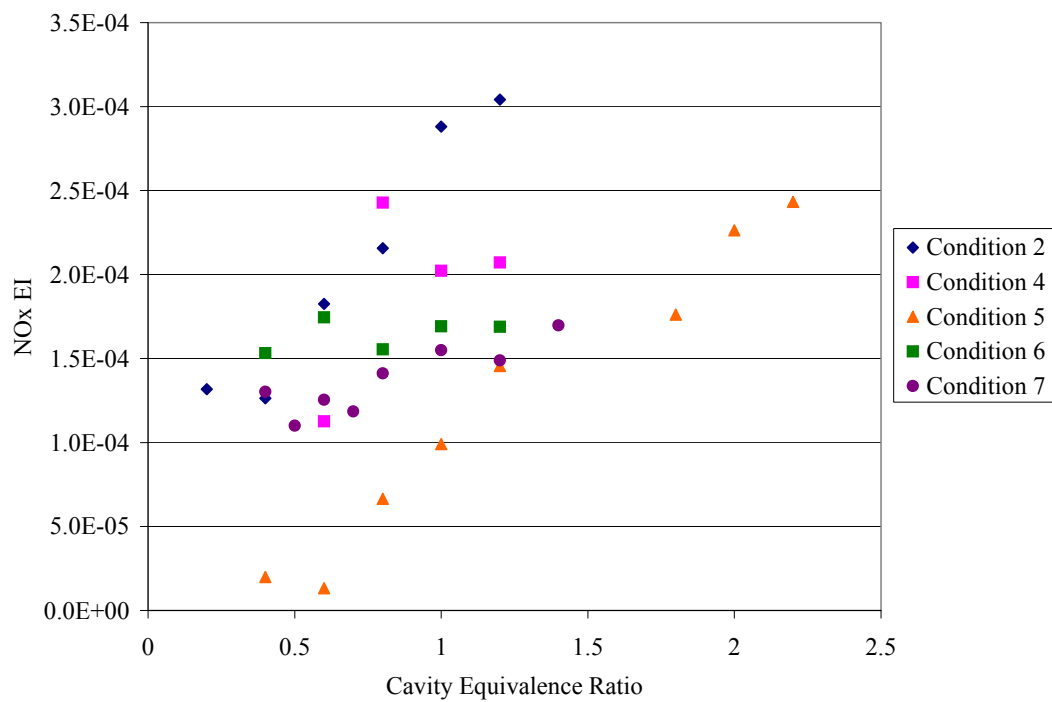Fig. 80. UCC CO emissions versus cavity equivalence ratio

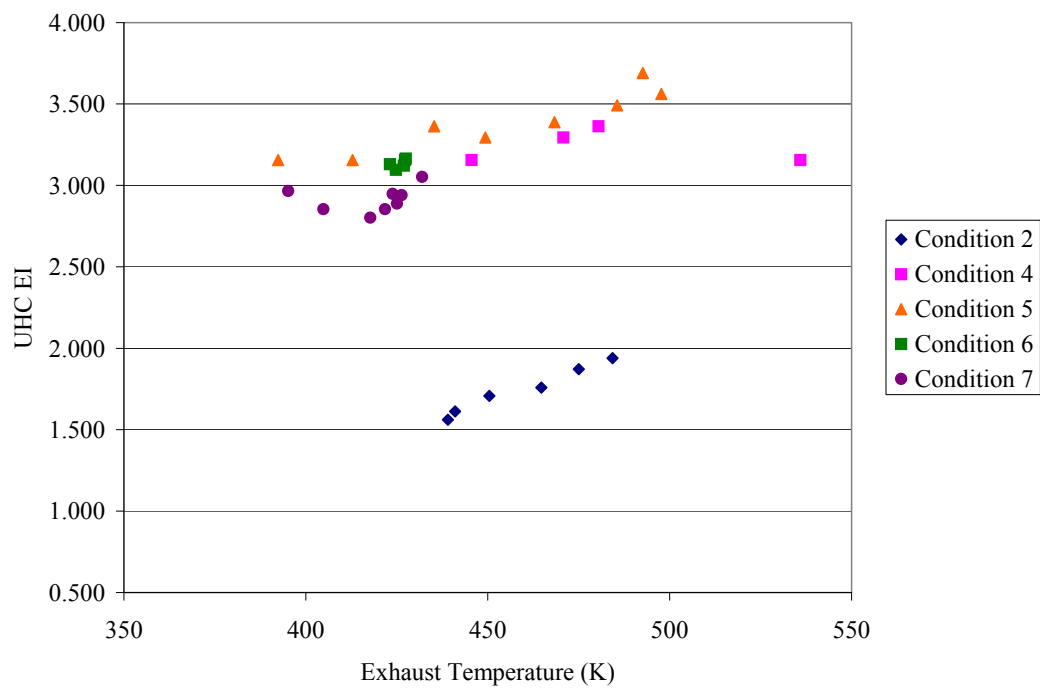Fig. 81. UCC NO$_x$ emissions versus cavity equivalence ratio

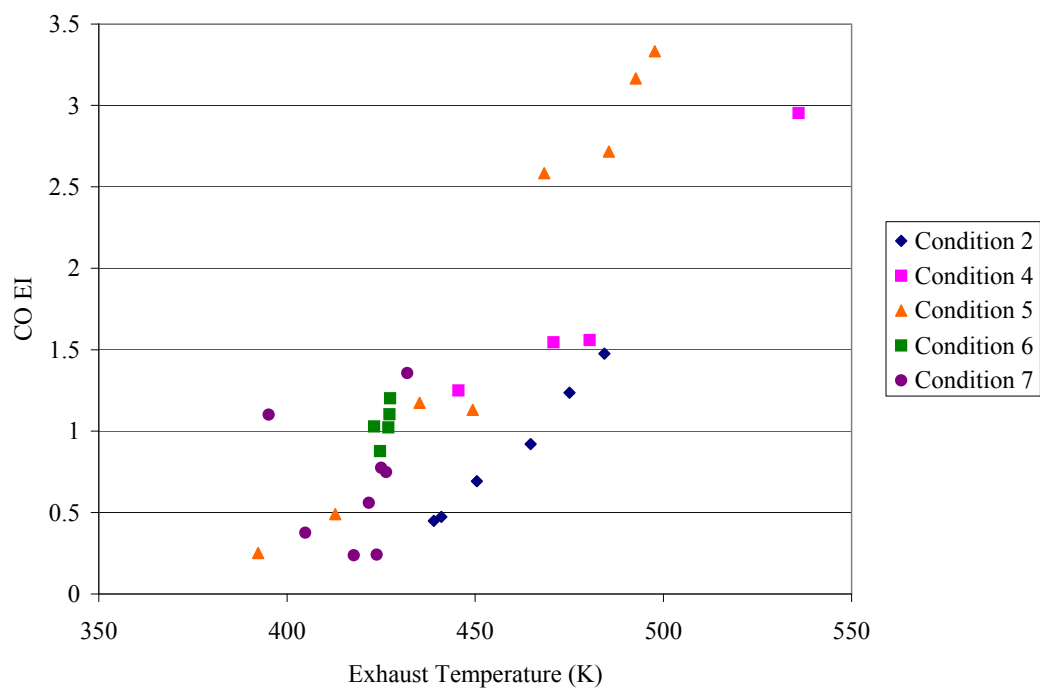Fig. 82. UCC UHC emissions data versus temperature

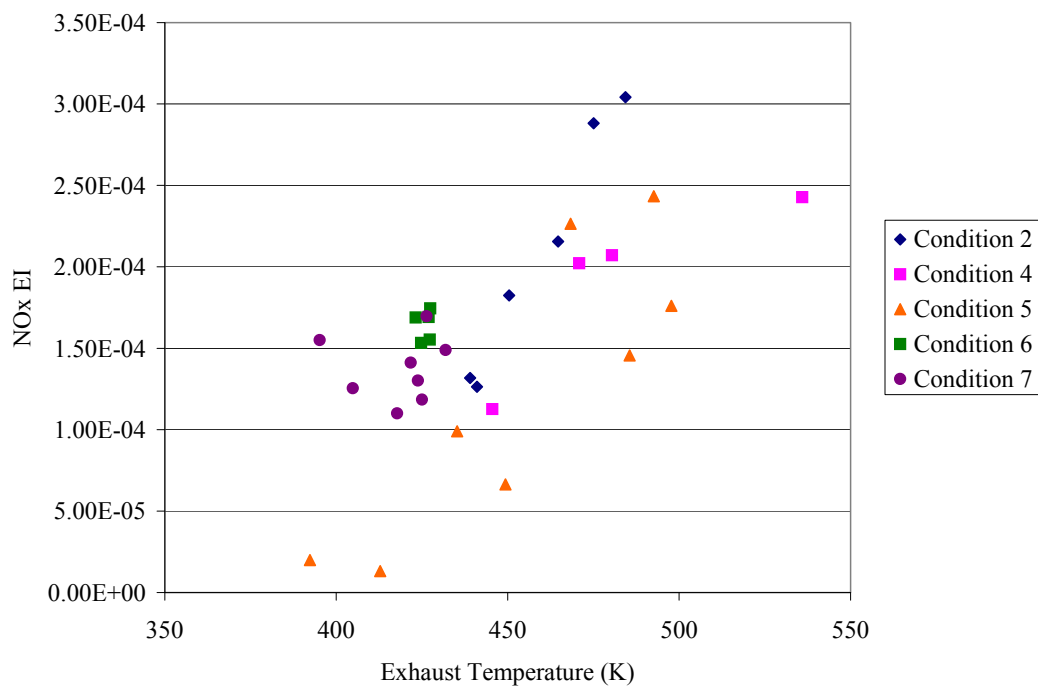Fig. 83. UCC CO emissions data versus temperature
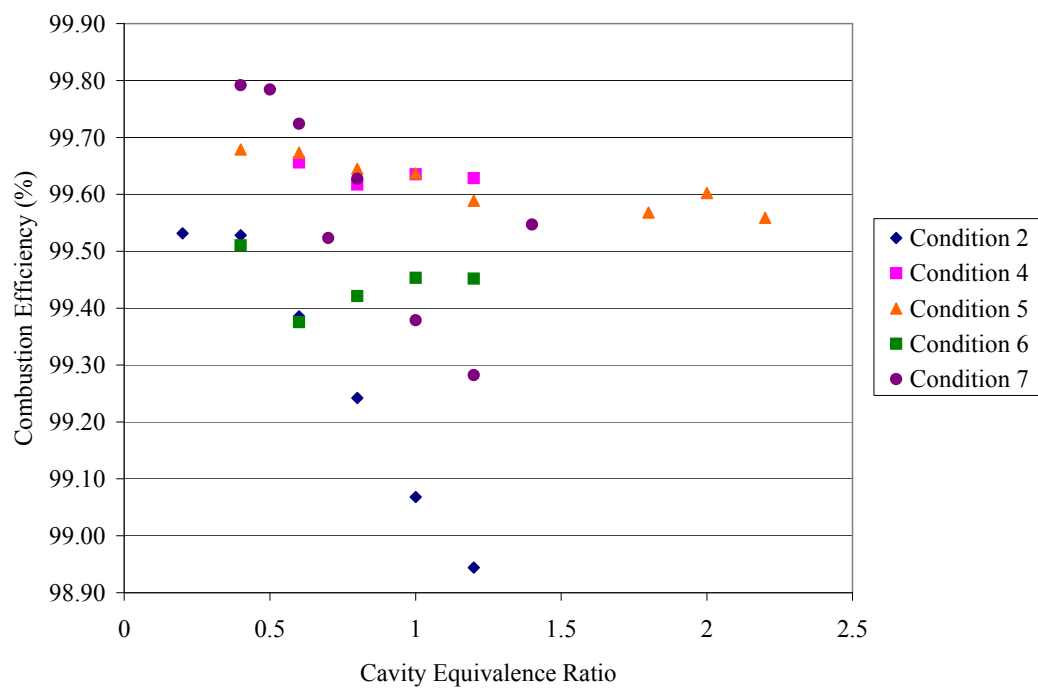
Fig. 84. UCC NO$_x$ emissions data versus temperature

Fig. 85. UCC efficiency as a function of cavity equivalence ratio

Table 23. Operating condition 2 emissions data

ϕ	CO (ppm)	NO (ppm)	NO$_2$ (ppm)	NO$_x$ (ppm)	UHC (ppm)	% CO$_2$ - IR
0.2	223	0.7	0.3	1.1	1810	0.44
0.4	235	0.6	0.5	1.1	1870	0.48
0.6	344	1.2	0.5	1.7	1980	0.53
0.8	457	1.6	0.5	2.1	2040	0.58
1	614	1.9	1	3	2170	0.62
1.2	733	2.3	1	3.3	2250	0.65

Table 24. Operating condition 4 emissions data

ϕ	CO (ppm)	NO (ppm)	NO$_2$ (ppm)	NO$_x$ (ppm)	UHC (ppm)	% CO$_2$ - IR
0.6	621.1	1.3	0.5	1.8	1983	0.59
0.8	1467.1	3.3	1	4.4	2153	1.18
1	767.9	2.4	1	3.5	2360	0.8
1.2	775	2.3	1.4	3.7	2530	0.88

Table 25. Operating condition 5 emissions data

ϕ	CO (ppm)	NO (ppm)	NO$_2$ (ppm)	NO$_x$ (ppm)	UHC (ppm)	% CO$_2$ - IR
0.4	125	0	0.3	0.3	3660	0.36
0.6	244	0	0.2	0.2	3660	0.39
0.8	562	0.7	0.3	1.1	3820	0.58
1	583	1	0.7	1.7	3900	0.68
1.2	1350	1.5	1.2	2.7	4050	0.86
1.8	1656	2.4	1	3.4	4130	0.97
2	1284	3.3	0.9	4.1	3930	0.87
2.2	1573	3.4	1.6	4.9	4280	1.06

Table 26. Operating condition 6 emissions data

ϕ	CO (ppm)	NO (ppm)	NO$_2$ (ppm)	NO$_x$ (ppm)	UHC (ppm)	% CO$_2$ - IR
0.4	436	1.5	0.9	2.4	3590	0.59
0.6	597	1.9	0.9	2.8	3670	0.6
0.8	548	1.6	0.9	2.5	3660	0.63
1	508	1.6	1	2.7	3620	0.64
1.2	511	1.6	1	2.7	3630	0.64

Table 27. Operating condition 7 emissions data

ϕ	CO (ppm)	NO (ppm)	NO$_2$ (ppm)	NO$_x$ (ppm)	UHC (ppm)	% CO$_2$ - IR
0.4	120	1.5	0.3	1.9	3420	0.49
0.5	118	1.2	0.3	1.5	3250	0.39
0.6	187	1.3	0.5	1.8	3310	0.54
0.7	385	1.4	0.3	1.7	3350	0.47
0.8	278	1.3	0.7	2	3310	0.47
1	547	1.6	0.7	2.3	3440	0.5
1.2	674	1.6	0.7	2.3	3540	0.56
1.4	372	1.8	0.7	2.5	3410	0.52

Bibliography

1. AIAA Position Paper, "Versatile Affordable Advanced Turbine Engines (VAATE) Initiative," *AIAA Air Breathing Propulsion Technical Committee*, Reston, VA, January 2006.

2. Anderson, W. S. *Design, Construction, and Validation of the AFIT Small Scale Combustion Facility and Sectional Model of the Ultra-compact Combustor.* MS thesis, AFIT/GAE/ENY/07-M01. Graduate School of Engineering and Management, Air Force Institute of Technology (AU), Wright-Patterson AFB OH, March 2007.

3. Koether, S. J. *Validation of the AFIT Small Scale Combustion Facility and OH Laser-Induced Fluorescence of an Atmospheric Laminar Premixed Flame.* MS thesis, AFIT/GAE/ENY/07-S03. Graduate School of Engineering and Management, Air Force Institute of Technology (AU), Wright-Patterson AFB OH, September 2007.

4. Mattingly, J. D. *Elements of Gas Turbine Propulsion.* New York: McGraw-Hill, Inc., 1996.

5. Zelina, J., Ehret, J., Hancock, R. D., Shouse, D. T., and Roquemore, W. M., "Ultra-Compact Combustion Technology Using High Swirl for Enhanced Burning Rate," *38th AIAA/SAE/ASME/ASEE Joint Propulsion Conference & Exhibit,* AIAA-2002-3725, Indianapolis, IN, July 2002.

6. Sirignano, W. A., and Liu, F., "Performance Increases for Gas-Turbine Engines Through Combustion Inside the Turbine," *Journal of Propulsion and Power,* 15:1 pp.111-118, 1999.

7. Liu, F., and Sirignano, W. A., "Turbojet and Turbofan Engine Performance Increases Through Turbine Burners," *38th Aerospace Sciences Meeting & Exhibit*, AIAA-2000-0741, Reno, NV, January 2000.

8. Zelina, J., Sturgess, G.J., Shouse, D. T., "The Behavior of an Ultra-Compact Combustor (UCC) Based On Centrifugally-Enhanced Turbulent Burning Rates," *40th AIAA/SAE/ASME/ASEE Joint Propulsion Conference & Exhibit,* AIAA-2004-3541, Fort Lauderdale, FL, July 2004.

9. Greenwood, R. T. *Numerical Analysis and Optimization of the Ultra-Compact Combustor.* MS thesis, AFIT/GAE/ENY/05-M10. Graduate School of Engineering and Management, Air Force Institute of Technology (AU), Wright-Patterson AFB OH, March 2005.

10. Mawid, M. A., Thornburg, H., Sekar, B., Zelina, J., "Performance of an Inter-Turbine Burner (ITB) Concept with Three-Different Vane Cavity Shapes," *42nd AIAA/SAE/ASME/ASEE Joint Propulsion Conference & Exhibit,* AIAA-2006-4740, Sacramento, CA, July 2006.

11. Thornburg, H., Sekar, B., Zelina, J., and Greenwood, R., "Numerical Study of an Inter-Turbine Burner (ITB) Concept with Curved Radial Vane," *45th AIAA Aerospace Sciences Meeting and Exhibit*, AIAA-2007-649, Reno, NV, January 2007.

12. Hsu, K-Y, and Goss, L. P., "Characteristics of a Trapped-Vortex Combustor," *Journal of Propulsion and Power,* Vol. 14, No. 1, 1998.

13. Roquermore, W. M., Shouse, D., and Burrus, D., "Trapped Vortex Combustor Concept of Gas Turbine Engines," *39th AIAA Aerospace Sciences Meeting & Exhibit*, AIAA 2001-0483, Reno, NV, January 2001.

14. Lewis, G. D., "Centrifugal-Force Effects on Combustion," *14th Symposium (International) on Combustion,* The Combustion Institute, pp.413-419, 1973.

15. Yonezawa, Y., Toh, H., Goto, S., and Obata, M., "Development of the Jet-Swirl High Loading Combustor," *26th AIAA/SAE/ASME/ASEE Joint Propulsion Conference,* Orlando, FL, AIAA-90-2451, Orlando, FL, March 1990.

16. Moenter, D. S. *Design and Numerical Simulation of Two-Dimensional Ultra-Compact Combustor Model Sections for Experimental Observation of Cavity-Vane Flow Interactions.* MS Thesis, AFIT/GAE/ENY/06-S07. Graduate School of Engineering and Management, Air Force Institute of Technology (AU), Wright-Patterson AFB, OH, September 2006.

17. Anisko, J. *Numerical Investigation of Cavity-Vane Interactions Within the Ultra-Compact Combustor.* MS thesis, AFIT/GAE/ENY/06-M01. Graduate School of Engineering and Management, Air Force Institute of Technology (AU), Wright-Patterson AFB OH, March 2006.

18. Turns, S. R. *An Introduction to Combustion* (2nd Ed.)*.* New York: McGraw-Hill, Inc., 1996.

19. Society of Automotive Engineers, Inc., "Aerospace Recommended Practice: Procedure for the Analysis and Evaluation of Gaseous Emissions from Aircraft Engines." ARP1533, Warrendale, PA: 2004.

20. Spectra-Physics Lasers & Photonics. *Quanta-Ray Lab-Series Pulsed Nd:YAG Lasers User's Manual.* Mountain View, CA: 2001.

21. Hitz, B., Ewing, J. J., Hecht, J. *Introduction to Laser Technology* (3rd Ed.). Piscatawa, NJ: IEEE, Inc., 2001.

22. Kohse-Hoinghaus, K., and Jefferies, J. *Applied Combustion Diagnostics.* New York, NY: Taylor & Francis, 2002.

23. Kohse-Hoinghaus, K. Laser Techniques for the Quantitative Detection of Reactive Intermediates in Combustion Systems. *Prog. Energy Combust. Sci. Vol. 20 pp. 203-279,* 1994.

24. Eckbreth, A. C. In Gupta A. K., Lilley D. G. (Eds.), *Laser Diagnostics for Combustion Temperature and Species* (1st ed.). Tunbridge Wells, Kentucky: Abacus Press, 1998.

25. Tamura, Masayuki, Pamela A. Berg, Joel E. Harrington, Jorge Luque, Jay B. Jefferies, Gregory P. Smith, and David R. Crosley. "Collisional Quenching of CH(A), OH(A), and NO(A) in Low Pressure Hydrocarbon Flames" *Combustion and Flame*, Vol 114, p 502-514, 1998.

26. Seitzman, J. M., R. K. Hanson, P. A. DeBarber, and C. F. Hess, "Application of quantitative two-line OH planar laser-induced fluorescence for temporally resolved planar thermometry in reacting flows," Applied Optics, Vol. 33, No. 18, June 1994.

27. J. Luque and D. R. Crosley, "LIFBASE: Database and Spectral Simulation Program (Version 2.0.55)," SRI International Report MP 99-009, 1999.

28. Giezendanner-Thoben, R., Meier, U., Meier, W., Heinze, J., Aigner, M., "Phase-locked two-line OH planar laser-induced fluorescence thermometry in a pulsating gas turbine model combustor at atmospheric pressure," Applied Optics, Vol. 44, No. 31, November 2005.

29. Welle, E. J., Roberts, W. L., Carter, C. D., Donbar, J. M. The Response of a Propane-Air Counter-Flow Diffusion Flame Subjected to a Transient Flow Field. *Combustion and Flame 135, pp. 285-297,* 2003.

30. Hancock, R. D., Bertagnolli, K. E., Lucht, R. P. Nitrogen and Hydrogen CARS Temperature Measurements in a Hydrogen / Air Flame Using a Near-Adiabatic Flat-Flame Burner. *Combustion and Flame 109, pp. 323-331*, 1997.

31. Kahler, J., Kompenhans, J. Fundamentals of Multiple Plane Stereo Particle Image Velocimetry. *Experiments in Fluids [Suppl.], pp. S70-S77,* 2005.

32. Jarvis, S. and Hargrave, G. A Temporal PIV Study of Flame/Obstacle Generated Vortex Interactions within a Semi-Confined Combustion Chamber. *Measurement Science and Technology 17, pp. 91-100,* 2005.

33. Filatyev S., Thariyan, R., Lucht, R., Gore, J.P. Application of Simultaneous Stereo PIV and Double Pulsed Acetone PLIF to Study Turbulent Premixed Flames. *35th AIAA Aerospace Sciences Meeting & Exhibit,* Reno, NV, January 2007.

34. Tanahashi, M., Murakami, S., Choi G., Fukuchi, Y., Miyauchi, T. Simultaneous CH-OH PLIF and Stereoscopic PIV Measurements of Turbulent Premixed Flames. *Proceedings of the Combustion Institute 30, pp. 1665-1672,* 2005.

35. Driscoll, J., Filatyev, S., Carter, C., Donbar, J. Measured Properties of Turbulent Premixed Flames for Model Assessment, including burning Velocities, Stretch Rates, and Surface Densities. *Combustion and Flame 141, pp. 1-21,* 2005.

36. Reynolds, William C. "STANJAN: Equilibrium solver." Stanford University, CA, 1995.

37. Dittman, E. R. *Design, Build, and Validation of a Small Scale Combustion Chamber Testing Facility.* MS thesis, AFIT/GAE/ENY/06-M06. Graduate School of Engineering and Management, Air Force Institute of Technology (AU), Wright-Patterson AFB, OH, March 2006.

38. Olivero, J.J. and Longbothum, R.L. Empirical Fits to the Voigt Line Width: A Brief Review. *Joint Quantitative Spectroscopy and Radiative Transfer* 17, pp. 233-236. 1977.

Vita

Captain Terry B. Hankins graduated from Decatur High School in Decatur, Texas. He enlisted in the Air Force in January 1996 and received an ROTC commissioning scholarship in February 2000. Graduating from the University of Texas at Arlington with a Bachelor of Science in Aerospace Engineering, he was commissioned as a Second Lieutenant in May 2003.

His first assignment was to the 28th Test and Evaluation Squadron, Eglin AFB, Florida where he served as an operational test engineer. There he coordinated live fire test of the AIM-120C7 AMRAAM missile from aircraft such as the F-15C. In September 2006, he entered the Graduate School of Engineering and Management, Air Force Institute of Technology. Upon graduation he will be assigned to the Propulsion Directorate at Wright-Patterson AFB, Ohio.

1. REPORT DATE (DD-MM-YYYY) 27 March 2008	**2. REPORT TYPE** Master's Thesis	**3. DATES COVERED** (From – To) October 2006-March 2008

4. TITLE AND SUBTITLE Laser Diagnostic System Validation and Ultra-Compact Combustor Characterization	**5a. CONTRACT NUMBER**
	5b. GRANT NUMBER
	5c. PROGRAM ELEMENT NUMBER
6. AUTHOR(S) Terry B. Hankins, Capt, USAF	**5d. PROJECT NUMBER**
	5e. TASK NUMBER
	5f. WORK UNIT NUMBER

7. PERFORMING ORGANIZATION NAMES(S) AND ADDRESS(S) Air Force Institute of Technology Graduate School of Engineering and Management (AFIT/EN) 2950 Hobson Way WPAFB OH 45433-7765	**8. PERFORMING ORGANIZATION REPORT NUMBER** AFIT/GAE/ENY/08-M14

9. SPONSORING/MONITORING AGENCY NAME(S) AND ADDRESS(ES) AFOSR Dr. Julian Tishkoff 4015 Wilson Boulevard Room 713 Arlington, VA 22203-1954	**10. SPONSOR/MONITOR'S ACRONYM(S)**
	11. SPONSOR/MONITOR'S REPORT NUMBER(S)

12. DISTRIBUTION/AVAILABILITY STATEMENT
     APPROVED FOR PUBLIC RELEASE; DISTRIBUTION UNLIMITED.

13. SUPPLEMENTARY NOTES

14. ABSTRACT
        The AFIT combustion optimization and analysis laser (COAL) lab is now completely operational and is state-of-the-art in combustion diagnostics. The objective of this research is to perform a validation of a laser diagnostic system and to begin the characterization of a small-scale model of an ultra-compact combustor (UCC). Validation of the laser system was accomplished by using planar laser induced fluorescence (PLIF) on a laminar premixed hydrogen-air flame produced by a Hencken burner. OH species concentrations are measured. Flame temperatures are determined with a two line fluorescence technique using different transitions in the (1,0) band of the OH (A-X) electronic transition system. Comparisons are made to existing research to prove accuracy. Characterization of the UCC began by developing an operational procedure. A proper starting condition and operating regime has been established. Pressures, temperature, and emissions data have been recorded for a range of equivalence ratios. Comparisons are made to previous computational fluid dynamic (CFD) research. Combustion efficiencies of over 99% have been recorded when operating the small-scale UCC. Future work will involve using PLIF to take non-intrusive measurements inside the combustor through optically clear quartz windows to study cavity-vane interactions.

15. SUBJECT TERMS
Combustion, Combustors, Experimental, Laboratory, Laser Diagnostics, Ultra-Compact Combustor, Laser-Induced Fluorescence, Hencken

16. SECURITY CLASSIFICATION OF:			**17. LIMITATION OF ABSTRACT**	**18. NUMBER OF PAGES**	**19a. NAME OF RESPONSIBLE PERSON** Maj Richard Branam, ENY
REPORT U	**ABSTRACT** U	**c. THIS PAGE** U	UU	172	**19b. TELEPHONE NUMBER** (Include area code) (937) 255-3636 x7485,

Standard Form 298 (Rev. 8–98)
Prescribed by ANSI Std. Z39.18